Investigating the Role of the Upper-Levels in Tropical Cyclogenesis

by

John Sears

A thesis submitted in partial fulfillment of

the requirements for the degree of

MASTER OF SCIENCE

(ATMOSPHERIC AND OCEANIC SCINCE)

at the

UNIVERSITY OF WISCONSIN-MADISON

2011

Abstract

Despite decades of theoretical research and observational studies, a good understanding of Tropical Cyclone Genesis (TCG) remains elusive. One recent theory proposes TCG is contingent upon a necessary condition in the lower tropospheric levels whereby a closed circulation exists in a Lagrangian framework forming a protective region for genesis. This thesis work contends that while lower-tropospheric forcing is necessary, it may not be sufficient, and the upper levels can have an influence on TCG. Specifically, enhanced divergence aloft as well as outflow vents are key differentiators between many developing and non-developing systems. Composite fields, 3-dimensional multivariate analyses, and case studies are examined to identify the roles that the upper-level flow environment can play in TCG events. While likely not a forcing mechanism per se, the upper tropospheric environment can provide a modulating effect on tropical disturbances trying to develop, and should not be ignored when forecasting impending genesis.

Acknowledgements

The utmost thanks to my research advisor, Chris Velden without whom tropical cyclones would have forever remained a mystery to me. His experience in scientific writing is almost entirely why my thesis is readable. Additionally, I would like to thank my readers, Dr. Steve Ackerman, Dr. Greg Tripoli and Dr. Larissa Back, their expertise is irreplaceable. My thanks goes out to those who contributed to the unfortunate number of different datasets that were utilized in this study, Dr. John Mecikalski and Dr. Greg Tripoli (again) for their UW-NMS model fields, Dave Settner for the CIMSS satellite AMVs and the New Mexico Technical University folks (Dr. Carlos Carrillo and Dr. David Raymond) for the 3-D Variational analysis. Also, without Dr. Michael Montgomery and Dr. Christopher Davis there would have been no PREDICT field experiment and no data to create datasets with.

Thanks to my wife, Sara for all her loving encouragement that makes life worth living. My family, both the one I was born with and married into have provided encouragement aplenty. My friends are to be thanked as well for keeping me sane... more or less.

Contents

1. Introduction

1.1 Background

Over the past few decades there have been great strides in improving tropical cyclone (TC) forecasting. Two formidable challenges that remain for TC forecasters are predicting TC intensity changes and forecasting TC Genesis (TCG). Genesis remains difficult to forecast for a number of reasons: 1) The structure and 3-dimensional flow fields associated with pre-genesis systems are poorly understood, in part due to the relative lack of reconnaissance aircraft data and research campaigns compared to mature TCs; 2) Competing theories for the fundamental processes involved, that transform a stochastic cluster of thunderstorms into an organized tropical cyclone (Tory and Frank, 2010); 3) TCG is not well handled by numerical models, in many cases due to the assumption of vortex axisymmetry in the initialization (Ooyama, 1987), which can often be an inadequate approximation for the actual formation stage of a TC .

There are two primary theories that have arisen to the forefront of TCG discussion in the last decade or two. The first includes two distinct variations, and both will be grouped together as "top-down" for the duration of this thesis. Variation 1, or "Top-down Merger" (Ritchie and Holland, 1997), features two mid-level vortices that interact, creating an area of enhanced vorticity that grows downward as a function of Rossby deformation. Extending to the surface, it promotes the spin-up of an organized system that can result in the initiation

of a tropical cyclone (TCG). Variation 2, or "Top-down Showerhead" (Bister and Emanuel, 1997), requires a single vortex that uses evaporatively-driven downdrafts from precipitation to advect cyclonic potential vorticity (PV) down to the surface to spin-up a cyclone. Both variations of "top-down" genesis require an initial mid-level vortex and the downward propagation of PV to establish a surface circulation.

The above concepts have in recent years been challenged by a "Bottom-up" theory of TCG. The basic principles of this theory are not new, but have been advanced primarily by Prof. Michael Montgomery and colleagues. This theory requires intense convection in the form of vortical hot towers (VHTs) to concentrate and spin-up relatively large areas of near-surface vorticity. The theory also necessitates the existence of a lower-tropospheric "sweet spot", referred to as a "Pouch," the name given to a protected area of vorticity and high moisture in a critical lower-tropospheric layer that moves along with a parent easterly wave (Wang et al., 2007), as shown schematically in Fig. 1. When these conditions are met, the circulation will build upwards and strengthen as the vorticity is amalgamated by the enhancement of the VHTs.
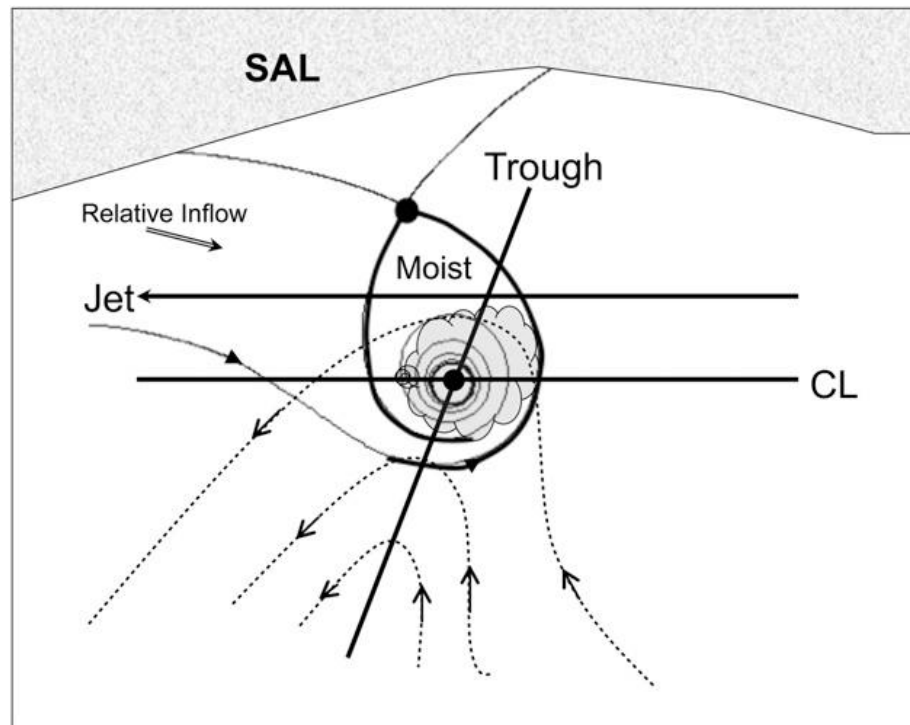
Figure 1. Schematic of a marsupial pouch in planar view showing the intersection of the .intersection of the critical layer (possessing suitable moisture and vorticity) propagating westward with the trough axis of the African Easterly Wave (AEW), creating a closed Lagrangian circulation.

The prevailing theories are not necessarily mutually exclusive, and a great deal of work remains to be done to determine what pieces of the theories best fit the limited observations of TCG. Bottom-up TCG was the focus of a recent field experiment called PREDICT (PRE-Depression Investigation of Cloud systems in the Tropics), which was designed to study pre-depression systems and test TCG hypotheses. The primary goals of PREDICT were to get a better understanding of the processes involved in TCG, and to specifically test the bottom-up hypothesis of Montgomery et al. The focus on TCG set this project apart from other TC field campaigns, such as NOAA's IFEX (Intensity Forecasting

EXperiment) or NASA's GRIP (Genesis and Rapid Intensification Processes) and provides a unique opportunity for the study of pre-depression cases. PREDICT builds on NASA's TCSP (Tropical Cloud Systems and Processes Experiment, Halverson et al., 2007) conducted in 2005 by adding many more new genesis cases to study, and also by targeting the sampling of non-developing systems.

While the focus of TCG and PREDICT is to better understand the pouch theory processes involved, in this study we employ the unique observations to examine the potential influence of the upper-tropospheric flow in the near-storm environment. Using various techniques, we show in a preliminary analysis that relies heavily on enhanced satellite data products, that upper-tropospheric environmental conditions may play a role in the TCG process.

This finding should not be too surprising. Observational analyses of mature TC systems (Davidson et. al., 1990; Hendricks et. al., 2010; Merrill and Velden, 1996; McBride, 1981; Zeng 2008; Jordan, 1952) indicate a relationship between storm intensity and upper-level influences. Several studies have cited the relevance of upper level asymmetries on mature TC's caused by tropical upper-tropospheric troughs (TUTTs) (Rodgers et al., 1991, Shi et al., 1997; 1990) or an established outflow channel (Wu and Cheng, 1999). Observational studies of the tropical upper troposphere and TC interactions are largely limited to satellite-based studies and focus mostly on mature storms. Therefore, this study which examines the genesis phase is in many ways charting new territory.

There are several documented instances of upper level influence on the intensification of mature storms. Observational studies (Chen, 1985; Molinari, 1989) feature asymmetries where interactions with mid-latitude disturbances allow for low eddy momentum flux values as an outflow channel is established from the inner radii to the outer radii (Molinari, 1990; 1995). Such outflow channels are typically found in the northeast sector of storms in association with trough interactions (Hanley, 2002), although she also found that identifying such signatures using satellite data was a formidable challenge.

Multiple modeling studies have shown the ability of the upper levels to modulate intensity of tropical cyclones. Montgomery and Farrell (1993) linked features in the upper troposphere to both mature tropical cyclone intensification and TCG. Similar studies have emphasized the importance of PV anomalies throughout the column (Kieu, 2009). There is a great deal of versatility in examining genesis in the upper troposphere from this perspective since it offers information regarding the tropopause and ambient vorticity which greatly affects inertial stability measures.

Composite studies of Blanchard et al. (1998) and others (Black and Anthes, 1971; McBride and Zehr, 1981; Merrill, 1988) identify a basic asymmetry in the upper troposphere above mature storms that allows for enhanced eddy flux convergence (EFC) of momentum and efficient mass transport. These asymmetries are also reproducible in modeling studies (Pfeffer and Challa, 1992; Challa and Pfeffer, 1980; 1990) that further emphasize the role of EFC in developing systems although Challa and Pfeffer characterized development as a TC

reaching tropical storm level. Additionally, statistical analysis of African Easterly Waves (AEW) show that the joint upper-level divergence-vertical velocity profiles were useful in differentiating developing waves and non-developing waves (Agudelo et. al., 2011).

Further model studies also suggest that the establishment of an outflow channel, either through TUTT influences or a storm's environmental modification, require inertial instabilities to be present (Schubert and Hack, 1982; Emanuel, 1982). Although the conditional instability of the second kind (CISK) is no longer considered the foundation of TCG low inertial stability in the upper levels, can create soft spots in the upper levels for outflow. Mecikalski and Tripoli (1998), hereafter referred to as MT98, use a diagnostic tool known as Inertial Available Kinetic Energy (IAKE, see Fig. 2) to study the role of upper-level inertial instabilities in mature storm development. IAKE can be portrayed as a horizontal analogy to convective available potential energy (CAPE), and they find that convectively active tropical waves without favorable IAKE conditions aloft can result in dissipation despite other favorable conditions.
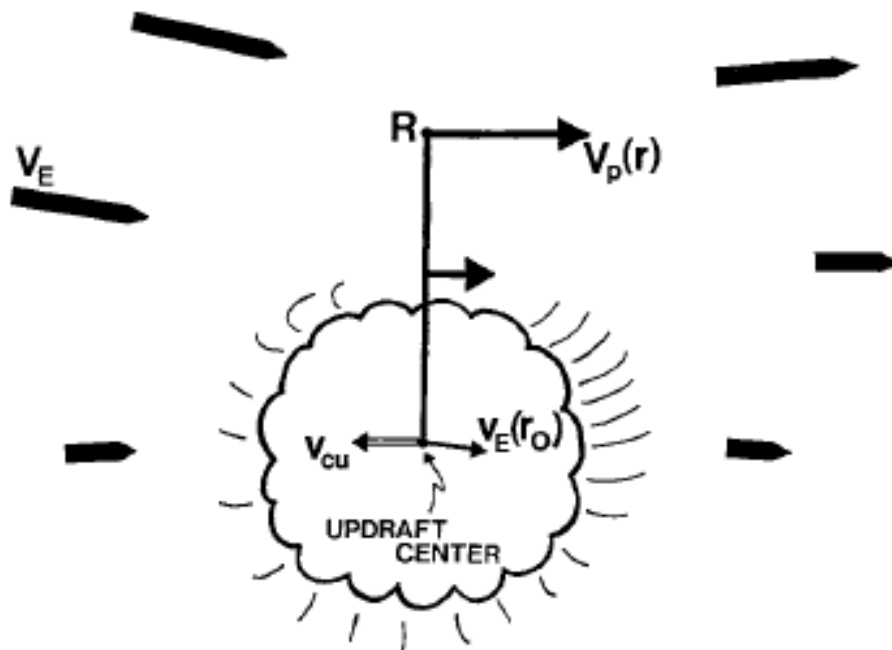
Figure 2. Top down view of a convective center and wind vectors used for determining IAKE. R is total distance from the updraft center. V_E is the environmental flow. $V_P(r)$ is the radial angular momentum about the updraft center *(Taken from: Mecikalski, John R., Gregory J. Tripoli, 1998: Inertial Available Kinetic Energy and the Dynamics of Tropical Plume Formation)*

The focus for this thesis paper is on using PREDICT and satellite observations to better understand how upper tropospheric processes may be involved in TC genesis and the importance of the asymmetric structures in outflow (Holland, 1984). Previous studies have shown imagery and derived products from geostationary satellites can provide crucial high-temporal observations of the upper-tropospheric flow evolution in the near-storm environment to supplement the available aircraft data. Using various analysis techniques, we show that upper-tropospheric environmental conditions may play a role in the TCG process.

1.2 Motivation

Bottom-up TCG and even top-down TCG theories usually don't put heavy consideration on the environmental flow conditions above 500hPa. However, as stated previously it has been shown that the upper-levels can play a significant role in the intensification of mature storms. Rapid TCG requires a substantial mass flux to sustain the secondary circulation similar to what drives mature storms (Rappin, Morgan and Tripoli, accepted; Merrill, 1988). Bottom-up dynamics require VHTs that transport vorticity upward through strong vertical motions (Montgomery et al., 2006). In order to evacuate the kind of mass necessary to allow persistent vortical hot tower activity and lowering MSLP, a divergent upper-troposphere over the pouch region would provide favorable conditions. Weak inertial stability aloft can often factor into the strength of the secondary circulation (Blanchard et al, 1998). Furthermore, if outflow ducts are available for mass transport away from the developing circulation, the TCG process could be made much easier, with less work (kinetic energy) required for the system to develop. Ventilation ducts connecting the core region with the outer environmental circulation allows the subsiding branch of the TC secondary circulation to occur well away from the pouch region, thereby minimizing the outer core downdrafts and subsiding dry air that if entrained back into the core region, could hinder VHT activity and TCG.

Besides strong vertical wind shear, the exact role of the upper-levels in TCG is uncertain for pre-depression systems, as it has received very little attention in the literature. Therefore, our motivation in this study is to examine this more carefully. We

hypothesize that the environmental flow conditions above the pouch may have important

TCG implications in many cases. Genesis forecasting (Schumacher et al., 2009; Tory et al.,

2007) and pouch diagnostics (Dunkerton et al., 2008; Montgomery et al., 2006) tend to

downplay upper-level conditions aside from the role that vertical wind shear plays in TCG

(Bell and Montgomery, 2010). The goal of this study is not to prove or disprove the validity

of "Pouch dynamics" as an instrumental piece of TCG, but rather cast it as a necessary but

possibly insufficient condition for genesis, requiring conditions to be favorable in the upper

troposphere as well as the lower troposphere.

1.3 Hypothesis

The primary hypothesis this study will address is that upper tropospheric

environmental flow conditions can play a role in genesis of tropical cyclones. Both case

studies and composite analyses are examined in order to identify any common flow

characteristics and their evolution in developing vs. non-developing events.

This study attempts to answer the question: *Can upper tropospheric conditions work

with or antithetically against favorable lower level conditions for TCG?* There are many

instances of promising tropical systems with strong pouch characteristics where

development was not observed, and this study will examine the possibility that unfavorable

upper troposphere conditions may have impeded such development. We hypothesize that

weak inertial stability aloft concentrated in outflow vents can provide the mass transport

channels necessary to sustain the VHT processes leading to TCG. This would suggest that

the upper-levels play at least a supporting role in the ability of the pouch dynamics to succeed in producing TCG. Furthermore, we believe enhanced satellite observations of the evolving upper-level cloud canopy along with model diagnostics may provide signatures of favorable vs. non-favorable conditions.

2. Research Approach

2.1 Data Sets

2.1.1 Period and Domain of Analysis

Easterly wave tracking is described by a Wang et. al. (2010). Identification of pouches requires a closed circulation from a Lagrangian perspective where the phase speed is contained in the critical layer (Figure 1). In contrast, previous studies (Davis et.al. 2008) primarily used only vorticity maxima to track features. Pouches are identified manually at three levels, 925, 850 and 700hPa and are tracked as long as it is present in a single layer. Pouch centers were identified in 00z model runs during the PREDICT field experiment July 15, 2010 to September 30, 2010, from analysis of four models, ECMWF, GFS, NOGAPS and UKMET although the tracking for this study requires only ECMWF. To smooth the analysis, the 6 hourly analyses between 00z were replaced with a linear interpolation.

The domain used for the 502 TC track locations analyzed in this study is 10°N to 50°N and 120°W to 20°W (FIGURE 3). The datasets employed for analysis of the upper-levels conditions in these cases are primarily derived from winds deduced by tracking clouds in

sequential satellite imagery (Velden et al. 2005): gridded U and V wind component fields at

150, 200, 250 and 300hPa running from 00Z 7/16/10 to 18Z 9/20/10. The wind data itself is

a conglomeration of infrared channel cloud drift winds, water vapor tracked winds and,

depending on daylight, either shortwave IR or visible channel cloud drift winds. The vectors

are analyzed onto an existing model grid, with weight given largely to the satellite wind

observations, creating fields of U and V wind components at 1 degree resolution. The

details of the wind derivation and grid analysis process can be found in Velden et al. (1998).

The winds and grids were produced at hourly intervals during PREDICT, but this study uses

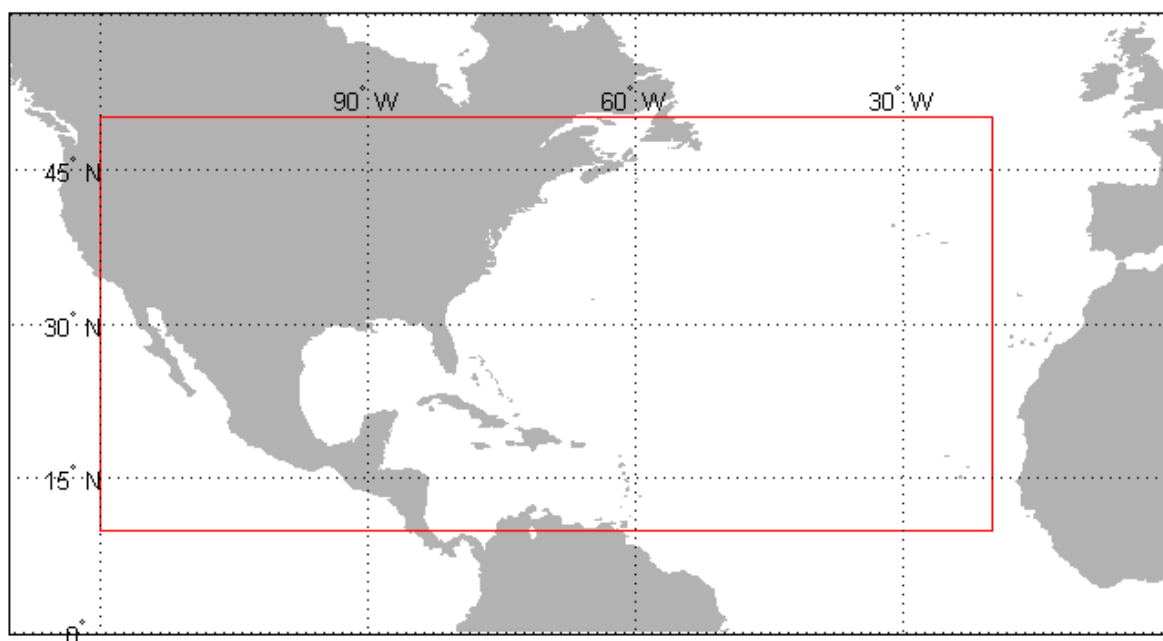only 6-hourly datasets to reduce serial correlation between analyses.

Figure 3. Region of observation for CIMSS satellite wind analysis dataset.

2.1.1.1 Multi-Storm Analyses

Thirty-five storms occurred over the course of the PREDICT experiment. The majority of these were easterly waves that propagated over the Atlantic, with many dissipating or developing before reaching 40 degrees west longitude. However, during this period a sizeable sample of both developing and non-developing systems were observed by satellite data, while a smaller sample were observed by the GV released dropsondes. Using primarily satellite and model observations, composite and EOF analysis was conducted to understand the general characteristics of the upper troposphere specific to either developing, non-developing or already developed systems. A more in depth discussion of the composite and EOF analyses will be done in a later section.

2.2.1.2 Case Studies

A pair of case studies are included in this work to further elaborate on points found in composite and convective analysis. Two storms are chosen to represent one developer (PGI44l- Karl) and one non-developer (PGI38L- Gaston). The track of these two storms, as well as dropsondes locations and intensity, is presented in Figure 4. Utilizing 3D-variational analysis of Gaston and Karl can be exploited to take advantage of higher horizontal and vertical resolution of dynamical variables along with derived vertical motion fields to identify patterns inferred in other analyses. Additional satellite analyses are also included in these case studies to supplement the 3-D Var analyses.
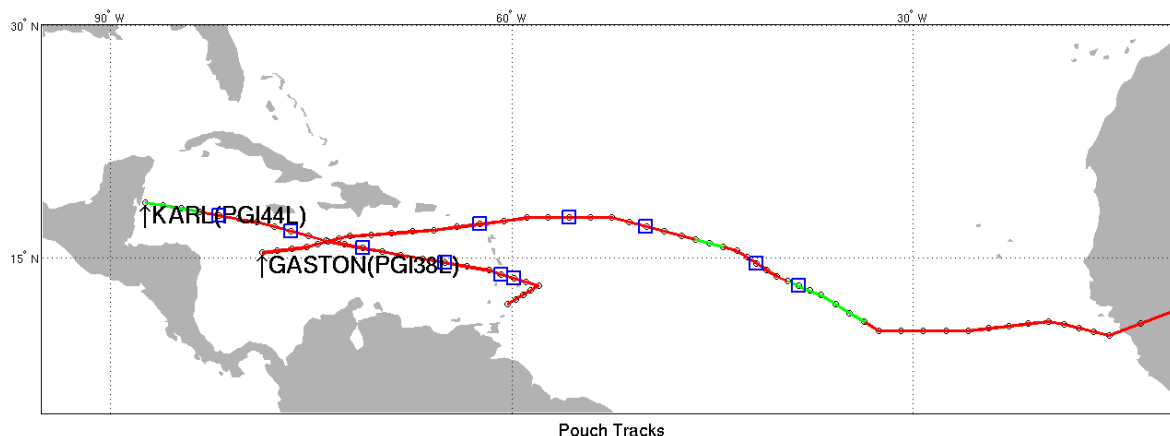
Figure 4. Daily interpolated 6-hr track locations of model derived pouch center locations for both case studies. Blue squares represent dropsondes analysis and green denotes TD strength or greater. Blue squares represent GV Missions.

2.1.2 Pouch Tracks

A summary of pouches identified throughout predict, as well as the location of every flight conducted by the GV throughout the PREDICT mission are presented in Fig. 5. The 6hr positions of the pouch locations are represented by the dots and storms stronger than tropical depressions are indicated by green tracks. Analysis of tracks east of 20 degreees West longitude and north of 10 degrees North latitude. were not part of the satellite winds analysis. The bulk of storms are traditional AEWs, thirty of the thirty-five storms in this dataset. Five storms have an origin west of 30 degrees west longitude, forming in the Carribean near the Gulf of Mexico or the West Atlantic. Flights were within 90°W longitude and 40 °W longitude, constrained by flight mission limitations.
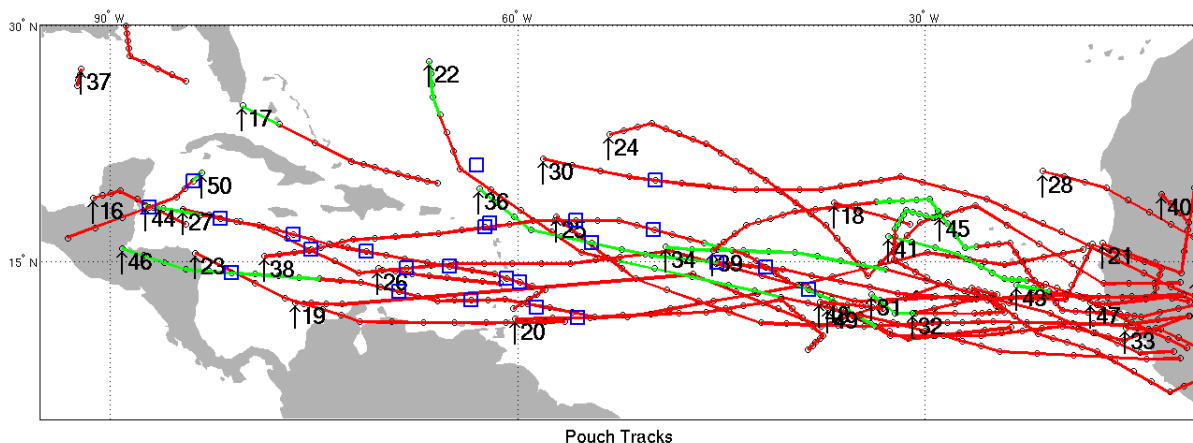
Figure 5. Daily interpolated 6-hr track locations of model derived pouch center locations for all 2010 pouches. Blue squares represent dropsondes analysis and green denotes TD strength or greater. Blue squares represent GV Missions.

2.1.3 PREDICT Observation Enhancements

Over 26 flights, between 15 and 30 dropsondes we used to take a vertical profile of temperature, humidity and winds. A summary of the flights is presented in Chart 1. A rigid quality control was applied for all dropsondes, eliminating several flagged as "fast falls" or flawed temperature or moisture sensors. Several individual dropsondes are included in this work as well as part of the New Mexico Technical University (NMTU) 3-D Variational data (from RF09-RF19) which will be discussed in more detail later in this thesis. Dropsonde analysis also provides a unique opportunity to provide a satellite wind validation dataset. Sounding analysis has been used to validate satellite wind analysis (Bedka et.al., 2009 and Velden and Bedka 2009) and a similar validation for tropical satellite wind datasets will be included in a later section.

Flight	Date	System	Operations Area	Maximum Intensity During System Lifetime	Notes
RF01	Aug 15	Disturbance	Western Atlantic	Disturbance	Shakedown/ Investigation of stalled frontal boundary and upper tropospheric shear line in the vicinity of the Bahamas.
RF02	Aug 17	PGI27L	Caribbean	Disturbance	First mission into PGI27L which had only recently begun to develop deep convection.
RF03	Aug 18	PGI27L	Caribbean	Disturbance	Second mission into PGI27L during which a large MCS developed in the northeastern part of the flight region.
RF04	Aug 21	PGI30L	Central Atlantic	Disturbance	First mission into PGI30L with weak convective activity. A small area of moderate convection was sampled in the northeastern corner of the lawnmower pattern.
RF05	Aug 23	PGI30L/Dropsonde Test	Central Atlantic	Disturbance	Test flight to confirm dropsonde noise/reception problems corrected.
RF06	Aug 30	PGI36L	Central Atlantic	Tropical Storm Fiona	First mission into PGI36L, while system still just below Tropical Storm Status. NHC named it TS Fiona on the update immediately following

					our flight
RF07	Aug 31	PGI36L	Central Atlantic	Tropical Storm Fiona	Second mission into PGI36L
RF08	Sep 1	PGI36L	Central Atlantic	Tropical Storm Fiona	Third mission into PGI36L
RF09	Sep 2	PGI38L	Central Atlantic	Tropical Storm Gaston	First mission into PGI38L (Gaston)
RF10	Sep 3	PGI38L	Central Atlantic	Tropical Storm Gaston	Second mission into PGI38L (Gaston)
RF11	Sep 5	PGI38L	Central Atlantic	Tropical Storm Gaston	Third mission into PGI38L (Gaston)
RF12	Sep 6	PGI38L	Central Atlantic	Tropical Storm Gaston	Fourth mission into PGI38L (Gaston)
RF13	Sep 7	PGI38L	Central Atlantic	Tropical Storm Gaston	Fifth mission into PGI38L (Gaston)
RF14	Sep 10	PGI44L	Trinidad-Tobago	Hurricane Karl	First mission into PGI44L
RF15	Sep 10	PGI44L	Trinidad-Tobago	Hurricane Karl	Second mission into PGI44L (First double mission day)
RF16	Sep 11	PGI44L	Trinidad-Tobago	Hurricane Karl	Third mission into PGI44L (AL92)
RF17	Sep 12	PGI44L	S. of Dominican Republic	Hurricane Karl	Fourth mission into PGI44L (AL92)
RF18	Sep 13	PGI44L	Jamaica	Hurricane Karl	Fifth mission into PGI44L (AL92)
RF19	Sep 14	PGI44L	W. of Jamaica	Hurricane Karl	Sixth mission into PGI44L (AL92). PGI44L was named Tropical Storm Karl after this mission.
RF20	Sep 20	PGI46L	Central Atlantic	Tropical Storm	First mission into PGI46L.
RF21	Sep 21	PGI46L	Central Atlantic	Tropical Storm	Second mission into PGI46L.
RF22	Sep 22	PGI46L	Central Caribbean	Tropical Storm	Third mission into PGI46L.
RF23	Sep 24	PGI46L	Western Caribbean	Tropical Storm	Fourth mission into PGI46L/Tropical Storm

Flight	Date	System	Operations Area	Maximum Intensity During System Lifetime	Notes
					Matthew.
RF24	Sep 27	PGI50L	Western Caribbean	Tropical Storm	First mission into PGI50L.
RF25	Sep 28	PGI50L	Western Caribbean	Tropical Storm	Second mission into PGI50L/Tropical Storm Nicole.
RF26	Sep 30	PGI48L	Central Atlantic	Disturbance	Mission into PGI48L/PGI51L.

Chart 1. GV mission fight summary (*Earth Observing Lab*).

2.1.4 Enhanced Satellite-Derived Atmospheric Motion Vectors

Since this study relies heavily on the quality of the satellite winds to determine the

upper-level structure of these developing systems, validation of the data to help determine

the accuracy and gain confidence in the use of the data for our analysis was conducted. To

do this, interpolation of the satellite derived gridded satellite winds to the locations of near-

coincident aircraft-deployed dropsondes at 250hPa for all flights with 250hPa level data was

necessary. The times of the dropsonde reports are rounded to the nearest 6 hour grid to

facilitate the validation. A scatter plot of the measured dropsonde winds vs. the gridded

satellite wind field (Fig. 6) has a U correlation of 0.6505 and a V correlation of 0. 4703.

Vector RMSE is on the order of 10kts. Biases between the two datasets are less than 0.15kts

for U and V. Given the spatial interpolation and temporal rounding, these comparison

statistics give us confidence that the satellite wind dataset accuracy is reasonably capable of

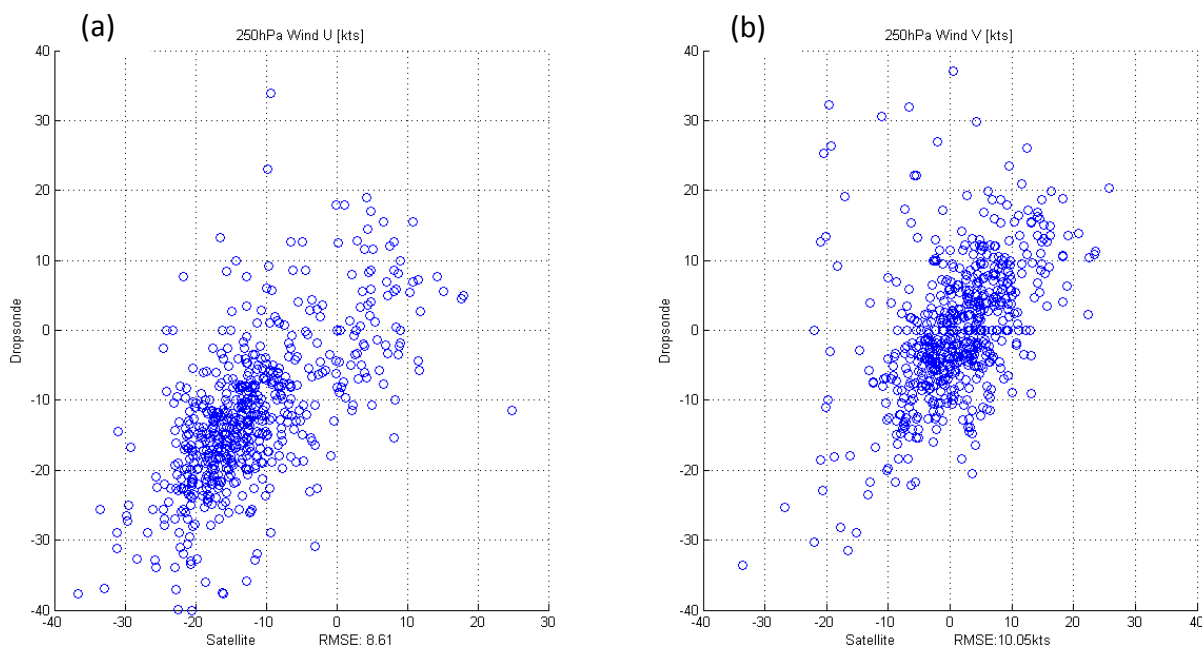representing upper-level flow trends and means near the 250hPa level of analysis.

Figure 6. Scatter plot of 250hpa interpolated CIMSS satellite gridded analysis (x-axis) vs. dropsonde observations (y-axis) for (a) the zonal(U) wind component and, (b) meridional (V) wind component from all 26 flights.

2.1.5 Validation Datasets

A subset of dropsondes from the flights into Gaston and Karl used in the 3-D Var will be compared to the satellite winds. The average number of dropsondes used for comparison per analysis is 19.82. The number of drops per analysis ranges between 22 and 17 although the total number of drops compared is less based on the requirement that satellite winds be within 1 degree and with enough coverage to reach an accurate interpolation of the satellite winds for the specific drop location. This is a particular challenge in the middle troposphere where cloud vectors are less common due to cloud tops obscuration or lack of clouds features in dry or subsidence dominated regions.

A similar analysis to the previous correlation analysis was conducted at 10.6km for

the non-gridded, raw CIMSS satellite winds, which is comparable to 250hPa based on

multiple sounding comparisons from the region. For each analysis the correlation

component of U and V satellite winds versus dropsondes U and V components at all levels is

plotted (Figure 7). There are only a few days where either U or V components have a

correlation coefficient higher than 0.5. Additionally, the range of correlation coefficients is

large, ranging from 0.78 to -0.04. The wide difference between U and V correlation

coefficients suggests large uncertainties in direction that might be linked to error in height

assignments of satellite winds. Larger errors are also associated with analysis with fewer

satellite winds due to no upper level cloud cover on weak convection days such as those

near the end of Gaston's lifetime where lacking sufficient wind coverage, limited the

number of comparisons.
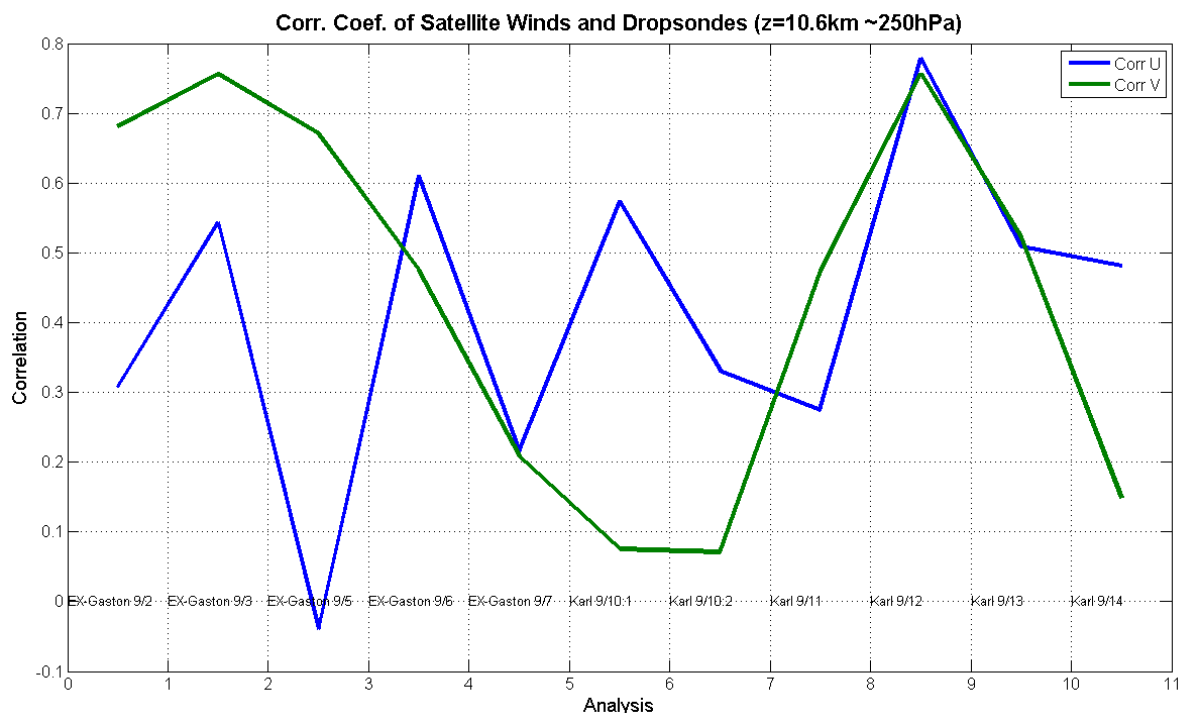
Figure 7. 10.6km correlation coefficient for U and V wind component comparing interpolated raw CIMSS satellite wind vectors to dropsondes limited to flights included in the 3D-Var analysis

Additionally, using the raw satellite winds assimilated into the 3D-Varriational dataset, there are fewer interpolation points but a breakdown root mean squared error by height (Figure 8, a). RMSE range between 3 and 4.5 m/s for both U and V components throughout the entire range of heights, which is roughly half of the estimate at 250hPa. Bias estimates (Figure 8, b) range between -3 and 2 m/s although for the lowest 9km the bias for U ranges between -1 and 1 although the mid-levels for the V component's bias is larger. In general, the statistics suggest that the raw winds are better than the winds projected on the GFS gridded satellite winds compared to dropsondes (Figure 6).
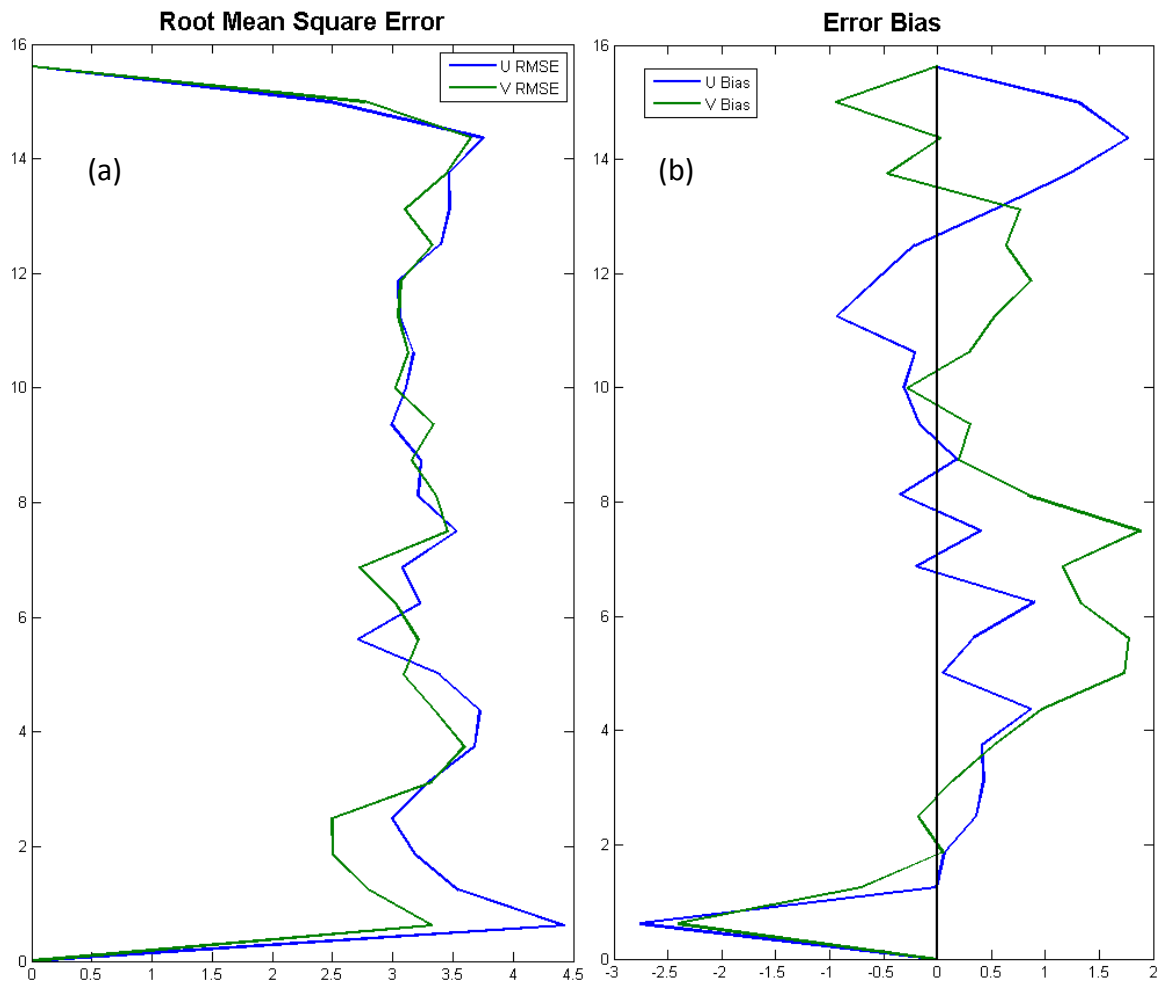
Figure 8. (a) Vertical profile of RMSE, raw CIMSS satellite AMVs validated against dropsondes. [m/s] (b) Vertical profile of bias, raw CIMSS satellite AMVs validated against dropsondes. [m/s]

2.2 Objective Analyses

2.2.1 Methods

2.2.1.1 CIMSS 3-D Recursive Filter

Roughly a third of this thesis is comprised of a multi-storm analysis of composite and

EOF analysis utilizing CIMSS satellite gridded wind datasets. The grids, which initially

covered the Atlantic basin, were broken down into 21x21 degree grid boxes centered on the

model consensus center of the pouch location. Cases were eliminated where the center of

the pouch was located poleward of 10 degrees latitude because the southern analysis

boundary was the equator. Additionally, cases were also constricted to be west of 20°W

degrees longitude to avoid direct interaction with the coast of Africa. This brought the total

of 6-hourly observations from 709 to 502 for the CIMSS satellite wind datasets investigated.

The computation of the IAKE and PV grids were created in an identical manner although the

period of usage of these fields was shorter, so the total number of grids created was less.

2.2.1.2 NMTU 3D-VAR

New Mexico Technical University (NMTU) provided storm relative 3D-Variational

analyses incorporating satellite winds and dropsonde information for selected PREDICT case

studies. Gridded fields were processed on constant height surfaces at half degree horizontal

resolution, once per day centered on GV dropsonde missions. The availability of these high

spatial resolution datasets with dropsonde observations allows for a more precise and

detailed study of the upper-level flow structure for our selected case studies.

To understand how the assimilated satellite winds impact the 3D-Var analyses, the

half degree resolution grids were dissected into a 10x10 array resulting in 2.1x2.1 degree

bins. The concentration of satellite wind data points in each bin tabulated for all of the 3D-

Var analyses (11 of them covering 2 storms). This is done in order to gauge the average

satellite winds concentration (per mission) and variation assimilated at 2 selected height

levels (Fig. 9). It is evident from Fig. 9a that (at least in these selected cases) upper level

cloud tracers are lacking in the northern hemisphere of the storm, allowing for better

coverage of low-level winds (Fig. 9b). Not surprisingly, upper level winds are more

concentrated over the storm center, and also in the southern quadrants.

(a) (b)

Figure 9. Binned concentration plots of satellite data ingested by 3D-Var analysis [# of observations per analysis] at (a) 0.625km and (b) 14.375km.
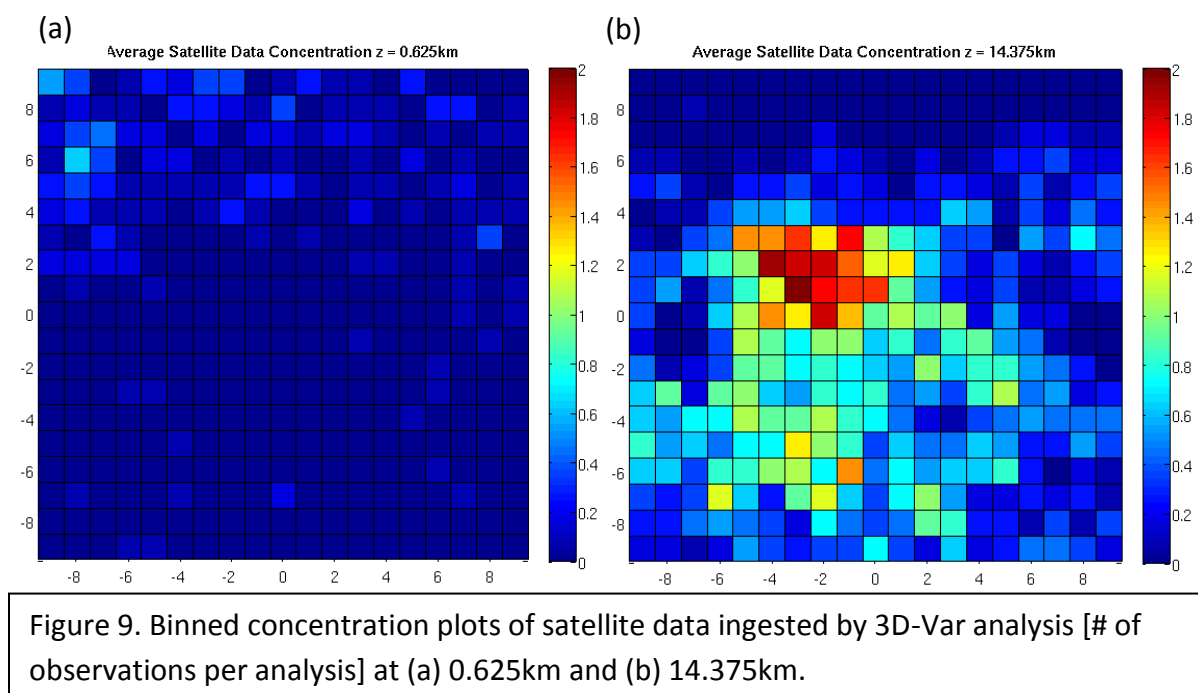
The relative sparsity of satellite winds in the northeast quadrant of the upper levels

is not mitigated in the 3D-Var analyses by the ingestion of dropsonde data (Figure 10).

Dropsonde concentration is limited primarily to the innermost radii. This still leaves a

noticeable data challenged region on the poleward side of storms beyond 5 degrees at this

height, which must be filled in by the 3-D Var process using observations from other levels

when available.
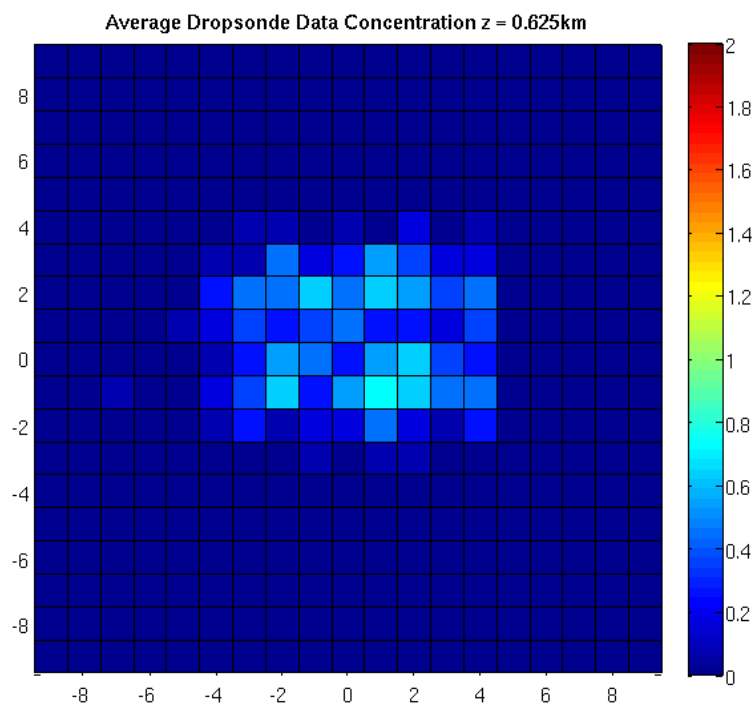
Figure 10. Binned concentration plot of dropsonde data ingested by 3D-Var analysis [# of observations per analysis].

Of note, this same data sparseness in the northern hemisphere present in the 3D-Var data is present in the CIMSS analyses, where the missing data is filled in by the GFS model analysis, accounting for some difference between the two analyses in addition to the resolution.

Figure 11 shows a comparison of the satellite wind observations against the 3D-Var field in which resulted from the final assimilation of drop and satellite information. Some differences are expected as the analysis attempts to achieve balance with dropsondes and mass continuity. The RMSEs above 4km for U and V run between 1.2 and 1.5 m/s (Figure 11a), with a minimal bias throughout the column (Figure 11b). The bias agreement and

RMSE of <2 m/s in the upper levels suggests enough agreement to draw similar conclusions between the 3D-Var data and other satellite wind datasets, despite irregularities in coordinate assignment and resolution since the 3D-Var datasets do not tremendously modify the raw satellite winds.
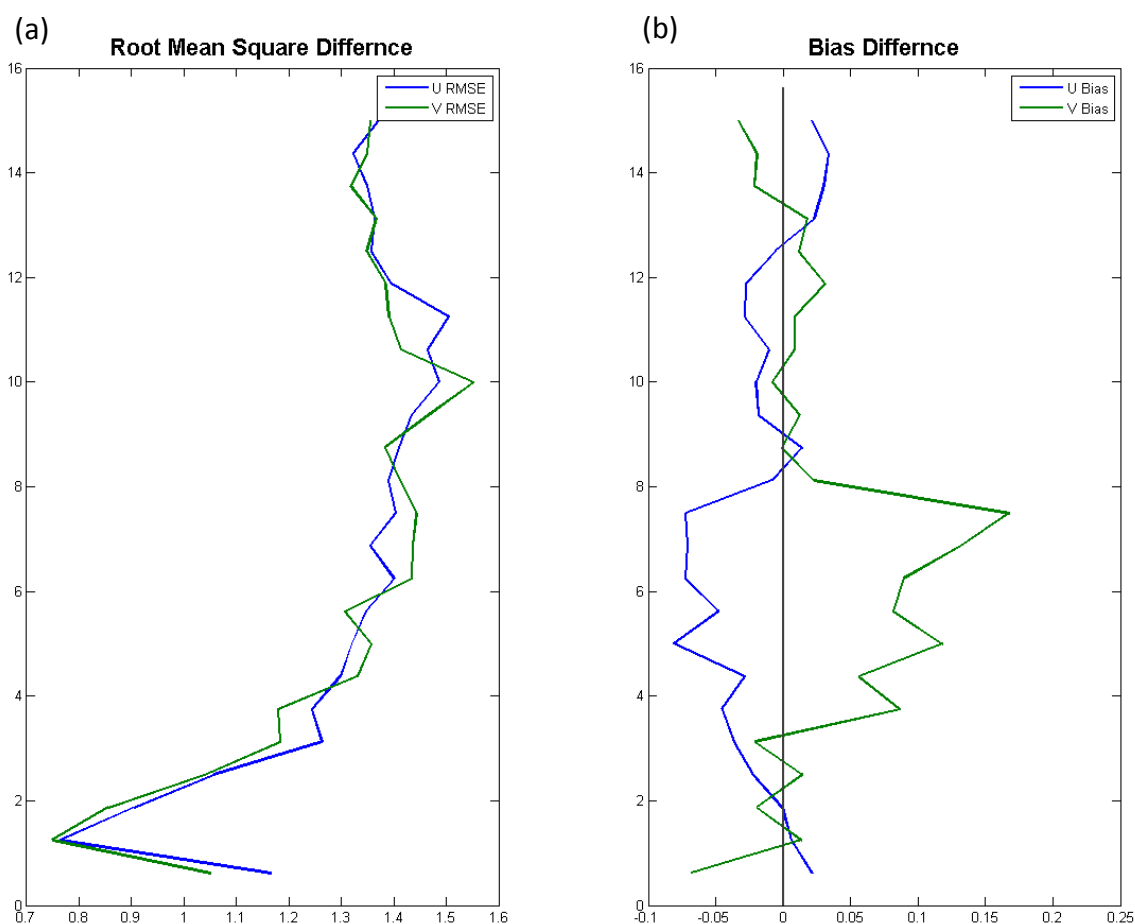

Figure 11. (a) Vertical profile of RMSE, raw CIMSS satellite AMVs validated against final 3D-Var analysis. [m/s] (b) Vertical profile of bias, raw CIMSS satellite AMVs validated against final 3-D Var analysis. [m/s].

2.2.1.3 UW-NMS Isentropic Analyses

As mentioned above, our hypothesis rests on the existence of upper-level "soft spots", in terms of low inertial stability and outflow ducts. The following diagnostic variables are calculated at 11 isentropic levels derived from GFS analysis fields which then utilize the University of Wisconsin Numerical Model Simulations (UW-NMS) model to compute Inertial Available Kinetic Energy (IAKE) and potential vorticity fields in isentropic coordinates. In order to perform the necessary calculations, the U and V wind fields used to derive these variables have not had storm motion removed and are thus Eulerian in nature:

Inertial Available Kinetic Energy	Ertel's Potential Vorticity
$$IAKE = \int_{r=0}^{RNA} \frac{dV_{rad}}{dt} dR$$	$$EPV = -g(\zeta_\theta + f)\frac{\partial \theta}{\partial p}$$
1 degree grids on isentropic surfaces (330K-380K)	1 grids evaluation on isentropic surfaces (330K-380K)

The derivation and further elaboration on IAKE is critical to understand its value, therefore much of the following is extracted from Mecikalski and Tripoli, 1998 (MT98) and presented here.

It begins with the isentropic coordinate form of Ertel's PV:

$$PV = -g\frac{\partial\theta}{\partial p}(\zeta_{\theta r} + f),\qquad(1)$$

where

$$\zeta_{\theta r} = \frac{\partial[rv_p(r)]}{r\partial r} - \frac{\partial u}{r\partial\varphi} = \frac{v_p(r)}{r} + \frac{\partial v_p(r)}{\partial r} - \frac{\partial u}{r\partial\varphi}\qquad(2)$$

(2) is the relative vorticity in cylindrical coordinates on an isentropic surface, with $v_p(r)$ being

the tangential wind of a parcel as a function of distance r from plume origin over deep

convection, u the radial wind, and g is gravity.

Putting (1) into differential form and solving for $v_p(r)$ (neglecting terms $v_p(r)/r$ and

du/rdφ as noted above), assuming PV1 = PV2 (i.e., PV conservation in plume outflow), gives

$$v_p(r) = r\left(\frac{\sigma_{d1}}{\sigma_{d2}}f_{d1} - f_{d2}\right),\qquad(3)$$

, where $\sigma_{d1} = d\theta/dp$ is the static stability of the plume outflow, $\sigma_{d2} = d\theta/dp$ is the

environmental static stability outside a plume, and r is as in (2). Also, subscripts d1 and d2

indicate radial distances from the plume origin, and we have taken dv/dr at d1 (the plume's

origin) to be zero when forming (3).

Assuming the above conservation principles provide a relationship describing the

behavior of plume expansion [$v_p(r)$], we form IAKE for measuring the kinetic energy

available to parcels exiting convective updrafts. We define inertial available kinetic energy

as

$$IAKE = \int_{r=0}^{RNA} \frac{dU_{rad}}{dt} \, dR, \qquad (4)$$

, where U_{rad} is the radial velocity relative to a given point (in cylindrical coordinates). The integration for IAKE would be over a total distance "R" from the plume origin (at r = 0) to the radius of neutral acceleration (RNA). A straight line is assumed for the integration path. An obvious extension to this is to evaluate IAKE, "following" convective outflow streamlines (i.e., a curved path of integration).

Given an environment initially near geostrophic balance, dU_{rad} /dt (neglecting advection) may be expanded to give

$$\frac{dU_{rad}}{dt} = fv + \frac{v^2}{r} - \frac{\partial M_\theta}{\partial r}, \qquad (5)$$

, which is the radial equation of motion on an isentropic surface, where y is tangential velocity and M is Montgomery streamfunction. We drop the centrifugal force term, v^2/r, under the aforementioned assumption of asymmetric outflow and because plume tangential flow components are assumed small near the plume's origin.

Next is an expansion of the tangential velocity into mean and perturbation components, $v = v_o + v'$ in the simplified (5), where v_o represents the geostrophically balanced environmental tangent wind with

$$\frac{dU(v_o)_{rad}}{dt} = 0 = fv_o + \frac{\partial M_o}{\partial r}, \qquad (6)$$

and v' represents the unbalanced portion of the flow. The environment's pressure gradient is assumed undisturbed by parcel displacements (by the outflow plume), an assumption that is also made when determining CAPE, as the parcel is defined to be an infinitesimal fluid element (Emanuel 1994). Upon substitution for v in (5) (excluding term v^2/r), and using (6), we arrive at

$$\frac{dU(v')_{rad}}{dt} = fv' = f[v_{pt}(r) - v_E], \qquad (7)$$

and thus,

$$v' = v_{pt}(r) - v_E. \qquad (8)$$

Equation (7) is the radial equation of motion we integrate along plume outflow paths to determine IAKE. In (8), the tangential wind $v_{pt}(r)$ is defined as the total parcel angular momentum and v_E is the environment's tangential wind.

IAKE values are generally negative and should only approach zero when environmental winds are assumed for the plume, that is, when $v_{cu} = 0$ in the Galelian transformed, updraft-relative system, where v_{cu} represents a parcels momentum relative to its parent convective system as it exits an updraft and is the dominant component of $v_{pt}(r)$. Positive IAKE (inertial instability) distant from the Tropics would not be expected except in cases of strong anticyclonic shear and/or very near convective updrafts where a diabatic source of low PV exists (i.e., in low PV environments). As shown below, it is only when the convective momentum transport v_{cu} is nonzero to provide a diabatic source of negative PV that positive IAKE occurs. Vector v_{cu} is taken to represent the collective momentums of a

number of processes within a cloud system including those formed by microphysical effects (e.g., precipitation drag), the momentum of the convective environment, and those that compose a system's internal mesoscale organization (Schneider and Lindzen 1976; LeMone 1983; Houze et al. 1989; Emanuel 1994).

As is often done for CAPE, this approach will initially neglect several important diabatic processes such as mixing, radiation, and friction when determining IAKE.

2.2.2 Other Analysis Approaches

2.2.2.1 Composites

Most of the previous TCG studies were limited by the number of cases investigated, resulting primarily in case studies. The large number of model-derived 6-hourly pouch track locations from 2010 in the tropical Atlantic allows the use of CIMSS satellite analyses for a number of developing and non-developing cases. Although case studies accompany this work, we can use this larger sample to create composite analysis that can be exploited to better understand systematic features pertaining to developing vs. non-developing systems.

Composite analyses were performed in two ways. The first set consisted of a breakdown based on storm stage: Non-developers, developing (pre-genesis) and already developed categories for 4 different pressure levels (150hPa, 200hPa, 250hPa and 300hPa). Development is defined as having reached tropical depression (TD) designation by the National Hurricane Center (NHC). Radially-averaged IAKE and PV analyses at selected isentropic levels (330-380K in intervals of 5) for the same storm stage categories are also

composited. Secondly, composites were created relative to the time of genesis, i.e.

compositing variables based on the time relative to declaration as tropical depression by

the NHC (developing cases only).

2.2.2.2 EOFs

Empirical orthogonal functions (EOFs) are used to find the primary modes of

variability in a dataset. Time series were broken down into loadings, principal components

and Eigenvalues; Eigenvalues regressed on the loadings provide a physical representation of

the dominant modes with units of per standard deviation. An Eigen Spectrum can be

computed using formula 1. λ, which is the vector of Eigenvalues and N is the number of

observations in the time series. The result is the % variance explained by each EOF. Using

North's Rule (Equation 2) error bars are calculated (North 1982). A well-defined EOF is one

without overlapping error bars, although for the purposes of this study, EOFs beyond the

third are not considered since they explained too little variance to be of value.

$$VAR = 100 \times \lambda/(sum(\lambda)) \qquad\qquad (1)$$

$$\lambda_{error} = VAR * \sqrt{2/N} \qquad\qquad (2)$$

2.2.3 Diagnostic Fields and Parameters

2.2.3.1 Upper-level Winds, Streamlines, Divergence and Vorticity

In addition to basic analyses of tangential and radial winds, the diagnostic variables used in this study, analyzed at four pressure levels (150hPa, 200hPa, 250hPa, 300hPa) with storm motion removed, are shown in Chart 1. The diagnostics are derived from the gridded CIMSS analyses described earlier using the equations shown in the chart. The diagnostic fields are produced at 6-hourly intervals throughout the PREDICT timeframe from June 20th 2010 to September 30th 2010.

Divergence/ Convergence	Relative Vorticity	Eddy Flux Convergence	Mass Flux
$D = \dfrac{du}{dx} + \dfrac{dv}{dy}$	$\zeta = \dfrac{dv}{dx} - \dfrac{du}{dy}$	$EFC = -\dfrac{1}{r^2}\dfrac{\partial}{\partial r}(r^2[u'v'])$	$M = \rho_{air} \oint V_{rad}\, d\theta$
1 degree grids	1 degree grids	Eddy flux convergence of relative angular momentum at radius r.	Mass of air moving through a circle of radius r.

The analyses for the diagnostic fields were created by sub-secting the CIMSS wind analyses into 21x21 degree grids, centered on a position fix of the PREDICT disturbances.. These fixes were derived from a consensus of global model estimates of the disturbance center locations. The center fixes were done every 24 hours, and linear interpolation is then used to create 6-hourly positions for the analyses described above. The motion of the

disturbance was then estimated from these position tracks and subtracted from the wind fields before the diagnostics were derived.

2.2.3.2 EFC and Mass Flux

Eddy Flux Convergence (EFC) and mass flux calculations are derived from the 21x21 gridded analyses used to compute divergence and vorticity fields. The computations require a radial average over selected rings around the center of the storm, ranging from 1 to 10 degrees. The values are found by averaging 16 points around the circle, interpolated from the surrounding gridded wind fields. An example mass flux calculation is shown in Figure 12, where the tangential wind component is averaged on interpolated points on the ring shown.

When considering storm quadrant analysis of these quantities, the averaging is limited to points in only the quadrant of interest. This results in a loss of radial resolution, or distance between interpolation points. For this reason, the interior 3 degree radial arcs consist of only four interpolation points, increasing to 16 for 3-8 degrees, and 32 for 8-10 degrees. In this way, a similar distance between points is maintained.
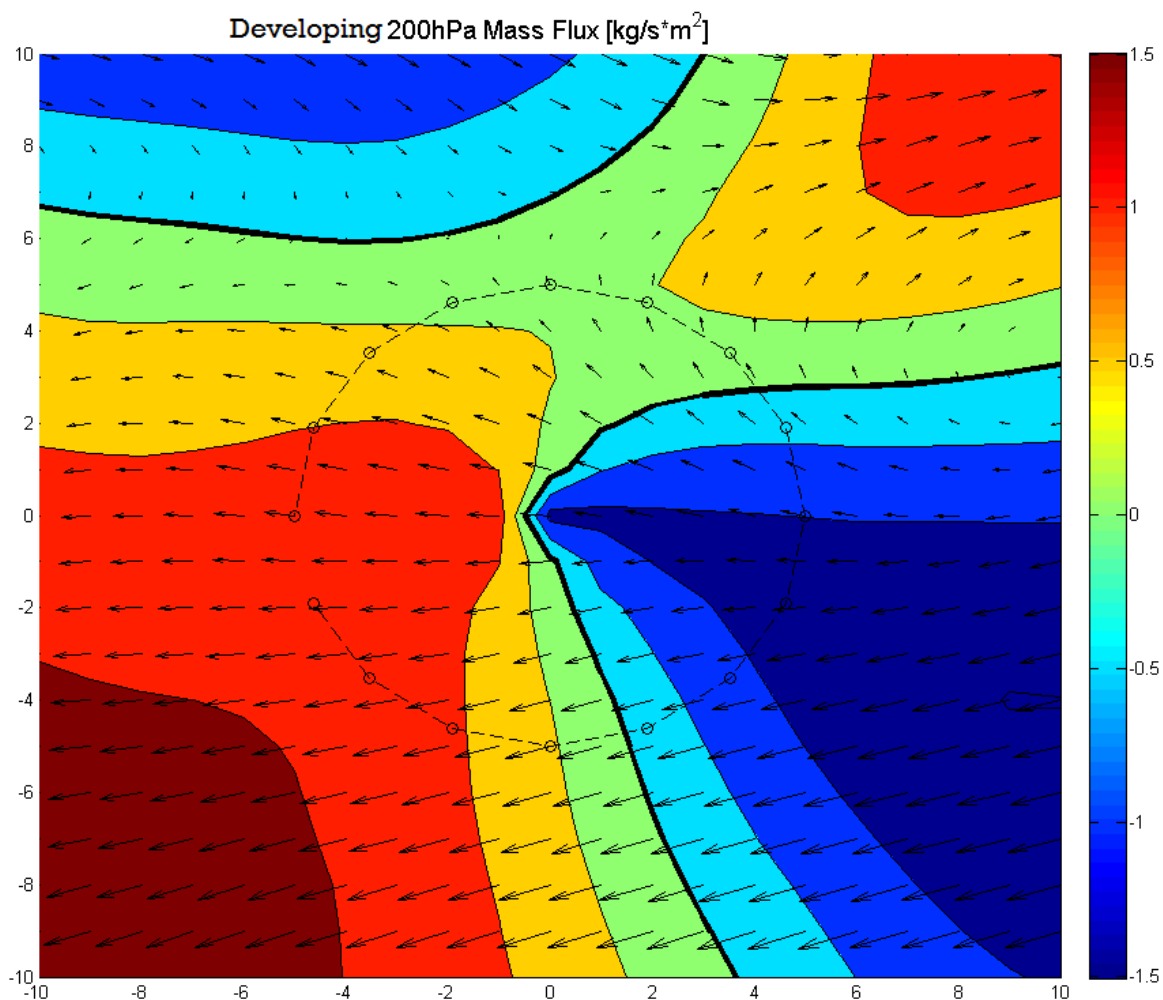
Figure 12. Example of method used for mass flux calculations with a sample 5 degree interpolation point ring used for analysis. Radial wind (contour) and gridded CIMSS satellite wind vectors.

2.2.3.3 IAKE and PV

IAKE and PV grids were derived in a manner similar to the divergence and vorticity grids, but from the Eulerian UW-NMS model fields; 21x21 degree grids, centered on the interpolated pouch center location with 10 degrees in every direction at 1 degree resolution. In cases where pressure analysis of the satellite winds (assigned at pressure heights) are compared to isentropic analysis (either IAKE or PV), the following

approximations were made, based on the mean of several sounding analyses from the

tropical Caribbean: 360K > 150hPa, 355K > 200hPa, 350K > 250hPa, 345K > 300hPa.

Therefore, the bulk of the upper level analyses considered in this study that are derived

from the CIMSS satellite winds fall in the 345-360K range of isentropic levels derived by the

UW-NMS model.

2.2.3.4 IR/WV/VIS Imagery

In addition to the quantitative diagnostics, satellite imagery can be an important tool

for observing the evolution of outflow structures and identifying environmental features

that may be playing an interactive role. Infrared (IR) and water vapor (WV) imagery cover

the domains of the GOES-EAST and METOSAT geostationary satellites, allowing complete

coverage of the tropical Atlantic with a spatial resolution of 3-4km. The WV imagery can

provide evidence of environmental subsidence that can affect the upper-level flow regimes

during pre-genesis. Additionally, the intensity of convective clusters can be tracked using IR

brightness temperatures. VIS imagery at 1km resolution allows tracking of even smaller

scale features such as arc clouds and overshooting tops that give insight into the convective

health of individual disturbances. The imagery can also be used to underlay the diagnostic

fields to better conceptualize and understand the various relationships being examined in

this study.

3. Results

3.1 Multi-Storm Analysis

3.1.1 Composite Analyses

The composite analyses (21x21 degree disturbance-centered boxes from the CIMSS Lagrangian wind analyses) of upper-level divergence were broken into three categories: the 36-hours previous to genesis, non-developing systems, and already-developed systems. In terms of the number of analyses contributing to each category, the most represented category is the non-developed systems, representing 60% of pouch observations in our sample. Correspondingly, the 36-hours-before genesis category constitutes 15% of the dataset, leaving 25% to be represented by TCs in the already-developed category. Thirteen of the 35 systems achieved TD or greater intensity in this dataset, representing 37.1% of pouches from the 20th of June to September 30th. Systems ceased to be followed upon hurricane declaration; therefore 'already-developed' systems represent entirely TD or TS systems, although some continued on to hurricane intensity, while others subsequently made landfall and weakened or weakened due to other adverse conditions

Composite divergence analyses for the full dataset and the 3 categories were created for the primary levels: 150hPa (Figure 13), 200hPa (Figure 14), 250hPa (Figure 15), 300hPa (Figure 16). Composite Lagrangian wind fields are also included in these figures. Fig. 13 shows that at 150hPa, the magnitude of divergence for developing systems is significantly greater than non-developing systems, especially over the interior 2 degrees.

The divergence patterns are similar in all four panels, which are found only at the 150hPa

level.
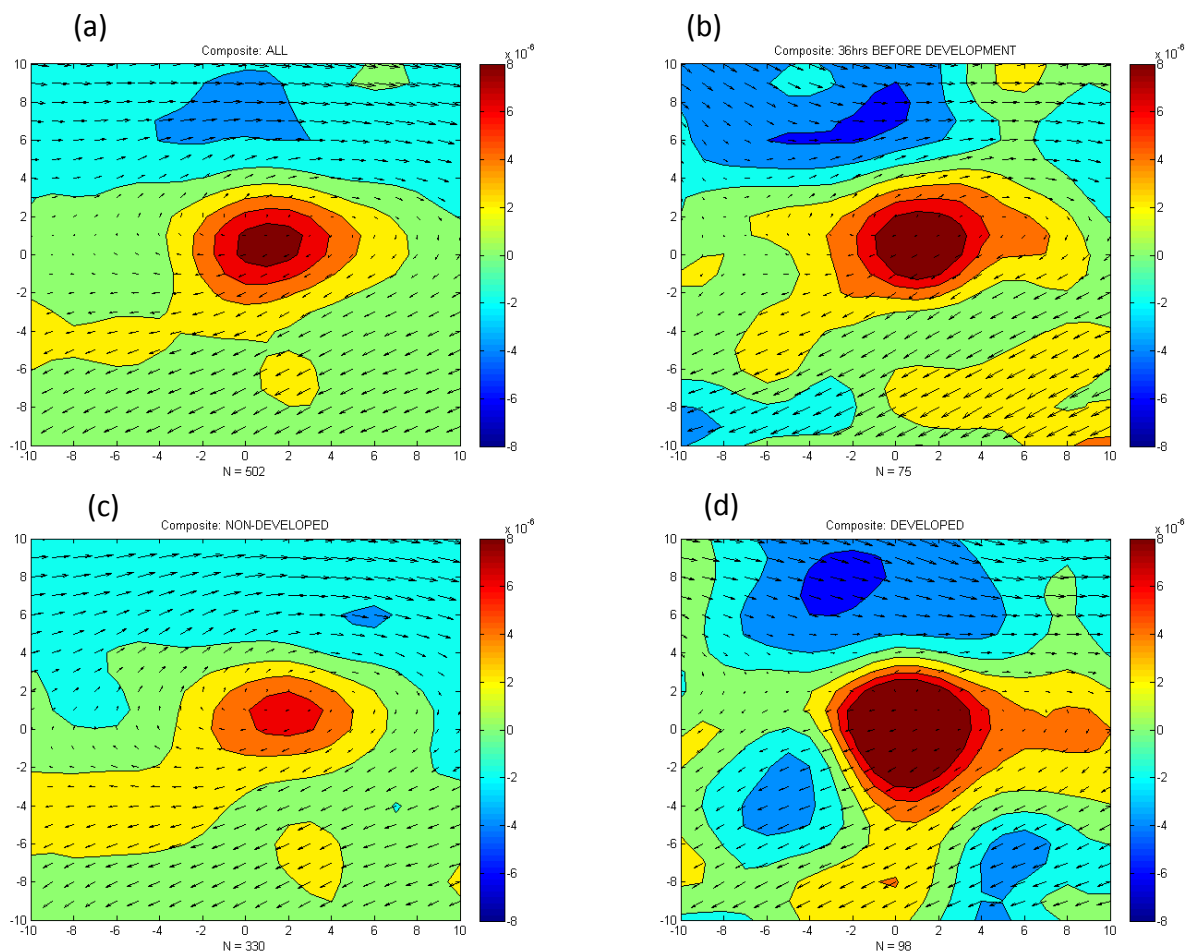
Figure 13. Composite divergence[s^{-1}] (fill) and gridded satellite wind vectors at 150hPa for (a) all grids, (b) the 36 hours before TCG, (c) non-developing systems , and (d) developed (TD and stronger) pouch classifications. Warm colors denote higher divergence.

The 200hPa composites (Fig. 14) are quite revealing. The developing cases show a

swath of strong divergence in excess of 8x10^{-6} s^{-1} from the southwest to the northeast

quadrants, a feature only weakly present in non-developing cases in the southwest

quadrant. ***The accompanying wind fields suggest these divergence "arms" represent outflow channels to the environment, which is a critical piece of information in support of our hypotheses.*** Developing cases also have an elevated divergence maximum near the center relative to the non-developers, similar to the pattern at 150hPa.
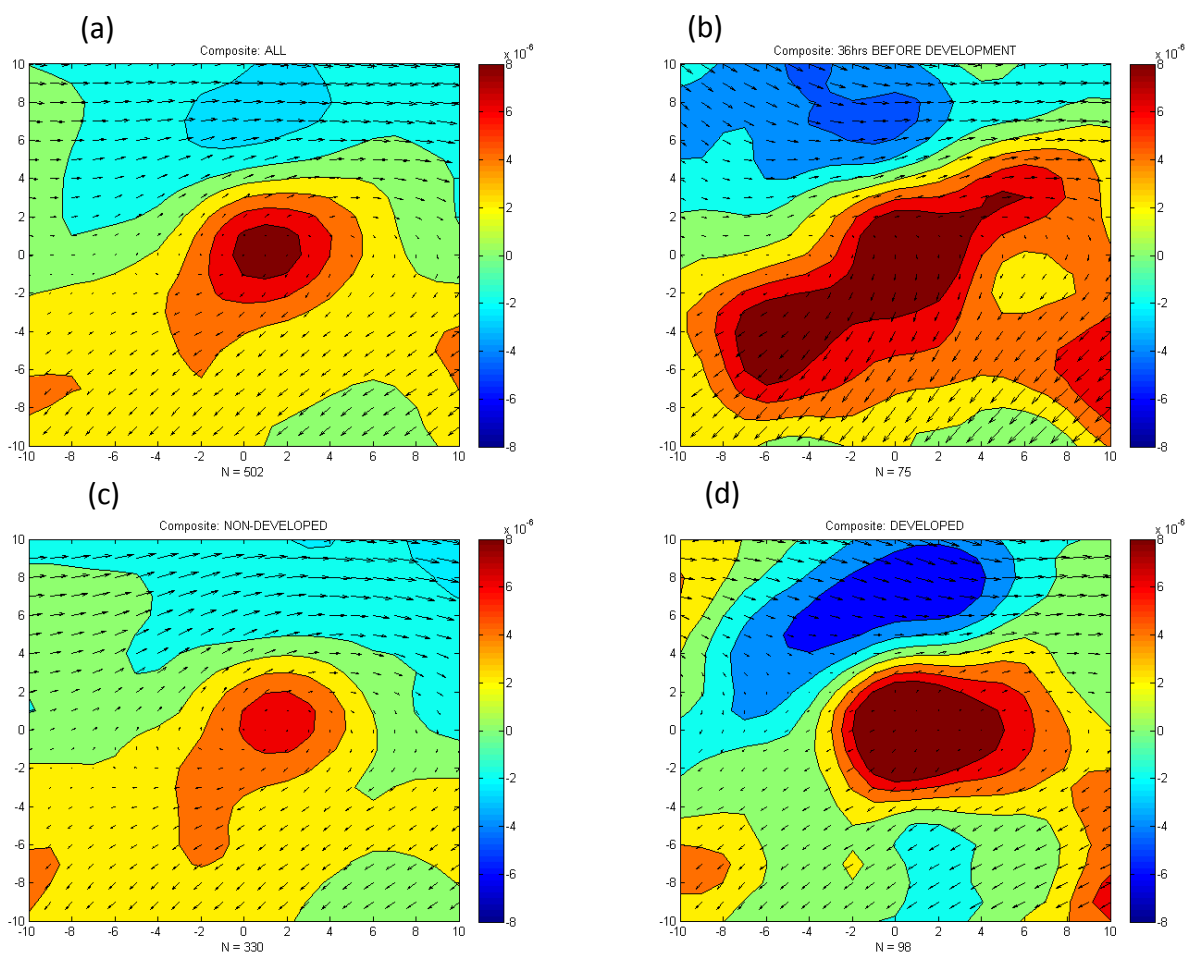
Figure 14. Composite divergence[s^{-1}] (fill) and gridded satellite wind vectors at 200hPa for (a) all grids, (b) the 36 hours before genesis, (c) non-developing systems , and (d) developed (TD and stronger) pouch classifications. Warm colors denote higher divergence.

The divergence analyses at 250hPa (Fig. 15) show a much broader pattern over the entire southern hemisphere for all categories, although the developing group has a much higher magnitude than the non-developing systems. This is also true at 300hPa (Fig, 16) where the signature at the center for non-developers is absent. In addition, the divergence and wind signals for developing and developed groups in these lower levels is an indication of much deeper outflow than is present for non-developed systems.

(a) (b)

(c) (d)
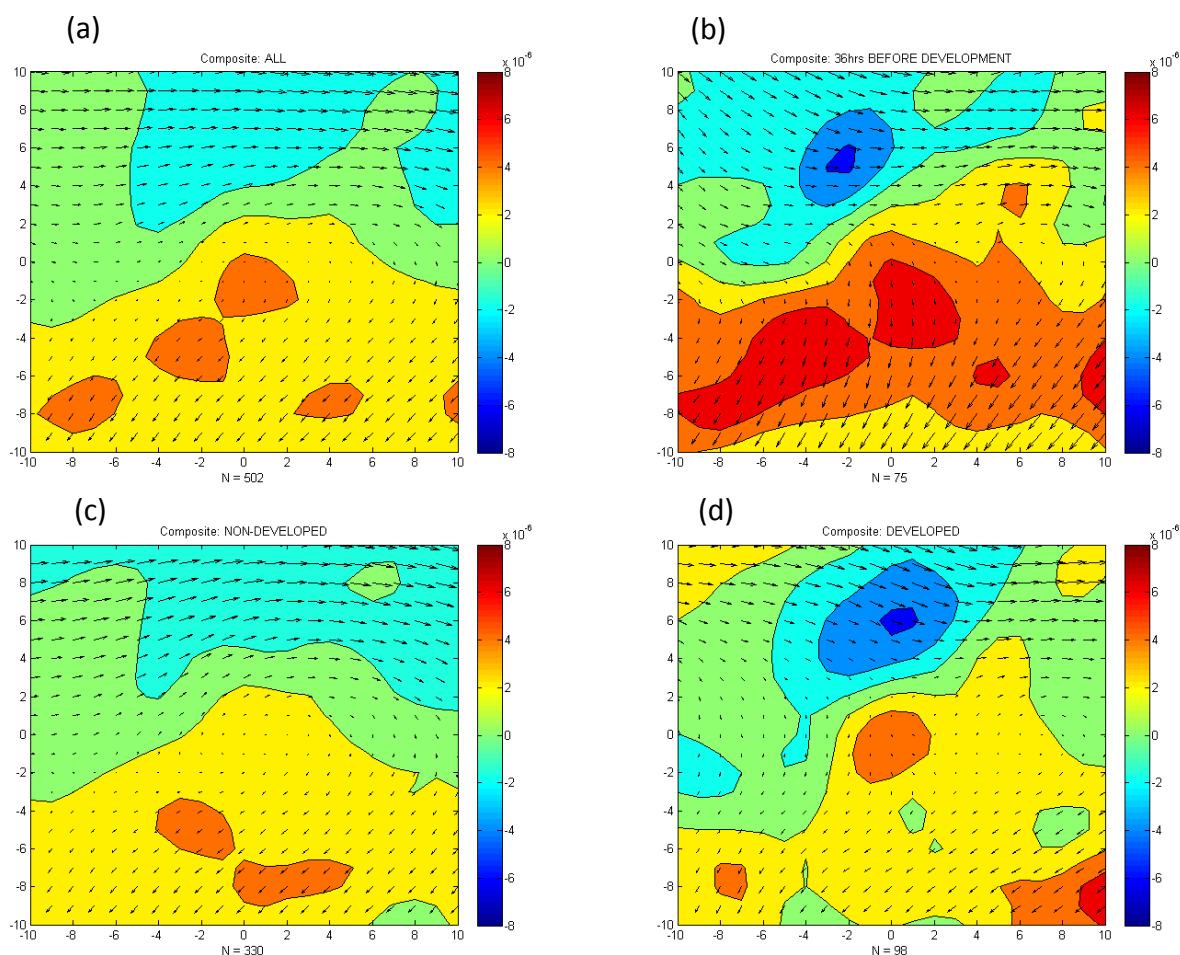
Figure 15. Composite divergence[s^{-1}] (fill) and gridded satellite wind vectors at 250hPa for (a) all grids, (b) the 36 hours before genesis, (c) non-developing systems , and (d) developed (TD and stronger) pouch classifications. Warm colors denote higher divergence.
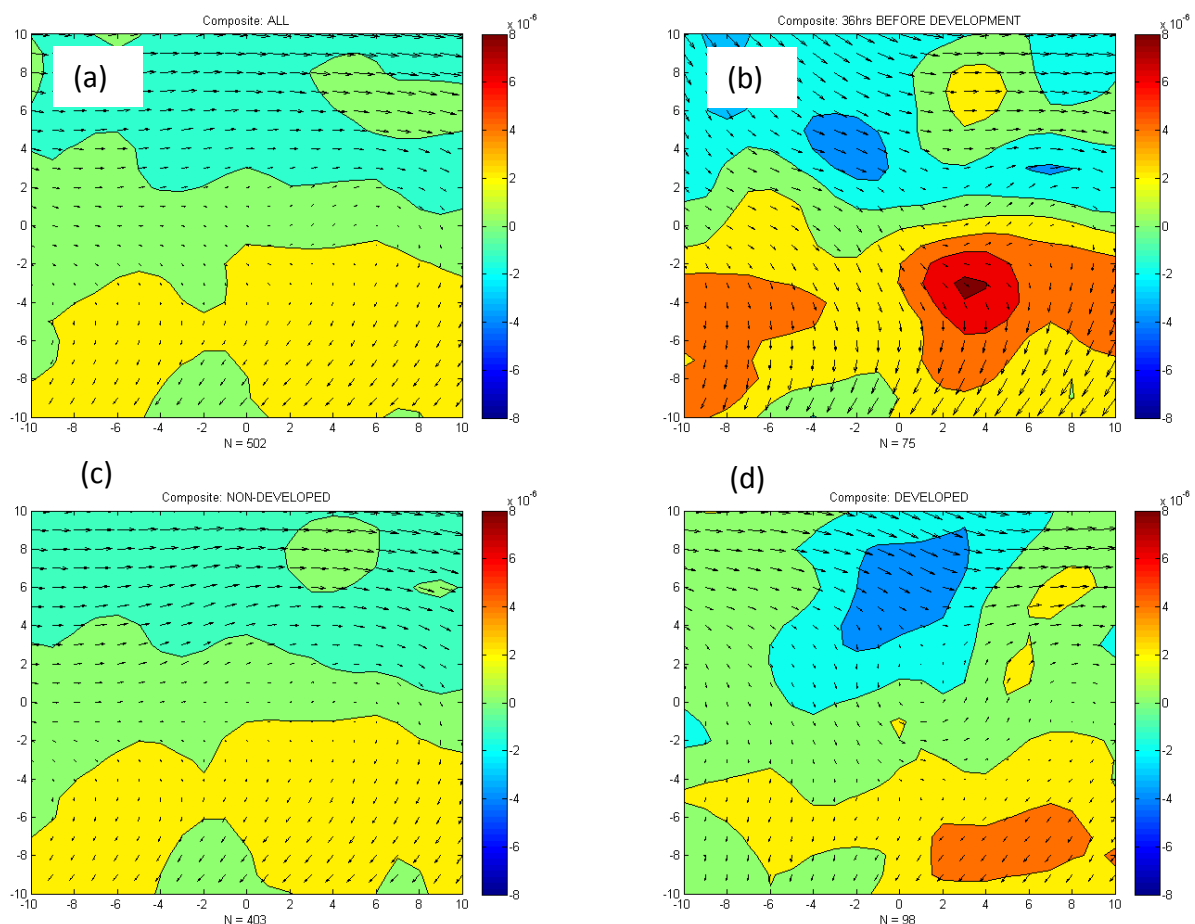
Figure 16. Composite divergence[s^{-1}] (fill) and gridded satellite wind vectors at 150hPa for (a) all grids, (b) the 36 hours before genesis, (c) non-developing systems , and (d) developed (TD and stronger) pouch classifications. Warm colors denote higher divergence.

Composite analyses of IAKE (Figure 17 and 18a) and potential vorticity (Figure 17 and 18b) on isentropic surfaces are radially averaged and presented in x-sections to view the vertical structure. The highest IAKE values are present in the inner radii where convection is the most robust and transition to horizontal outflow is critical for the secondary circulation to develop. Differences between developing and non-developing systems occur in the inner radii below 345K, which is typically at or below 250hPa for this

period, consistent with the horizontal composites shown earlier indicating increased divergence with the developing group at and below 250hPa.

The IAKE composite plots are very consistent and along the lines of what the theory predict (MT 98). First, the IAKE for developing events is much lower and over a deeper layer (300-375 K) versus being higher and over a shallow layer. This suggests that the PV is lower over developing systems (supported by Fig. 18b), and the low IAKE implies an ease for horizontal outflow in these low PV environments. The IAKE difference (Fig. 18a) being negative, again shows that values are smaller for developing cases, which is favorable for outflow. The deep layer over which these low/negative differences exist strongly points to the outflow being deeper and more structured for developing events.
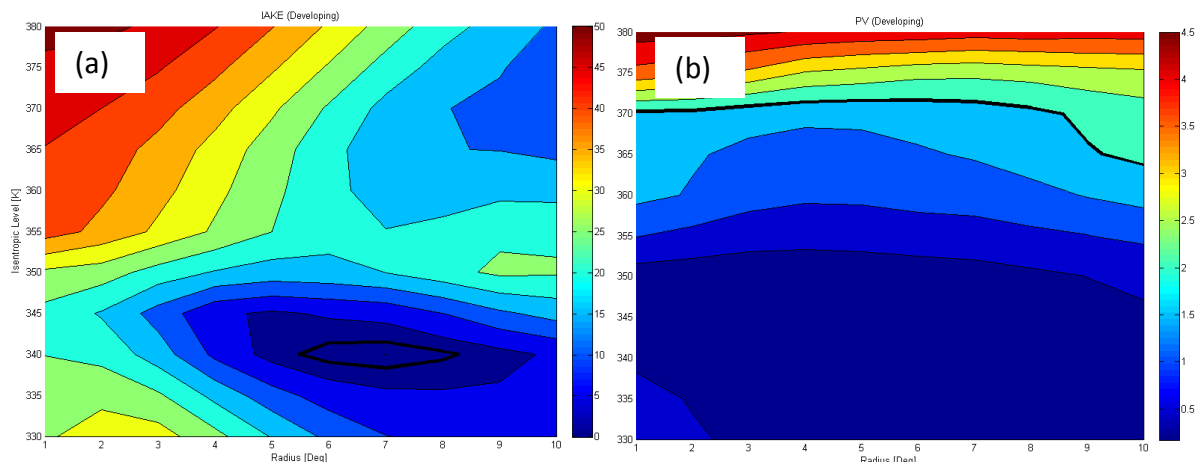
Figure 17. Developing (36 hours before TCG) radially averaged x-section for (a) IAKE [m^2/s^2] and (b) Potential Vorticity [PVUs]
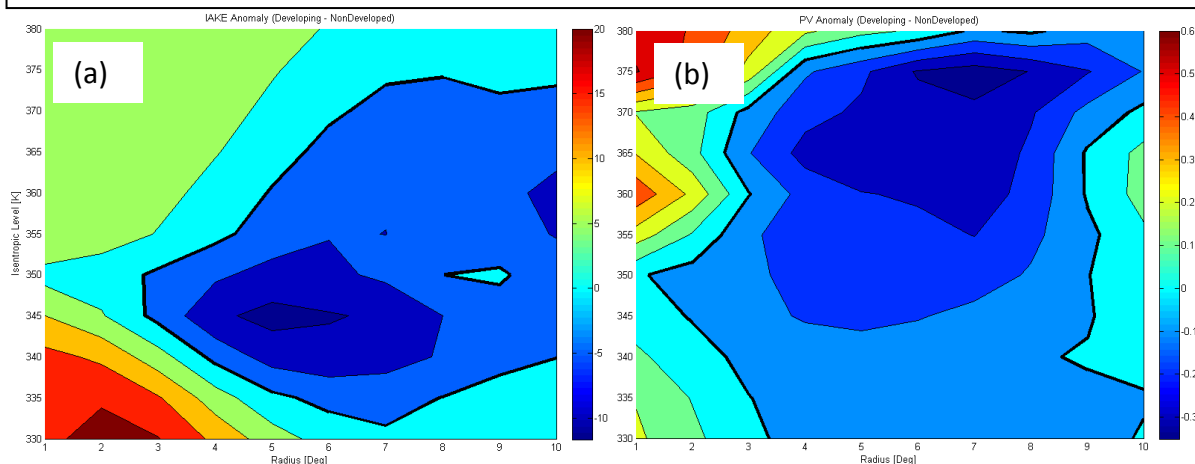
Figure 18. Difference between developing (36 hours before TCG) and non-developing radially averaged x-section for (a) IAKE [m^2/s^2] and (b) Potential Vorticity [PVUs]

Confounding the results of this radially averaged analysis is the work by Merrill and

Velden (1996) that showed outflow can occur at different levels depending on the sectors of

the storm in which outflow is taking place (i.e. poleward vs. equatorward). A dominant

region of outflow, but occurring at different levels, could be washed out in composite

analyses (especially constant-pressure analyses). Therefore, composite analysis x-sections

are also examined to account for this potential variability.

The composite analyses are sectioned into quadrants to isolate key regions of outflow channeling or ducting. While some quadrants feature negative or weakly positive upper-level mass flux in the 60 hours before genesis, the strongest signal occurs in the northeast sector. This clearly preferential region for horizontal mass flux occurs in nearly every system investigated. Understanding the attributes of this region and the conditions for the setup are important to understanding the influence of upper-level conditions on TC genesis.

Figure 19 shows a time vs. height x-section of radially-averaged (at 10 degree radius) horizontal mass flux relative to the time of genesis, for the northeast sector of the composite analysis (developing sample). Fig. 19 indicates an increase in outward mass flux starting around 40 hours before development and reaching a maximum 6-10 hours after genesis. This signature is consistent with the development of an outflow channel in the northeast sector of the composite, and a feature observed in several cases during the PREDICT experiment.
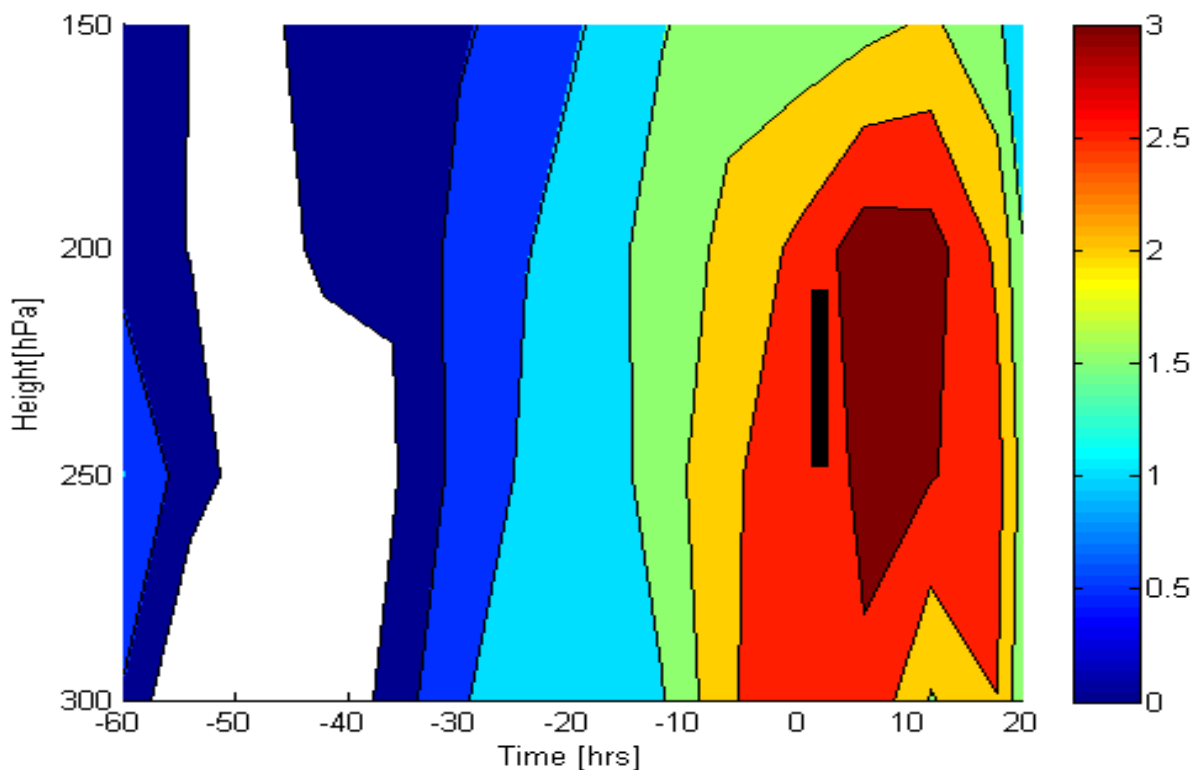
Figure 19. Time-section composite of upper-level radially-averaged (northeast quadrant) horizontal mass flux [s^{-1} x10^{-6}] in developing cases. Time 0 = genesis time, and negative time values indicate pre-genesis.

In summary, the upper-level composite analyses highlight several key differences between developing and non-developing systems. Elevated divergence values at several levels concurrent with IAKE and low PV found in the developing (pre-genesis) sample are all characteristics of enhanced outflow, which is also supported by the mass flux analyses. Spatially, the enhanced divergence in the northeast corridor fits with the establishment of an outflow channel in this sector, which was observed in several of the developing pouches. This is further supported in the increase of northeast sector's outward mass flux as genesis time is approached.

3.1.2 Empirical Orthogonal Functions (EOF) Analyses

EOF analysis is valuable in identifying dominant modes of variability in a dataset. The

first two EOFs (two modes that explain the most variability) for the composite IAKE

evaluated at 365K are shown in Figure 20. The first two EOFs explain 56% of the variability

in the dataset. The first explains 38% of the variability and the structure is similar to the

developing sample composite analysis of divergence at 150hPa, with a bull's-eye near the

storm center where convective activity is most rigorous, and extended structure in the

northeast and southwest quadrants that favor the establishment of accelerated outflow in

those directions. The second EOF, explaining 18% of the variance, is positive equatorward of

the composite center and negative poleward of the composite center, similar to the 250hPa

divergence composites. Higher IAKE is present at warmer isentropic surfaces in the inner 3

degrees (Figure17A), therefore the core accesses higher IAKE as outflow moves to higher

pressure surfaces and this is reflected in the elevated IAKE at 365K of the first EOF.
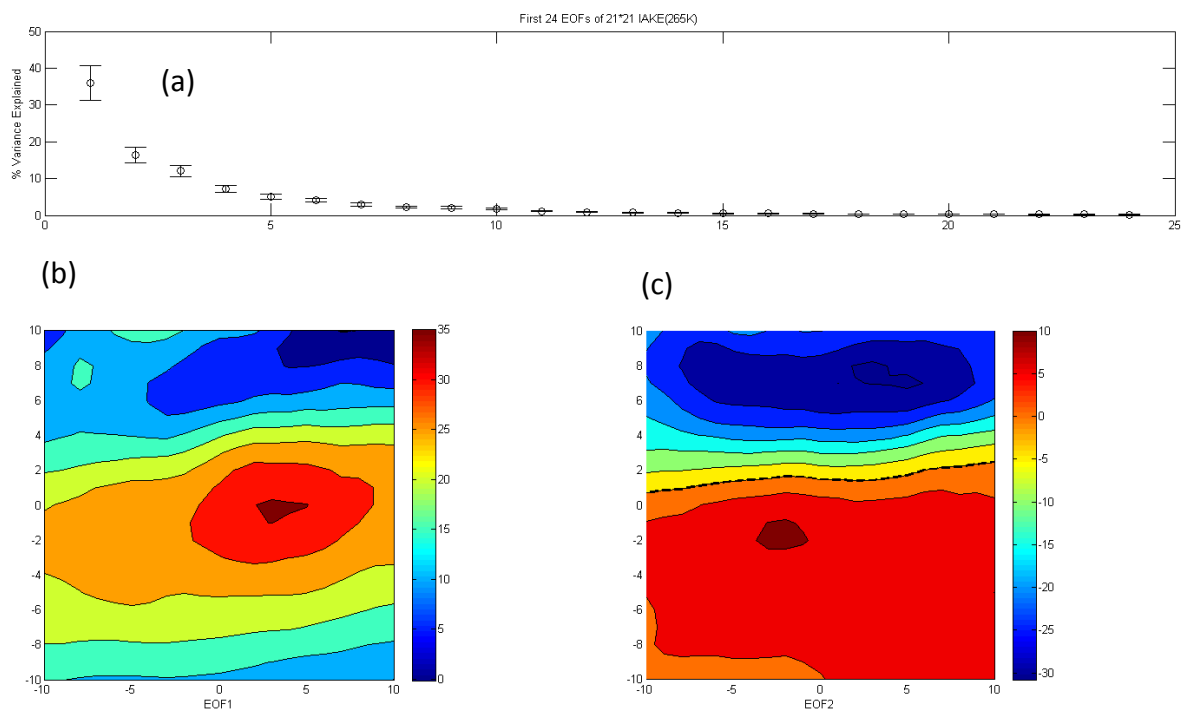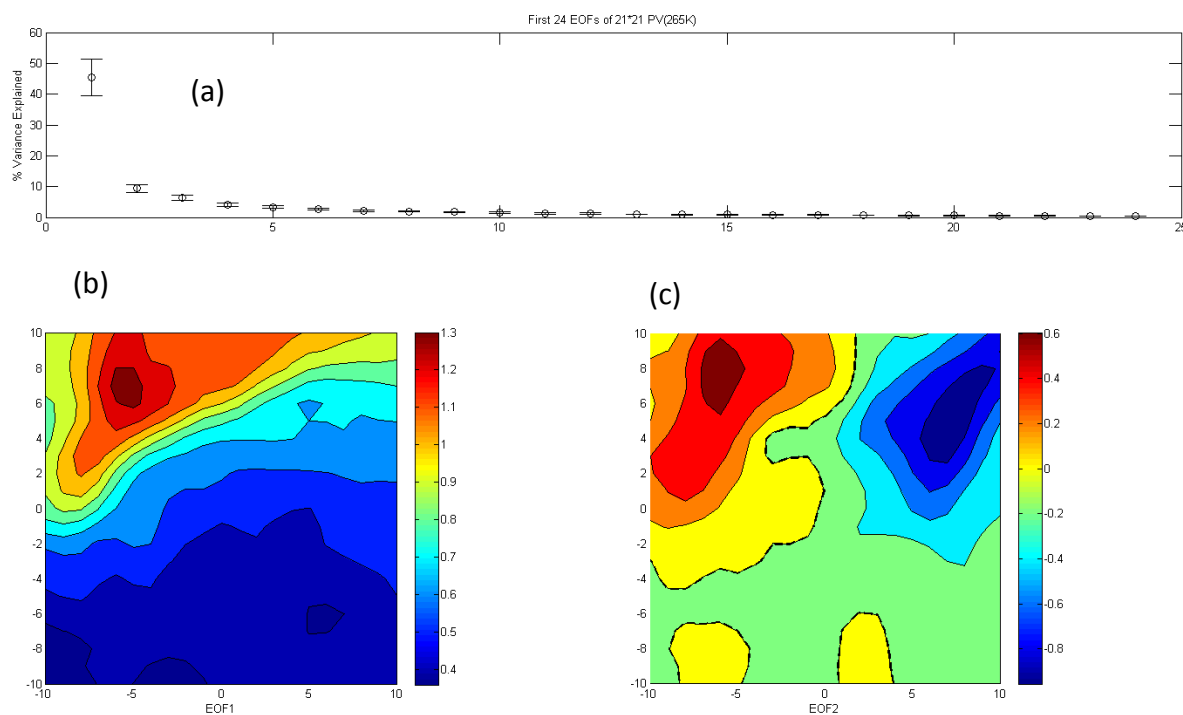
Figure 20. (a) Breakdown of variance explained by the first 24 EOFs of IAKE with bars of uncertainty derived by North's Rule of Thumb. (b) Structure of the first EOF of IAKE. (c) Structure of the second EOF of IAKE.

The first two EOFs of the potential vorticity field at 365K (figure 21) represent 55% of the variability of the PV dataset although the breakdown between the two is quite different. The first EOF represents 45% of the variability, while the second explains only 10%. The structure of the first EOF greatly resembles an upstream upper-level trough, which features a cyclonic turning of the winds around the area of high PV, leading the upper level winds over the developing sample composite center to turn from easterlies to southwesterlies, thereby increasing mass flux in the northeast quadrant noted earlier. The second EOF represents a sharpening of the pattern of EOF 1, turning the southwesterlies to a more southerly flow. Together, these patterns suggest that the preferential shape to the outflow

of waves during pre-genesis begins to take on a shape often seen in mature tropical

cyclones.

Figure 21. (a) Breakdown of variance explained by the first 24 EOFs of PV with bars of uncertainty derived by North's Rule of Thumb. (b) Structure of the first EOF of PV. (c) Structure of the second EOF of PV.

3.1.3 Individual Storm Examples

During the PREDICT period, there are several good examples of organizing outflow

before genesis. Figure 22 shows pre-Earl's (PGI34L) upper-level wind structure 6 hours

before reaching tropical depression strength. The most common outflow pattern, with a

northeast sector outflow turning anticyclonically to the south and then east equatorward of

the center is the most common structure of outflow. Figure 23 shows a slightly elongated

extension of divergence north of the storm center and a secondary maximum to the south

as the outflow wraps around to the east and south of the pouch center. This robust outflow

developed over the course of the previous 36 hours beginning as a narrow divergence

extension to the north. The strength of this outflow channel may have contributed to the

rapid deepening to Tropical Storm strength 6 hours later on 12Z the 25th.
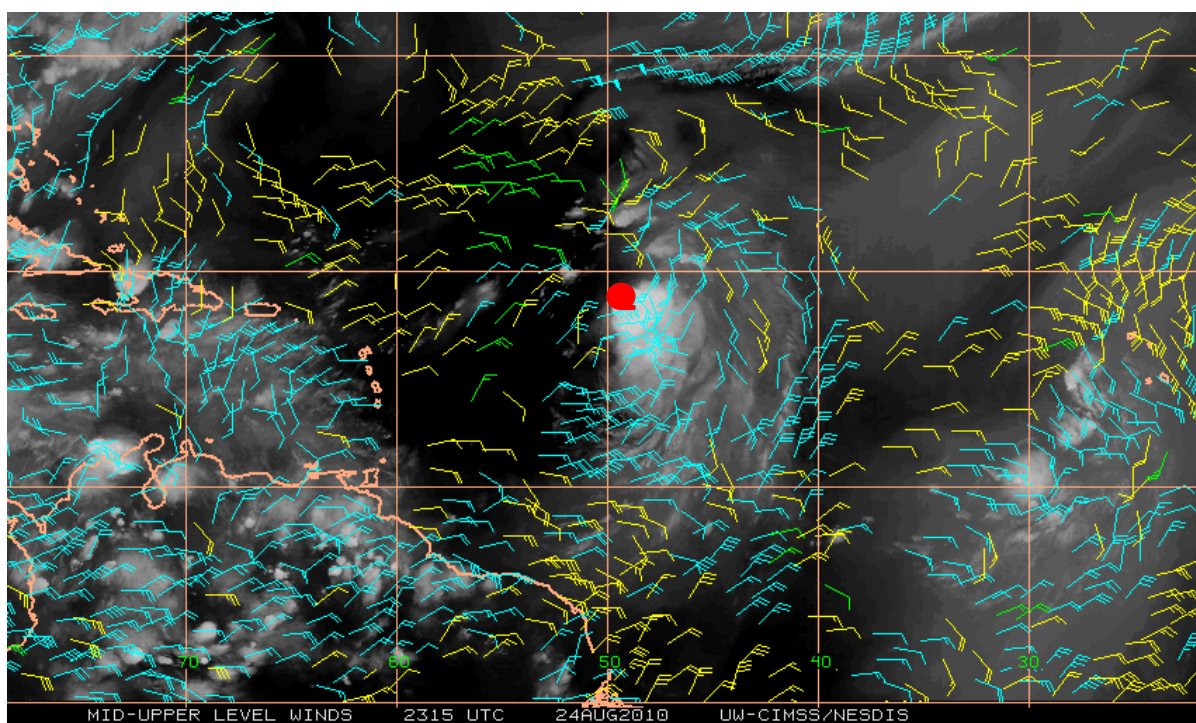
Figure 22. Raw CIMSS Satellite wind barbs for upper level winds [kts] above500hPa and IR for 6 hours before PGI34L (EARL) undergoes TCG.
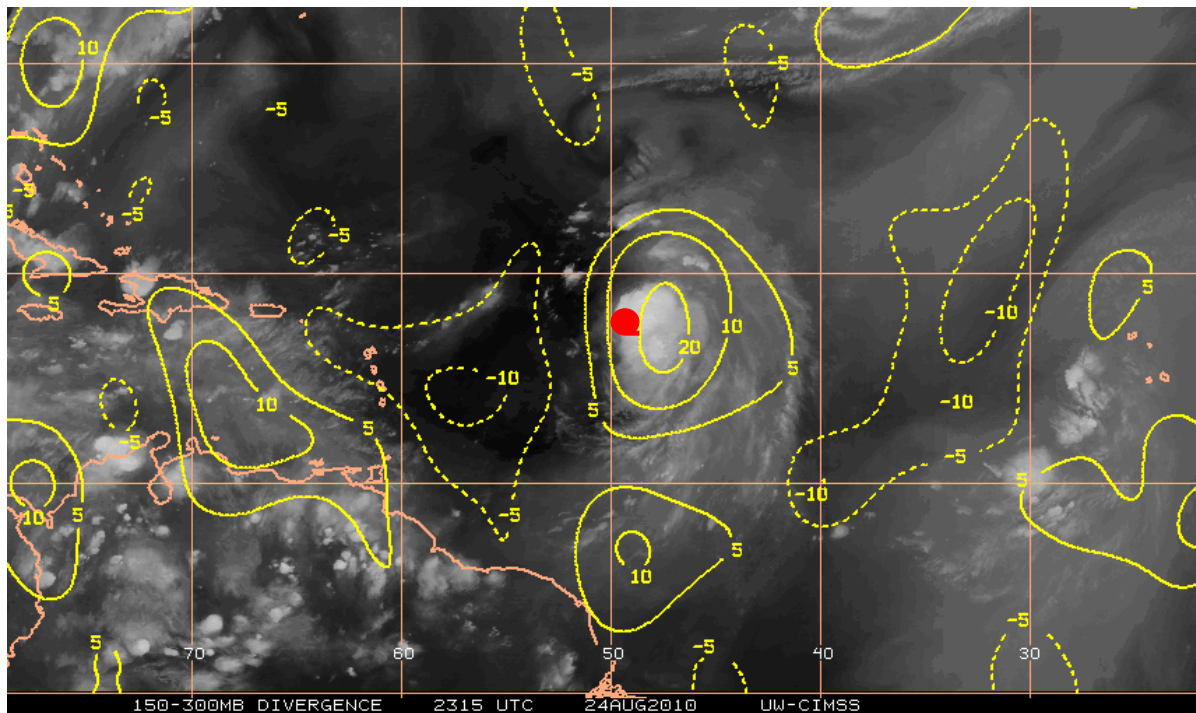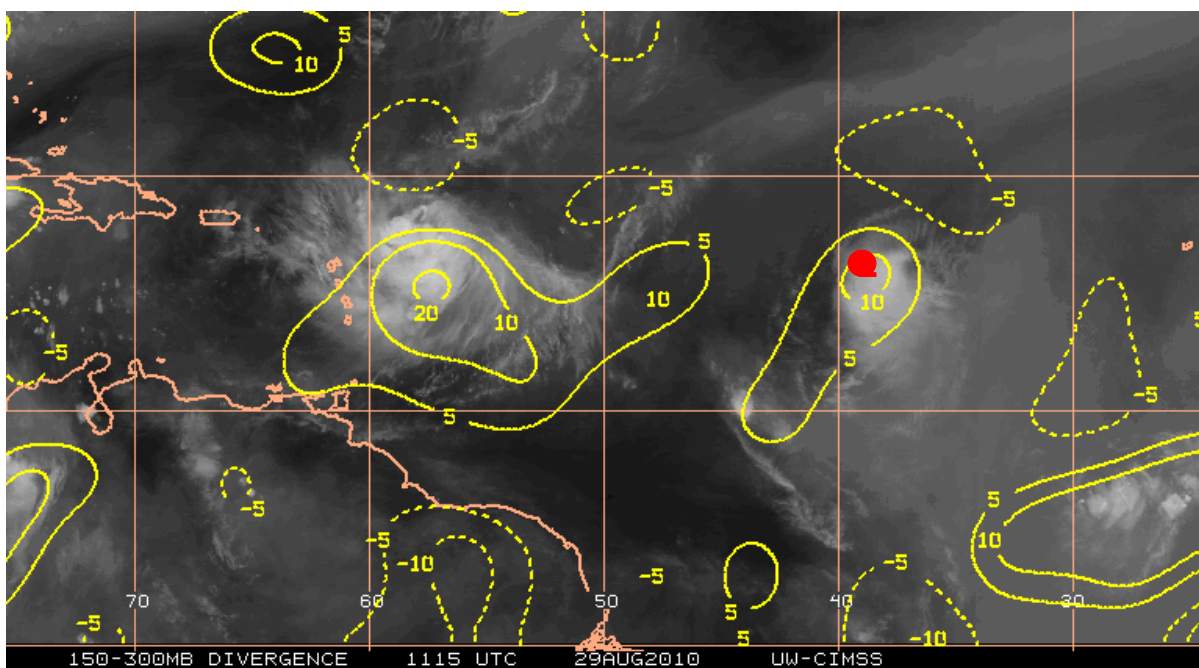
Figure 23. CIMSS Satellite grid derived divergence for upper level [s^{-1} x10^{-6}] above300hPa (contour) and WV imagery for 6 hours before PGI34L (EARL) undergoes TCG.

Pre-Fiona's (PGI36L) outflow pattern (Fig. 24) is establishing primarily to the southwest of the system 24 hours before genesis, and striving to link with the trough to the north as seen in the WV imagery and winds. An extension of divergence (Fig.25) verifies the existence of a narrow outflow channel bridging an upper-level moisture gap and preventing the entrainment into the inner core of the system. Future interaction with Earl, located 20 degrees to the west, prevents full development of a Fiona outflow channel to the west. As a consequence convergence develops in the space between storms halting the development of Fiona.
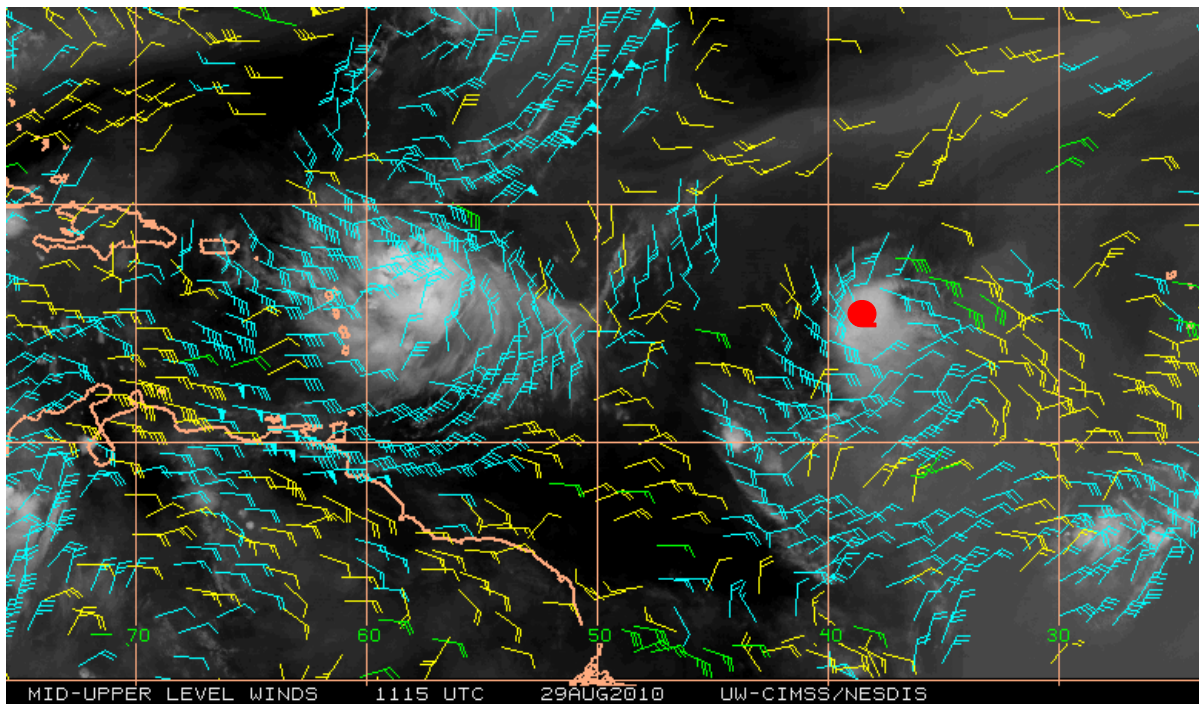
Figure 24. Raw CIMSS Satellite wind barbs for upper level winds [kts] above500hPa and IR for 24 hours before PGI36L (FIONA) undergoes TCG.
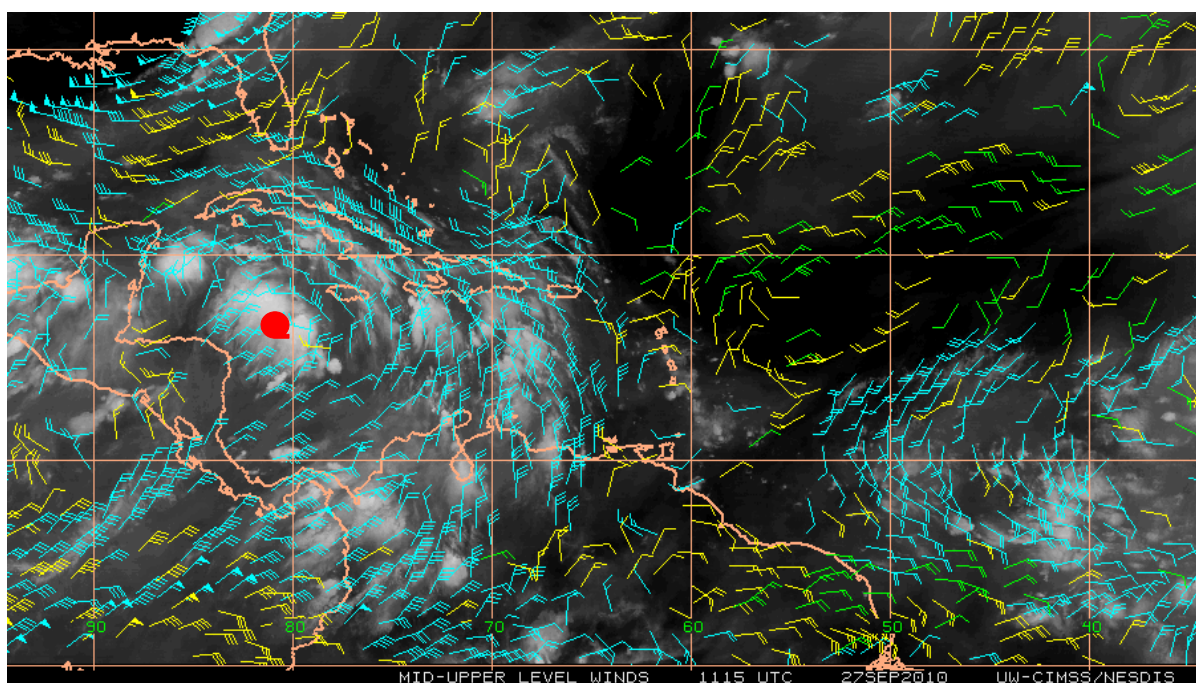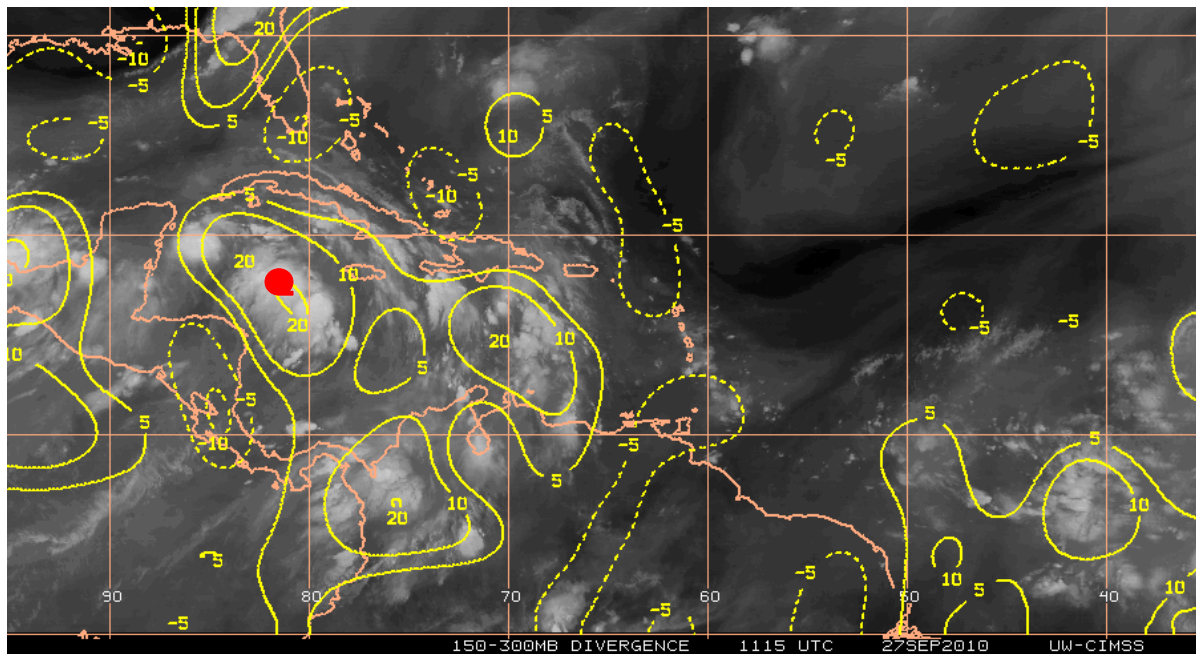

Figure 25. CIMSS Satellite grid derived divergence for upper level [s^{-1} x10^{-6}] above300hPa (contour) and WV imagery for 24 hours before PGI36L (FIONA) undergoes TCG.

Figure 26 shows an example of how the formation of outflow controls the outward mass flux of PGI36L (Fiona). While large upper-level horizontal mass flux values at the inner most radii can be associated with the strong core convection, fluxes of similar magnitudes at larger radii represent organized outflow under environmentally favorable conditions. After the 31st of August, the dominant anticyclonic upper-level flow from a fully formed nearby Hurricane Earl began to conflict with the outflow pattern of Fiona, suppressing further development. This confluence forced subsidence in the front quadrant of the storm path, resulting in entrainment of dry air into the storm core, preventing further deepening. The role of the dry air entrainment will be discussed in a following section.
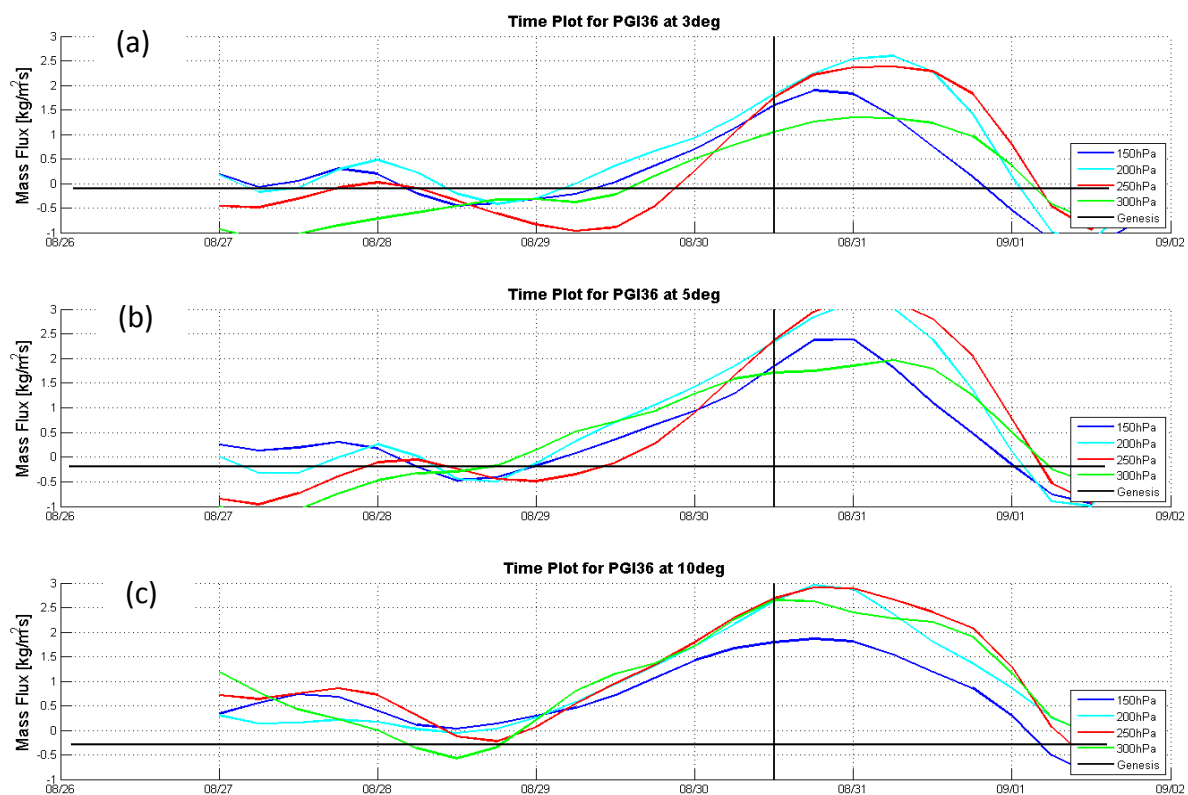
Figure 26. 300, 250, 200 and 150hPa mass flux profile [kg/m²s] time series for PGI36L (FIONA) evaluated at (a) 3degrees, (b) 5 degrees and (c) 10 degrees.

Nicole (PGI 51L) has strongly divergent outflow to the northeast ahead of an upper-trough in the Gulf of Mexico, and also open to the south and southwest. This allowed the storm to develop quickly even after recently emerging from land. While ample outflow existed, the large collection of convective activity in the region prevented the organization of a singular outflow channel necessary to sustain Nicole (Fig. 27). While the storm eventually reached TS intensity with favorable low-level pouch conditions, the lack of organized outflow channels inhibited further significant deepening (Fig. 28).

Figure 27. Raw CIMSS Satellite wind barbs for upper level winds [kts] above500hPa and IR for 24 hours before PGI50L (NICOLE) undergoes TCG.

Figure 28. CIMSS satellite grid derived divergence for upper level [s^{-1} x10^{-6}] above300hPa (contour) and WV imagery for 24 hours before PGI50L (NICOLE) undergoes TCG.

In contrast to the cases that underwent TCG, PGI39L initially looked likely to develop, with favorable low level conditions imbedded in an easterly wave and appearing safe from surface level dry air intrusion. However, convergence in the upper levels to the north, west and south impedes the establishment of an organized upper level outflow channel even while the model forecast had the highest likelihood for genesis (Fig. 29). Without sufficient mass flux to maintain the convection, the system's convection continued to pulsate for the entire lifetime of the pouch. In addition, subsidence-based dry air to the north driven by convergence is directly adjacent to the storm core. The effect this could have on convection is discussed in the following section.
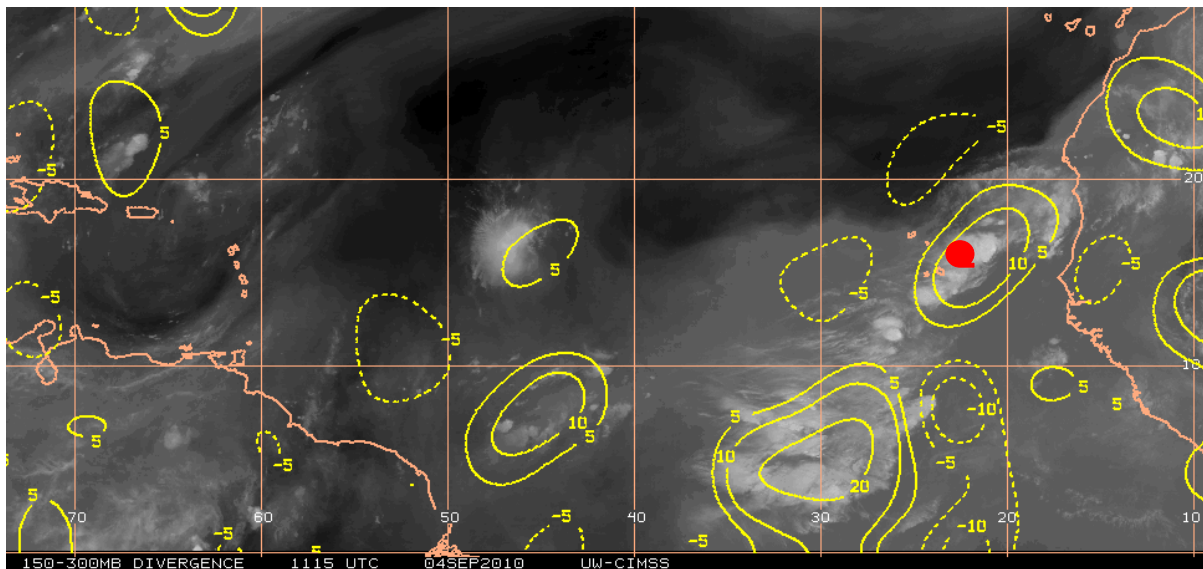
Figure 29. CIMSS satellite grid derived divergence for upper level [s^{-1}x10^{-6}] above300hPa (contour) and WV imagery PGI39L.

3.1.4 Multi-Storm Summary

There are several distinct upper-level differences between developing and non-developing Atlantic wave-type systems that feature robust enough signals to be quantified in composite analysis. Elevated divergence values and depressed inertial stability are the most identifiable features of the upper levels of developing systems. There is also sufficient evidence that organized upper-level mass evacuation from the storm core is an important regulator of Atlantic wave TC genesis. This manifests in organized outflow patterns in developing systems that's distinguishable by 24-48 hours before genesis. Supporting the composite analyses, most developing storms form the PREDICT field experiment feature some combination of northeast and/or southwest outflow. Non-developing systems often lack this organized outflow, although the influence of other environmental inhibiting factors makes it difficult to isolate the lack of outflow as the primary cause for failed genesis.

3.2 Enhanced Divergence Aloft: Is it Just the Response to Convection?

A key differentiator between a convectively active African Easterly Wave (AEW) and a tropical cyclone is the establishment of sustained deep convection rather than the diurnally pulsating convection that is often the dominant mode of AEWs. To show this, a power spectrum of convective activity during the large multi-pouch sample was produced. Figure 30 indicates a peak well in excess of the 95% confidence level of a representative first-order autoregressive process (Wilks, 2006) at just under 1 cycle per day for average IR brightness temperatures (BT) within a three degree circle around the pouch center. This diurnally-associated signature is typical for AEWs as they propagate westward following the solar cycle. A good example is presented in Figure 31, where the diurnal pattern of PGI44 is evident in an IR BT Index until genesis at 12z on the 14th September. Another example of the suspension of the diurnal variation occurs while Gaston is declared a TD from 00z September first to 00z September second (Figure 32).
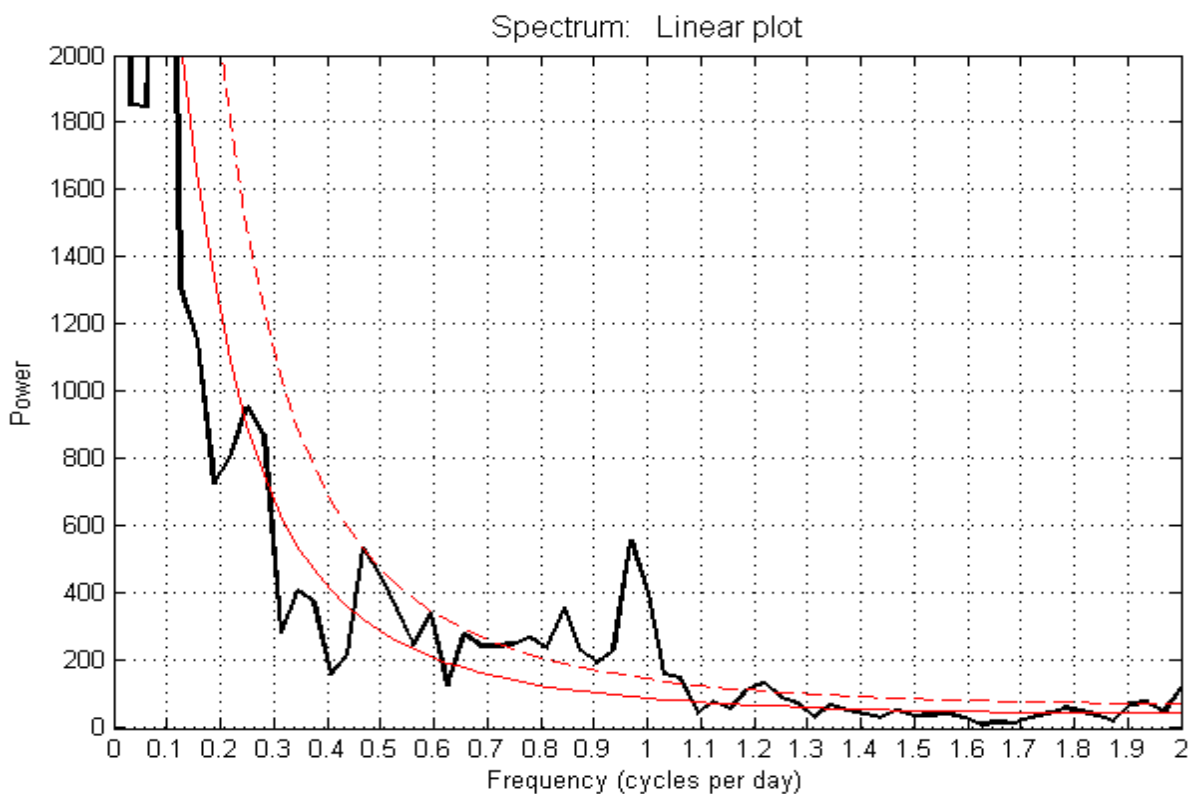
Figure 30. Power spectrum analysis of average IR index in 3 degree circle. AR(1) process is shown by a red Line. With 95% confidence level given by dotted red line.
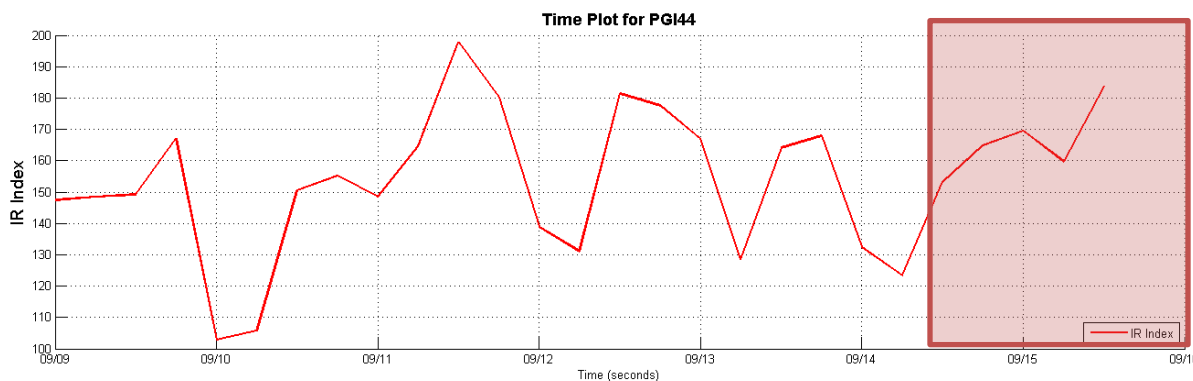

Figure 31. Average IR index in 3 degree radius circle for PGI44L (Karl), where high convective active are indicated by high values.
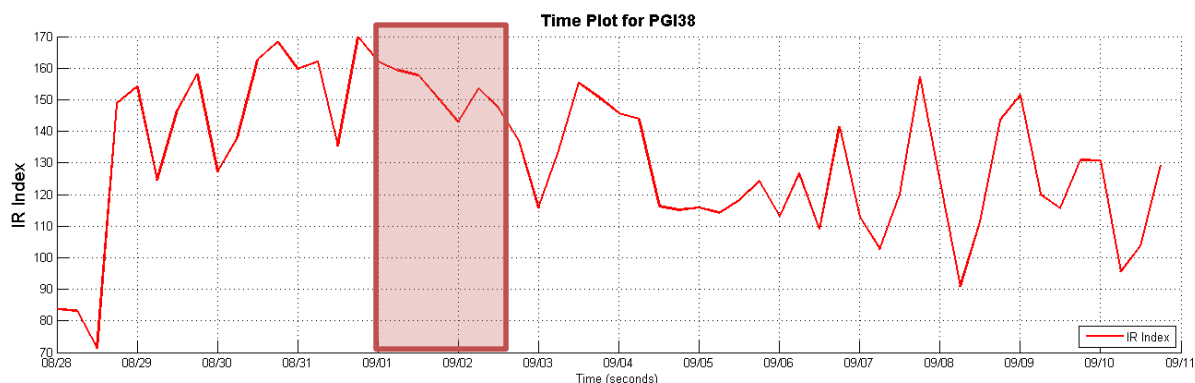
Figure 32. Average IR index in 3 degree radius circle for PGI38L (Gaston), where high convective active are indicated by high values.

Understanding the complex relationship of the ambient upper level environment and organizing tropical disturbance convective activity is difficult since upper-level divergence is naturally driven by the convection itself, although weak inertial instability may have a role in its horizontal extent. Using mainly satellite-based tools and analyses, can we distinguish a pre-existing favorable upper-level divergent environment from the convective influences? For example, a time lag analysis of from the entire dataset of 200hPa horizontal mass flux though a three degree ring correlated with inner core averaged convective activity shows increased convective activity and increased mass flux occur simultaneously (Fig. 33). However, the correlation with the flux at ten degrees radius from the center shows a very different response when compared to inner-core convective activity. The outer mass flux signal leads the convection signal by 1-2 days for three of the four storms shown.
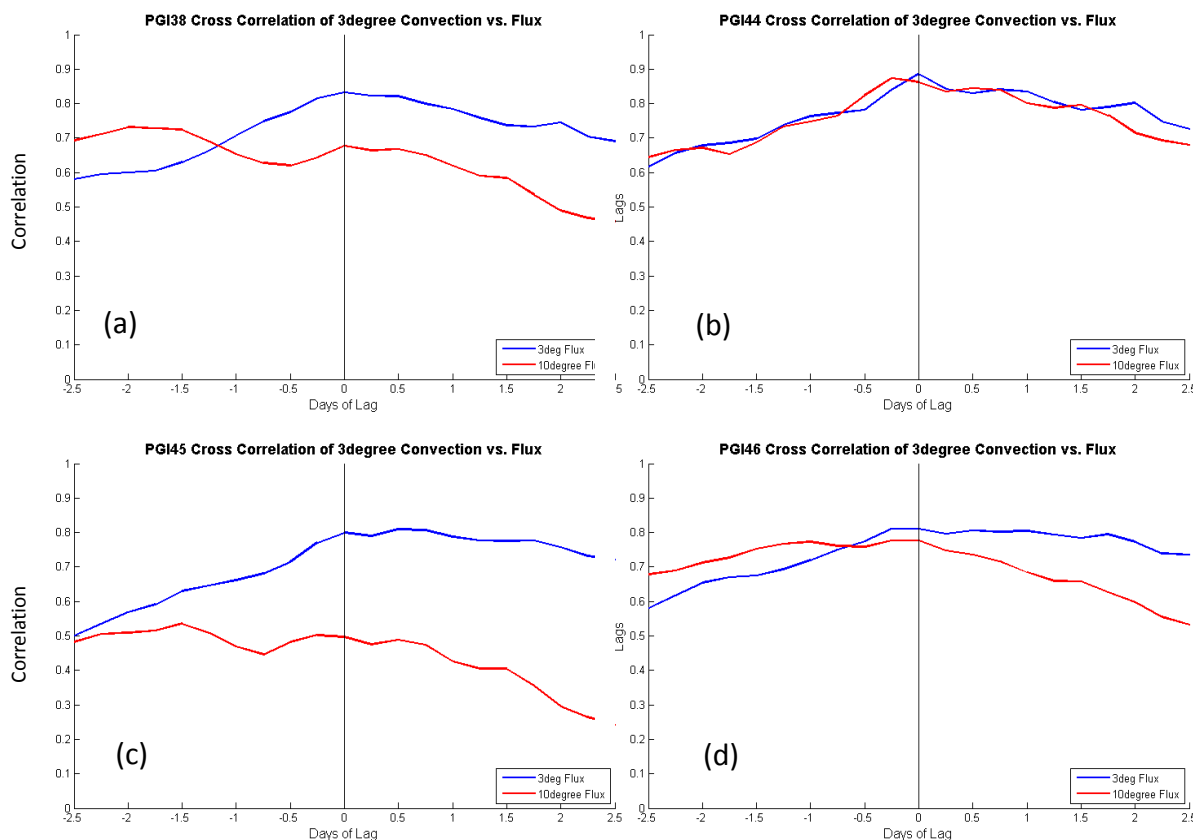
Figure 33. Cross correlation (lagged correlation between inner-core convection and 200hPa horizontal mass flux) for several pouches at two selected radii for (a) PGI38L (Gaston), (b) PGI44L (Karl), (c) PGI45L (Lisa) and (d) PGI46L (Matthew).

The significance of this 1-2 day upper-level mass flux precursor to inner core convection at 200hPa is explained by the establishment of divergent outflow independent of that associated with the convection. This is also indicated in a composite analysis of horizontal mass flux at 10 degree radius, relative to the time of genesis, for all 13 genesis cases (Fig. 34). The analysis shows a maximum at 200hPa from 40-18hrs before genesis, consistent with the signature present in the 10 degree time-lagged correlation plots.
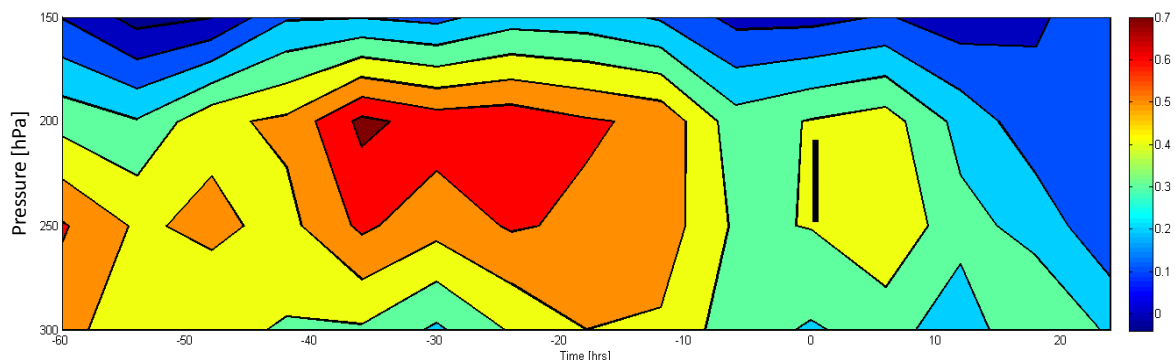
Figure 34. Composite analysis of radially averaged horizontal mass flux [kg/m²s] at 10 degree radius from storm center, relative to the time of genesis for the 13 genesis cases in our sample.

In the absence of favorable divergent upper-level environmental conditions that can support sufficient outward horizontal mass flux, such as the early lifetime of pre-Karl when diurnal pulsing was the dominant mode of convective activity, subsidence is in evidence in the region immediately outside of the inner core of convection. Subsidence is evident in a number of soundings from the near eastern perimeter of PRE-Karl on the 11th of September from a GV aircraft dropsonde (example in Figure 35). Moist lower levels with dry air above 500hPa and an inversion suggest a convectively-induced subsidence adjacent to the convection, which could easily be entrained into the convective circulation, enhancing the downdrafts, and disrupting the establishment of persistent inner core convection necessary to develop a warm core and lower surface pressures as well as stabilizing the atmosphere. This scenario is present in the early stages of pre-Karl, several days before genesis, even though lower-level pouch conditions were optimal.
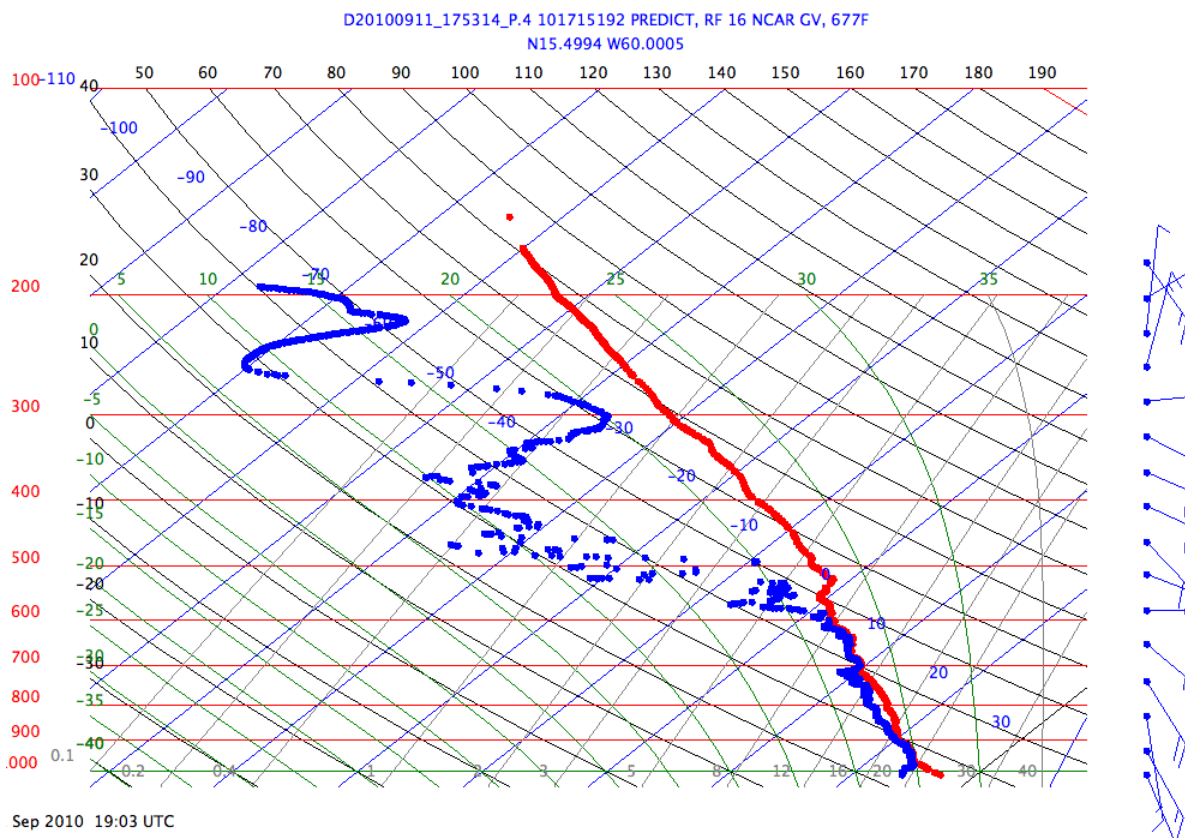
Figure 35. Dropsonde in northeast sector of pre-Karl.

By contrast, a sounding from the same region of the storm on the 14th of September,

2 hours after designation as a tropical storm, and under the outflow region of Karl, the

evidence of locally-enhanced subsidence is completely gone (Figure 36). The modulation of

the convection by the dry air induced by adjacent subsidence is absent, allowing sustained

convection to flourish, and organize into a mature tropical cyclone. The more robust and

sustained convection occurring in the less dilute vortical hot towers allows a more favorable

condition for the spin-up of the disturbance to occur in line with the pouch hypothesis.
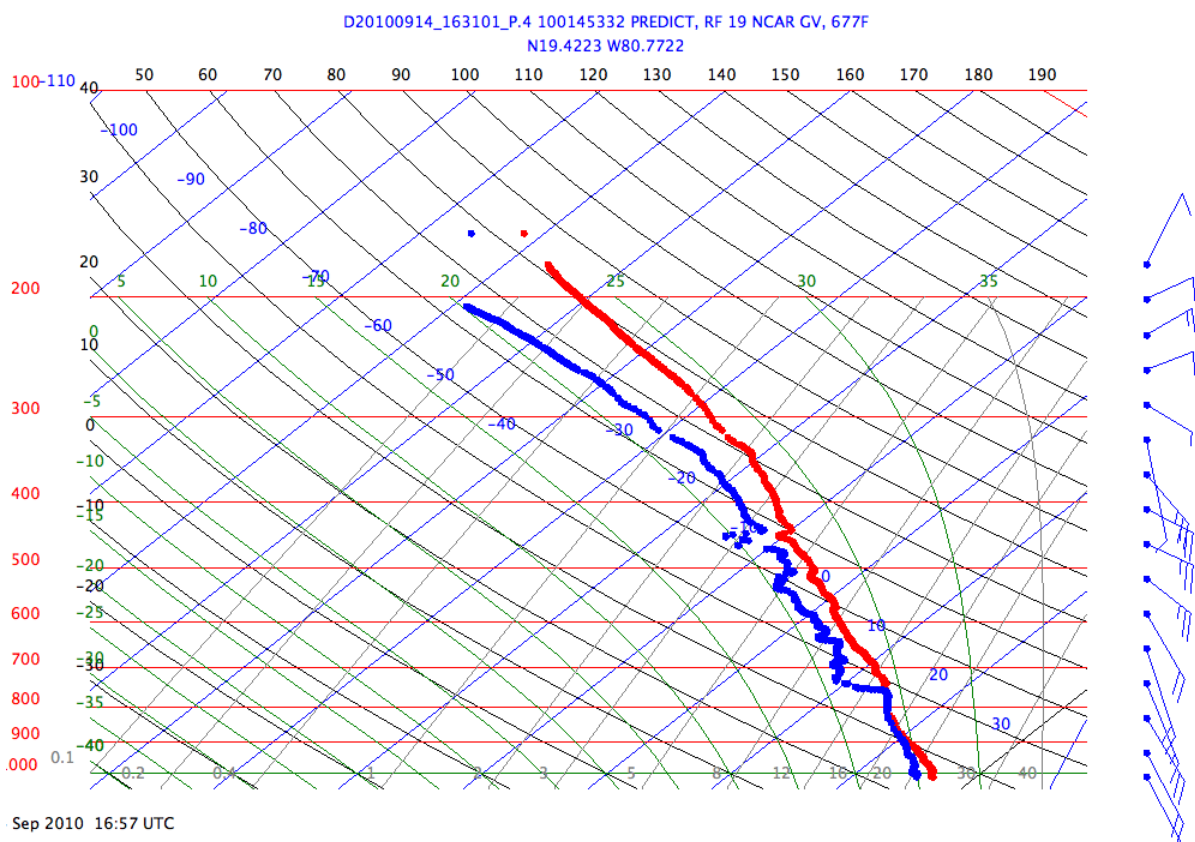
Figure 36. Dropsonde in northeast sector of Karl, 2 hours after being declared a tropical storm.

Of course, there are other sources of dry air above 700hPa, including the infusion of the Saharan Air Layer (SAL), which has been suggested to play a role in suppressing development in a number of storms (Dunion and Velden 2004). A good example from our study is PGI38L (Gaston). Gaston's convection was a great deal weaker than Karl's and the extent of the surrounding dry air is much more extreme (Figure 37). The suppression in convection is evident in IR trends, and suggests the SAL penetration into the core of the storm. Sources of dry air from locally-produced subsidence, and transient mid-latitude and SAL airmasses, were present in several of the non-developing systems during PREDICT, including especially PGIs 27L and 30L.
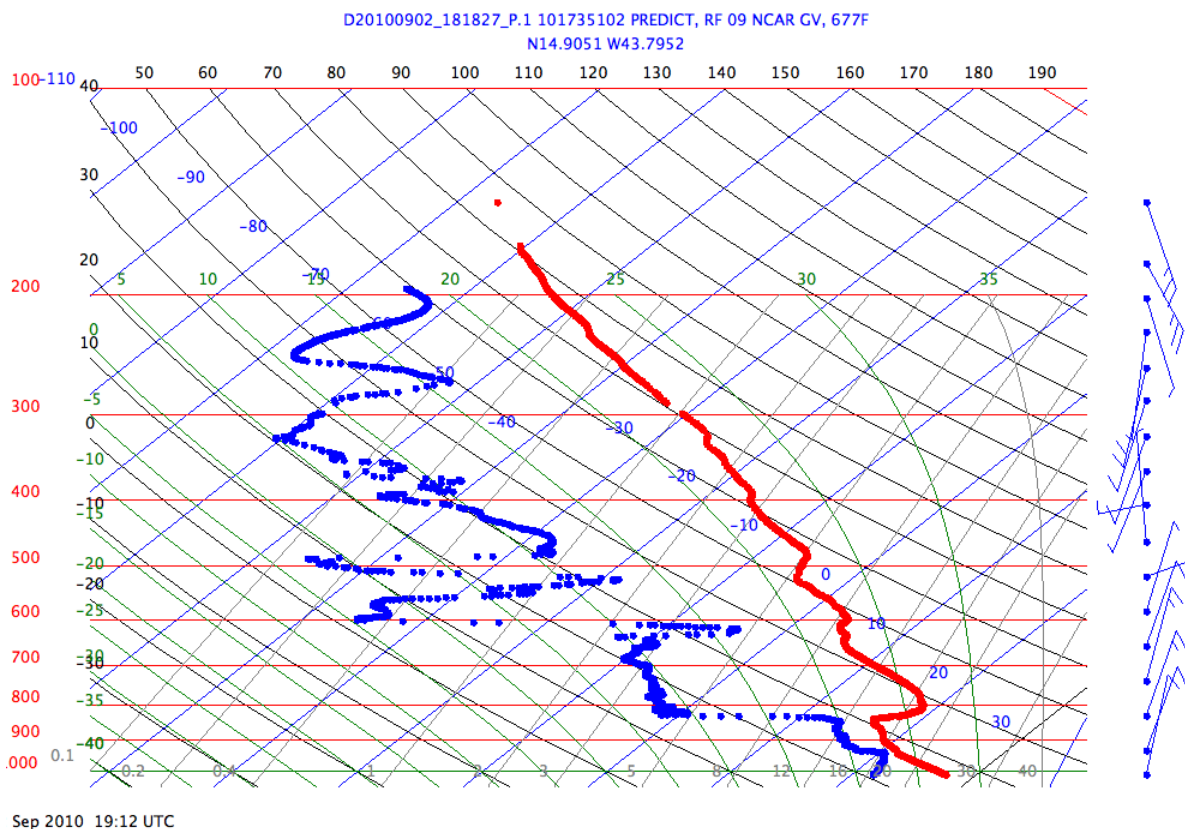
Figure 37. Dropsonde in northeast sector of PGI38L.

Evidence for enhanced downdrafts from dry air entrainment can quite frequently be seen in visible imagery in the form of arc clouds. However, sounding analysis features dry air throughout the mid-levels and the vicinity of the storm to Africa prevents distinguishing between subsidence based dry air and SAL air wrapping around from the north. Despite a well-developed low level vortex, entrainment from the mid-levels supported enhanced downdrafts and stabilization from upper level warming, preventing the establishment of persistent robust convection. Evidence of strong downdrafts in the form of arc clouds in satellite imagery is present during this period (Fig. 38 shows an example in the southwest portion of the disturbance on Sept. 3rd).
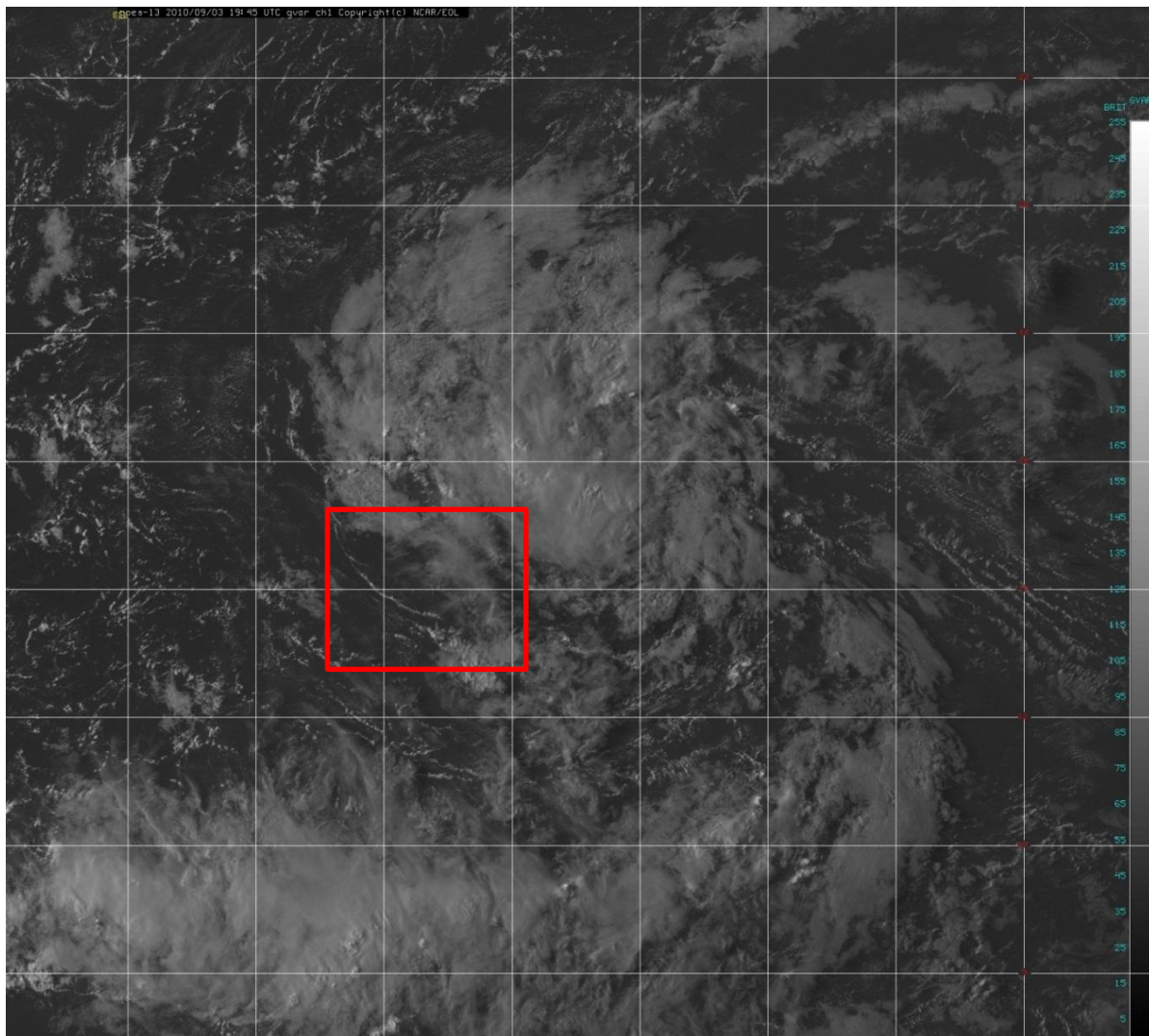
Figure 38. GOES Visibile satellite imagery on Sept. 3, 2010 at 1615Z. of PGI38L

In summary, in order for a TC to form, sustained convection is critical to build and

amalgamate vorticity and enable a warm core to develop. Dry air can often be entrained

into the disturbance convective cluster at the mid-levels, enhancing downdrafts and

disrupting further convection. This dry air can be environmental or locally produced

through forced subsidence adjacent to the convection if upper levels conditions are non-

divergent. In this regard, the establishment of outflow vents is essential, not only to

enhance the upper branch of the secondary circulation to evacuate mass from the storm center allowing pressure falls at the surface, but also to ameliorate adjacent subsidence.

3.3 Karl Case Study

a. Storm History

A pouch was first identified in the 0000 UTC 9 September GFS in the vicinity of the Windward Islands, and was subsequently followed until the 15th at 1200 UTC when it crossed from the Caribbean Sea and made landfall on the Yucatan Peninsula (refer back to Fig. 4 for the track). Forming north of Venezuela as a disorganized area of convection, PGI44L drifting slowly northeast, and the first GV flight revealed that the low level circulation was not identifiable by initial dropsonde analyses. The system then moved in a west-northwest direction with a zonal phase speed between 6 and 8 m/s. During the period of September 10th to September 13th dropsonde analyses show the development of a closed (in a Lagrangian framework) low-level circulation. Satellite analysis of total precipitable water showed a region of high moisture during the entire period in a broad area surrounding the pouch location. It appeared to the PREDICT analysts and forecasters during this period that PGI44 could form into a TC at any time based on the low-level conditions and pouch diagnostics. However, genesis did not officially occur until September 14th.

A striking feature of this storms development was the pulsating nature of the convection. Consecutive 06z images on the 11th, 12th and 13th of September feature robust convection, with very cold cloud tops within 3-5 degrees of the model diagnosed center of

circulation. In contrast, the corresponding prior 18z analyses featured mainly cirrus debris with little active convection. This cycle of unsustainable convective blowout continued despite strong low-level pouch characteristics. At 12z on the 14th, the NHC declared the system a tropical depression, and the storm quickly reached hurricane strength before landfall on the Yucatan. The system subsequently weakened over land, but then re-intensified in the bay of Campeche. However, the final PREDICT mission flight occurred just before the Yucatan landfall, and therefore that is when our case study analysis ends.

b. Analysis

The pulsating nature of the convection is also evident in radially averaged upper-level horizontal mass flux calculations (figure 39). A regular diurnal variation can be seen in the 3 degree fluctuations, however the mass flux (outflow) at the outer radii doesn't really pick up until late on the 13th, coinciding with an earlier maximum on the 13th at 3 degree radius. This coupling of inner and outer mass flux observations is the signature of an outflow channel being established, which will be supported by satellite wind analyses in later figures.
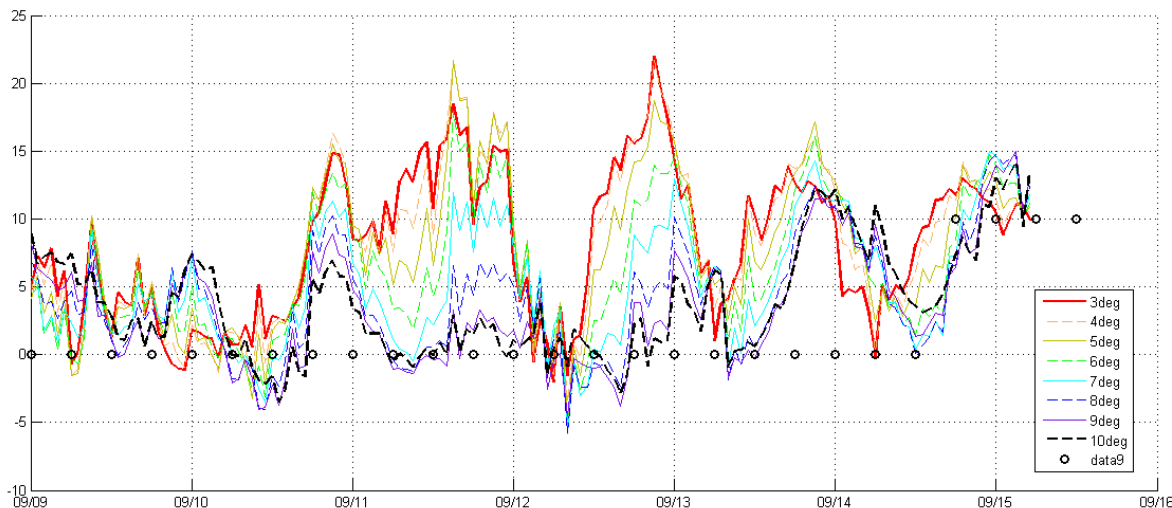
Figure 39. A time-series of radially averaged horizontal mass flux [kg/m²s] at 200hPa at various radii from the pouch center, for PGI44L (Karl). Dots indicate TCG on Sep. 14th, 12Z.

Using the dropsonde 3-D Variational analyses of radially averaged horizontal mass flux, Figure 40 features a few signatures that prior analyses suggested would be present on the 13th. First, a pocket of high outward mass flux at 11-13km (~250-200hPa) exists in the inner 5 degree radii with a relatively uniform signature from the inner radii to the outer radii. Despite a higher magnitude of upper-level outward flux on the 11th, it appears isolated from the inner core, which suggests there is not a strong coupling of this horizontal mass flux with the inner core upward vertical motion shown in Figure 41. It is likely this temporary surge in outward mass flux on the 11th has an invigorated outer rainband as its source. This is a crucial distinction, as it would not reflect sustained inner core convection which is more closely linked to TC genesis. The vertical motion field on the 11th shows an expanded radial profile, and is likely due to the analysis not being able to discretely resolve the convective influences from inner core and outer bands at 3-4 degrees.

Another significant feature identifiable in Fig. 41 is the deterioration of subsidence adjacent to the system core (5-10 degrees radius) that slowly gets eroded as the outflow develops. This is consistent with the concepts discussed in the previous section, and provides further evidence that the establishment of outflow acts to ventilate mass well away from the disturbance core, and at the same time diminishing locally produced subsidence which can hinder sustained inner core convection.
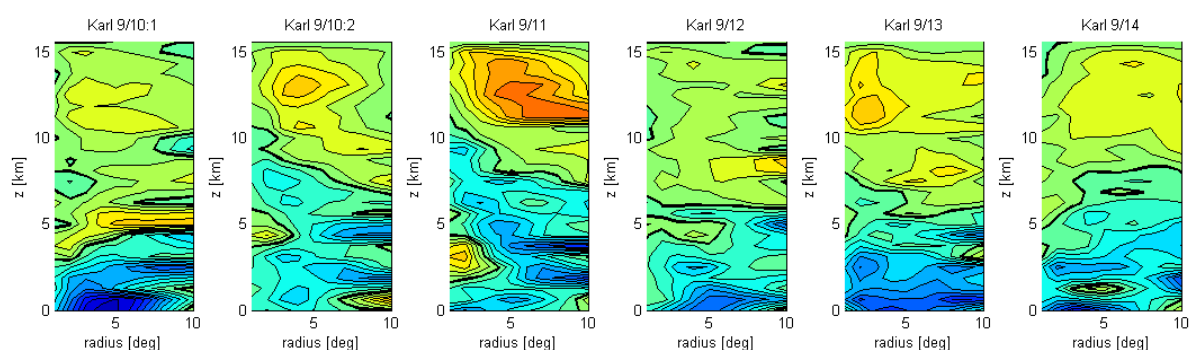

Figure 40. Vertical profile of radially averaged horizontal mass flux at various radii for mission (a) RF14, (b) RF15, (c) RF16, (d) RF17, (e) RF18 and (f) RF19.
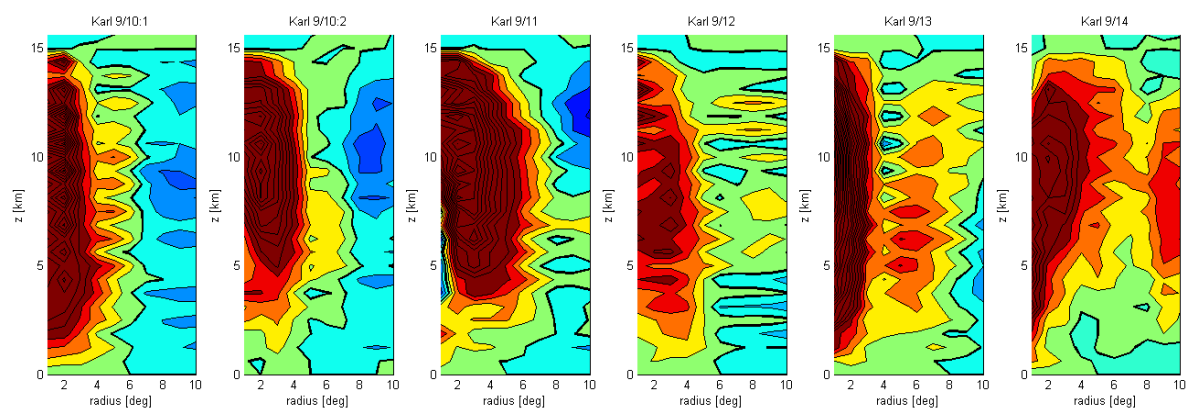

Figure 41. Vertical profile of radially averaged vertical motion at various radii for mission (a) RF14, (b) RF15, (c) RF16, (d) RF17, (e) RF18 and (f) RF19.

The outward mass flux through all radii is a signal that the inner core convective circulation is connected to the environmental flow, which is evacuating mass well away from the center. Compensating subsidence will therefore occur well away from inhibitive influences crucial to sustain the inner core convection. The profiles on the 14th even suggest the beginnings of a tilted eyewall and strong outer band. But the critical piece to development is the overcoming of the subsidence surrounding the core upward motion that can induce drier air into the boundary layer that recirculates back into the core below 4km. The enhanced mass flux out through 10 degrees allows moist static energy to accumulate and the surface low to deepen.

Radially averaged tangential wind (figure 42) shows the growth of the vortex during the analysis period. Once the anticyclone aloft develops, the lower vortex grows in height, eventually reaching 11-12km as the vorticity amplifies. This spinup is identified in the pouch hypothesis as a crucial mechanism for genesis, but in this case it would appear the process is modulated by the ventilation characteristics in the upper levels, allowing the transition of the convection from pulsating to persistent in nature.
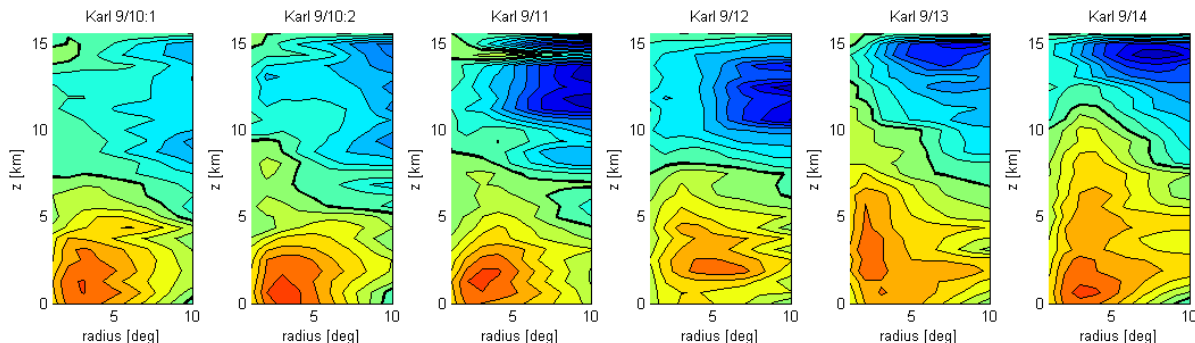
Figure 42. Vertical profile of radially averaged tangential wind flux at various radii for mission (a) RF14, (b) RF15, (c) RF16, (d) RF17, (e) RF18 and (f) RF19.

Qualitative analysis of satellite imagery and derived products can help support the evidence and interpretation discussed above. Water vapor imagery and an upper-level divergence analysis derived from the CIMSS fields at 12z on the 11th shows dry air/subsidence (dark areas in the image) in close proximity to and surrounding most of the vigorous convection in the core of PGI44 (Figure 43). This is supported by weakly convergent flow in the analysis. The corresponding satellite-derived winds plot (Figure 44) shows weak (but constrained) outflow in the form of southerlies just to the north of the center, and strong easterlies to the south in the southern hemisphere. The outflow to the north leads directly to the area of convergence/subsidence, and the easterlies to the south do not yet appear well connected to the core outflow.
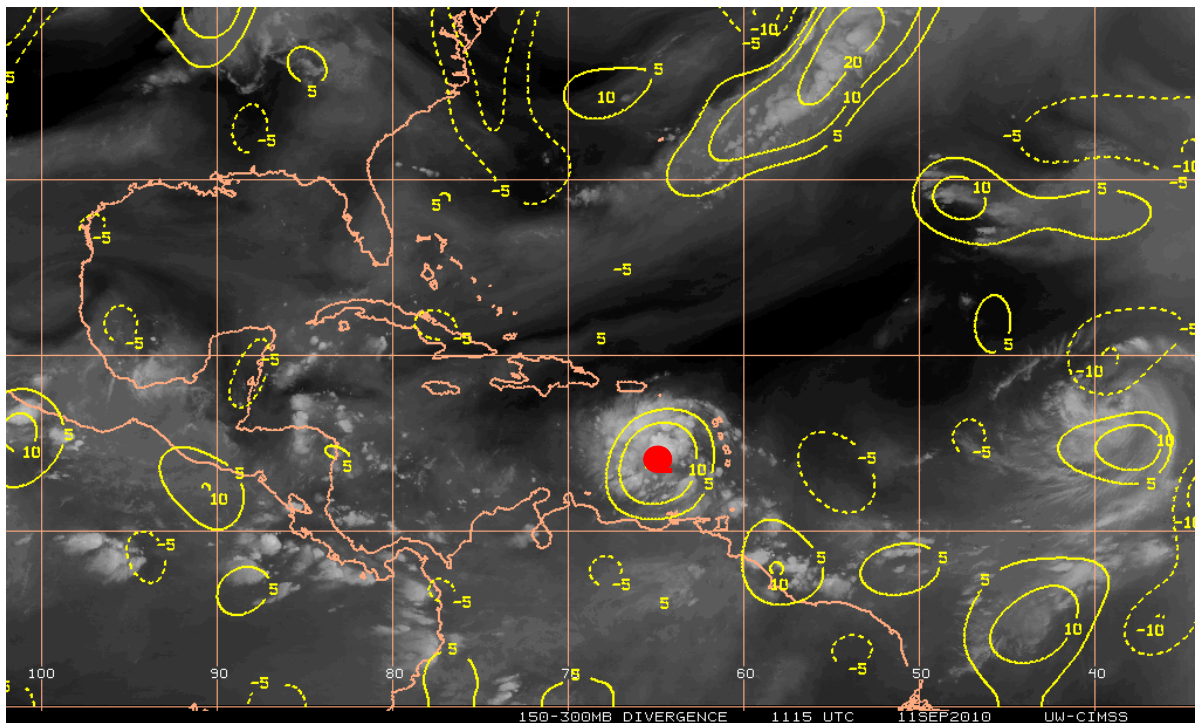
Figure 43. CIMSS satellite grid derived divergence for upper level [s^{-1} x10^{-6}] above300hPa (contour) and WV imagery PGI44L (Karl) on Sep. 11th 1115Z.
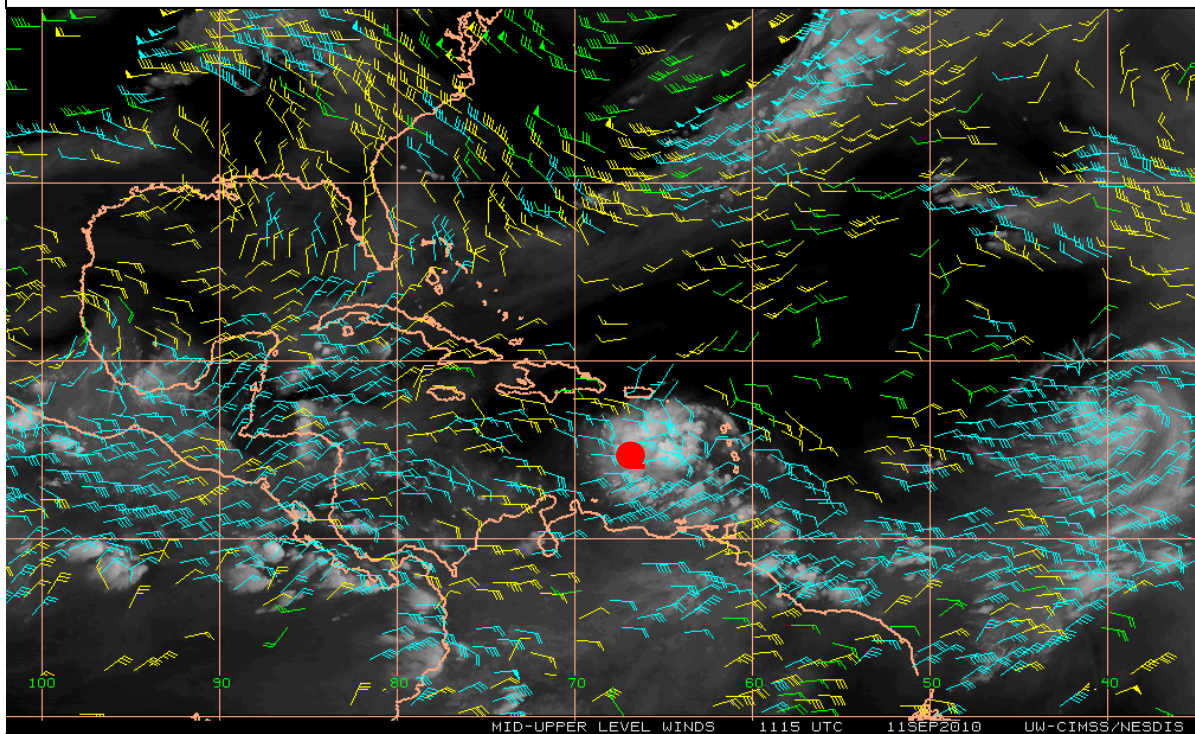

Figure 44. Raw CIMSS Satellite wind barbs for upper level winds [kts] above500hPa and IR for PGI44L (Karl) on Sep. 11th 1115Z.

This analysis provides further evidence of an unfavorable upper-level flow environment, preventing sufficient mass flux away from the center. Instead, the ambient convergent upper-levels encourage compensating subsidence to occur adjacent to the core convection, and the system has a hard time overcoming the dry air entrainment. Despite rigorous convection and a solid low-level vortex, the pouch is unable to deepen due to insufficient mass evacuation. Local divergence associated with the inner convection is insufficient to allow deepening without a larger environmental linkage.

Evidence of subsidence induced dry air's intrusion into the convection around the storm core can be seen in visible imagery. Arc clouds can be seen being expelled form PGI 44 associated with downdrafts (Figure 45). Subsequent analysis showed suppressed convection following this period. The downdrafts enhanced by dry air entrainment reflects the start of the ascent in average IR temperatures (Fig. 31) as the convective towers fail to grow due to expanding downdraft induced cold pools.
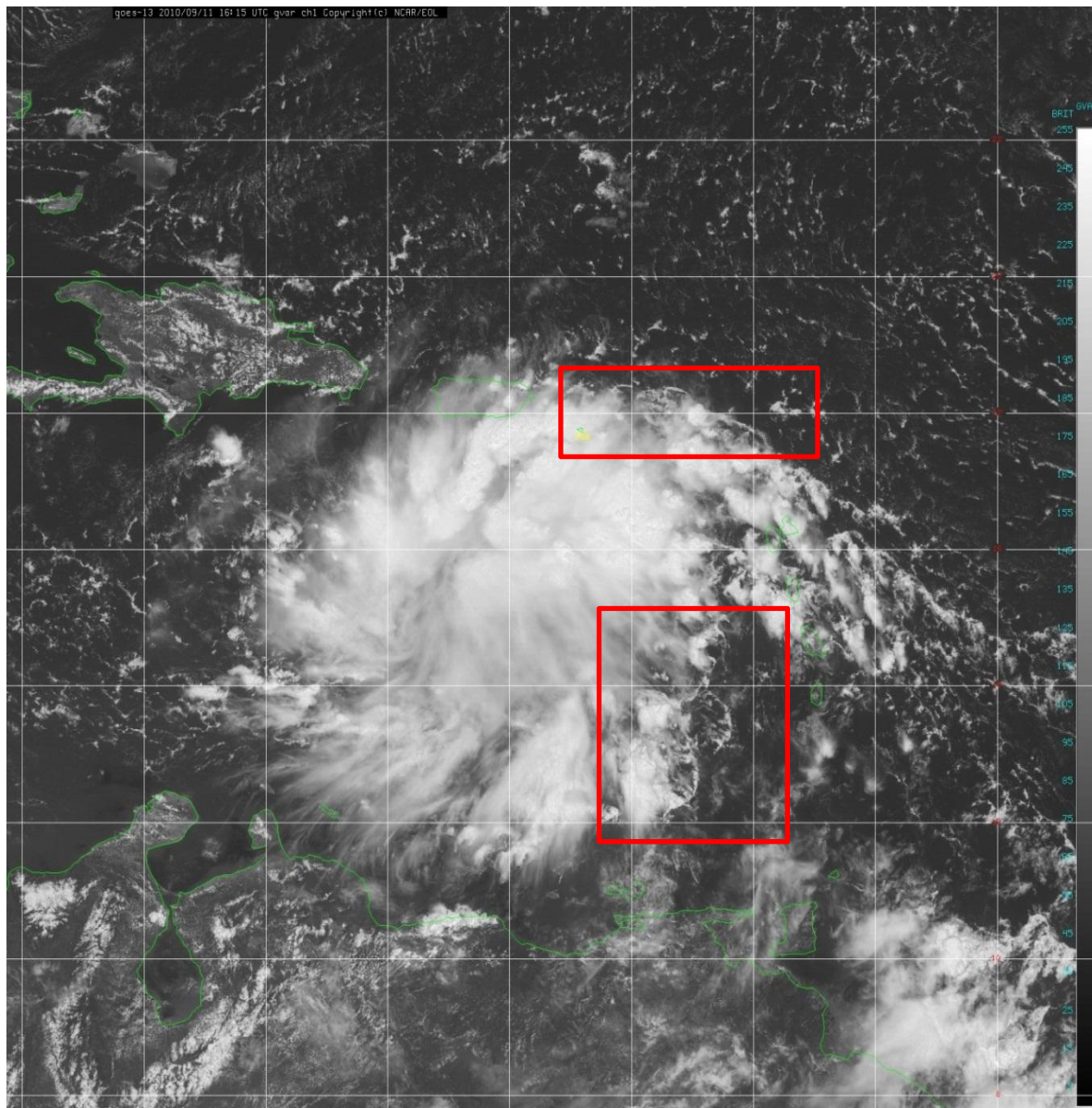
Figure 45. Visible imagery on Sept. 11, 2010 at 1615Z of PGI 44L. Arc clouds shown in blue boxes.

By comparison, at 18z on the 13th, about a day before Karl was declared a tropical storm, the divergence profile is very different (Figure 46). Evidence for a developing outflow channel to the northeast of the pouch system can be seen in an extension of the elevated divergence from the storm center between Cuba and Hispaniola. This extension of

divergence is not present on the 11th creating a region of sufficient mass evacuation well

away from the storm center and is reflected in the satellite winds from that period (Figure

47). Weak outflow is present equatorward of the storm as well, and there is no obstruction

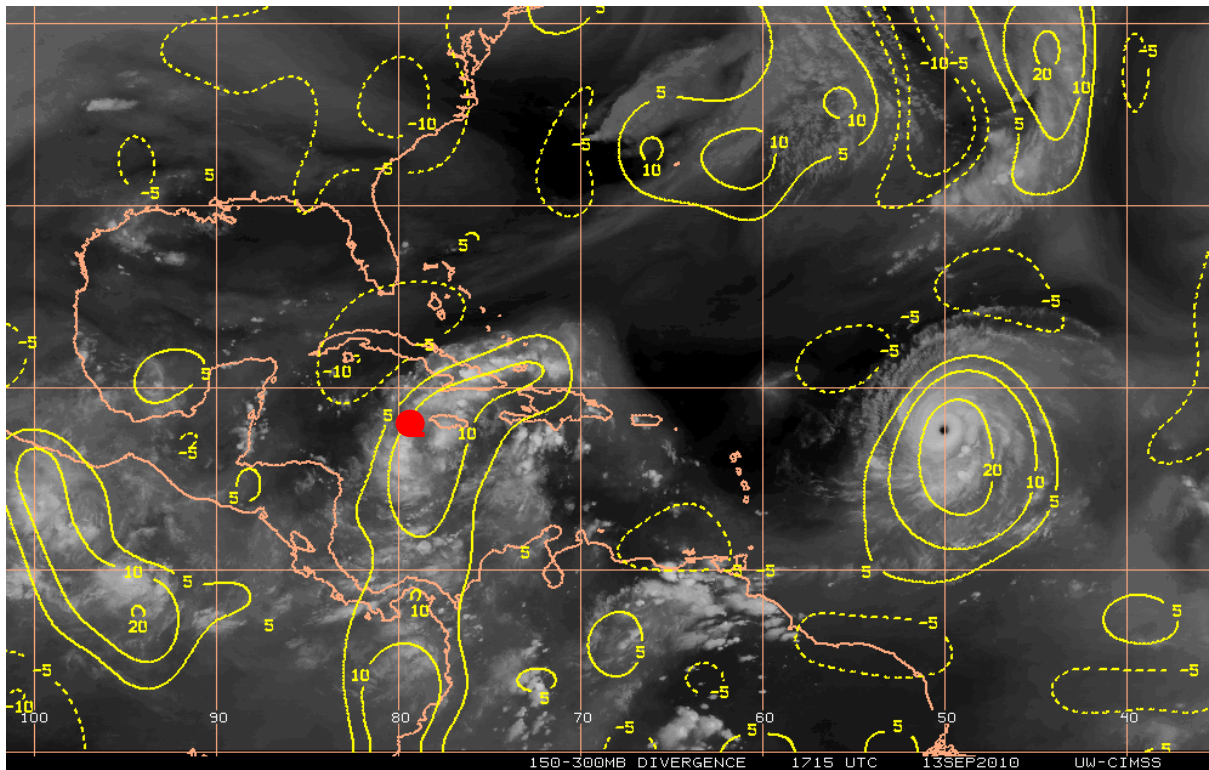as it turns anti-cyclonically to the west side of the storm.

Figure 46. CIMSS satellite grid derived divergence for upper level [s^{-1} $x10^{-6}$] above300hPa (contour) and WV imagery PGI44L (Karl) on Sep. 13th 1715Z.
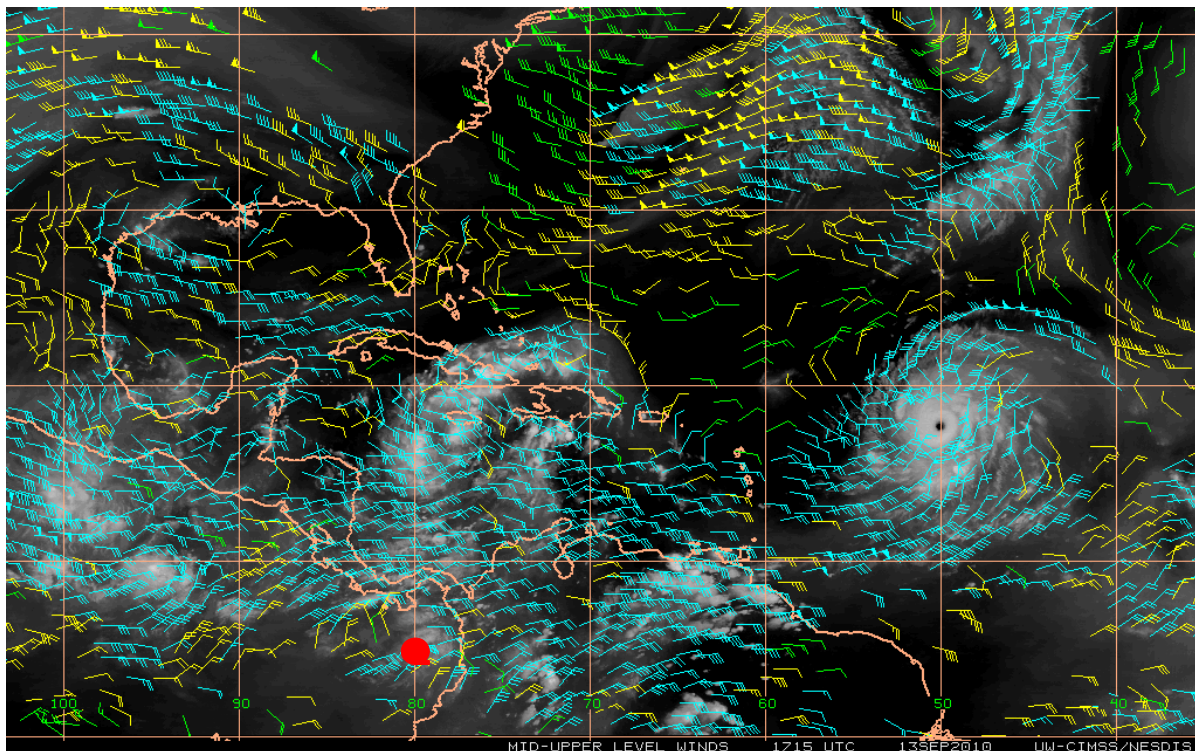
Figure 47. Raw CIMSS Satellite wind barbs for upper level winds [kts] above500hPa and IR for PGI44L (Karl) on Sep. 13th 1715Z.

The IAKE profile for the 11th at 12Z features a weakly positive or neutral signal near the storm core at 355K (Figure 48), with a ribbon of low IAKE just to the north associated with a narrow, weak PV streamer also evident in the water vapor imagery. As the PV streamer weakens and moves off to the northeast, it allows for a region of higher IAKE to settle in over the storm by the 13th at 12Z (Figure 49). This encourages the establishment of the outflow before the storm's declaration as TS 24 hours later.
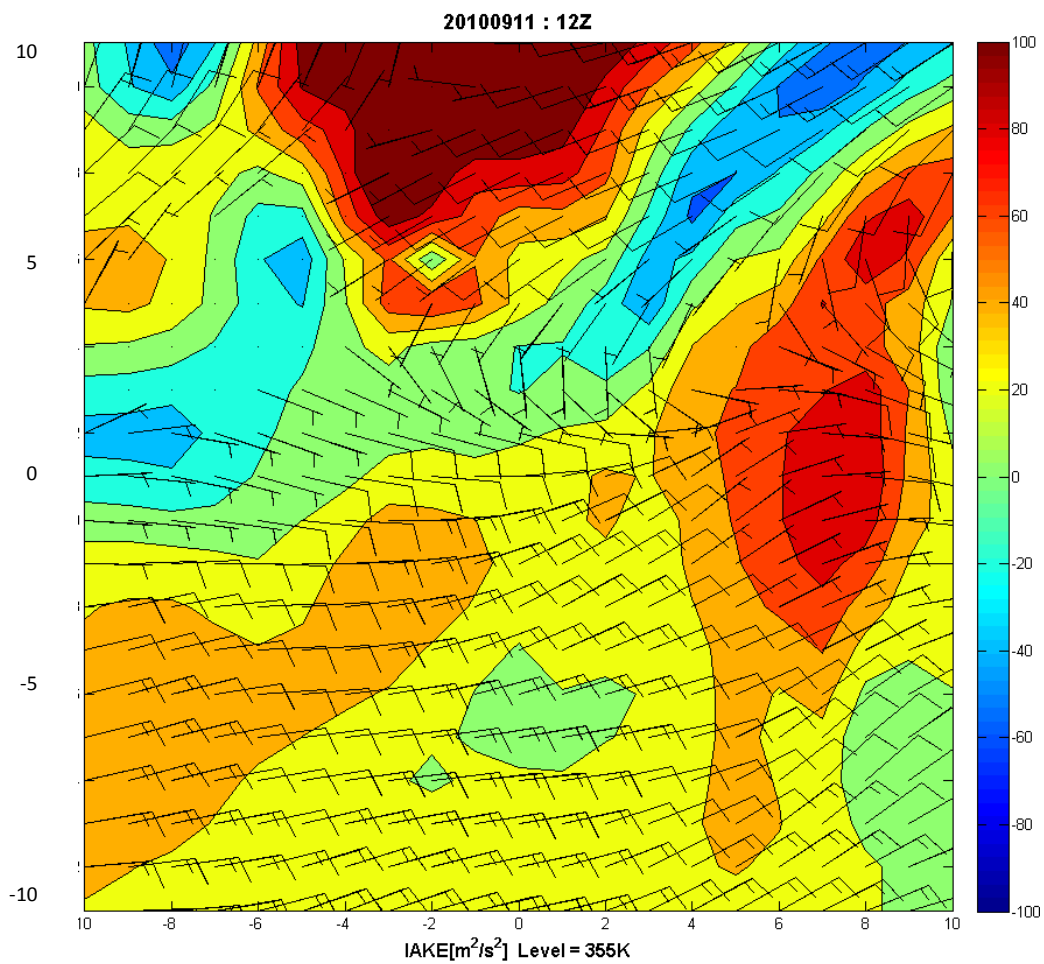
Figure 48. UW-NMS IAKE [m^2/s^2] (fill) with gridded satellite CIMSS gridded wind [m/s] at 355K on Sep.11th, 12Z.
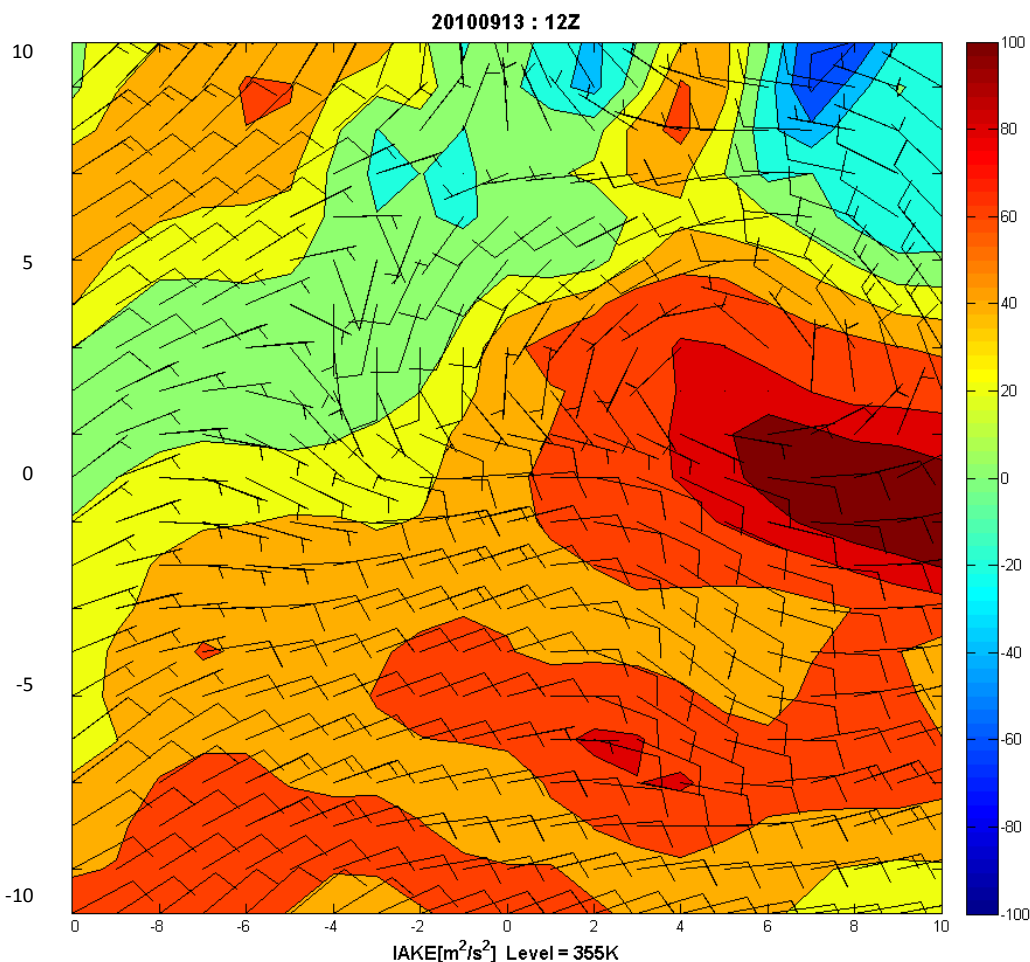
Figure 49. UW-NMS IAKE [m^2/s^2] (fill) with gridded satellite CIMSS gridded wind [m/s] at 355K on Sep.13th, 12Z.

In summary, PGI44 was expected to develop at an accelerated pace based on low-level pouch hypotheses and conditions present. Our hypothesis based on the presented evidence is that the delay in the genesis of Karl is linked to an upper-level flow pattern that was not conducive for outflow (and hence mass flux). This resulted in the entrainment of dry air caused by subsidence adjacent to the storm core. Once environmental conditions became more favorable for the establishment of outflow vents, the near-core subsidence eroded, and the disturbance rapidly deepened before making landfall. This case study

supports our overarching hypothesis that upper levels conditions can modulate TC genesis forced primarily by lower-level processes.

3.4 Gaston Case Study

a. Storm History

Initially identified at 00z on the 28th of July as an easterly wave still over Africa, PGI38L subsequently tracked generally westward, moving between 4 and 9 m/s (Fig. 4). The disturbance was quick to spin up after coming off the coast, reaching TD designation by the NHC early on September 1st and tropical storm designation for a brief period, until weakening caused it to be unclassified at 00z on the 2nd of September. PGI38L (Gaston) was briefly re-declared a TD operationally by the NHC on the 4th of September before being un-declared again for the remainder of the time it was followed in this case study (until September 11th). PREDICT flights into Gaston began on September 2nd as the storm passed the 40 degree west longitude line and was in the range of the GV aircraft from its base in St. Croix, USVI.

Convection was initially very robust as the storm left the coast of Africa although a strong diurnal signal was evident until Sept 1st when it was first declared a TD. From there, the average IR BT within a three degree ring around the center drops (Fig. 28), and dropsonde analyses on the 2nd of September provided the information used to de-classify the storm since a sufficient circulation was not present. A brief rebound in brightness temperatures on the 4th prompted the second TD declaration, but the convection did not

persist. Despite a closed Lagrangian circulation, Gaston never rebounded, even with favorable low-level pouch characteristics.

b. Analysis

PGI38L (Gaston) has some similarities to Karl, in that both systems had favorable pouch characteristics and were forecast to develop based these and numerical models, and both featured strongly evident pulsating convection on a nearly diurnal timescale. However, Gaston's vortex weakened substantially during its trek across the Atlantic after being declared a tropical depression on the first of September. Figure 50 shows the trend in the tangential wind profiles during the period of analysis. The strong low-mid level vortex steadily weakens, extending only to ~4-5km by the 7th of September.

Figure 50. Vertical profile of radially averaged tangential wind at various radii for mission (a) RF09, (b) RF10, (c) RF11, (d) RF12 and (e) RF13.

The horizontal mass flux profiles above 11km are sporadic during the analysis period (Fig. 51). There is a hint of outflow especially on Sept. 3 that could be responsible for the brief strengthening of PGI38 on the 4th. This elevated mass flux on the third occurs at the

same time as a broader area of positive vertical motion develops, replacing previous subsidence adjacent to the core (Fig. 52). However, while the upper-level wind flow patterns appear divergent over the system on the 3rd, there is no anticyclone apparent (Figure 53). The unfocused broad area of outflow proved unsustainable, and an area of subsidence re-establishes adjacent to the inner core, hindering persistent convection and deepening of the system.

Figure 51. Vertical profile of radially averaged horizontal mass flux at various radii for mission (a) RF09, (b) RF10, (c) RF11, (d) RF12 and (e) RF13.

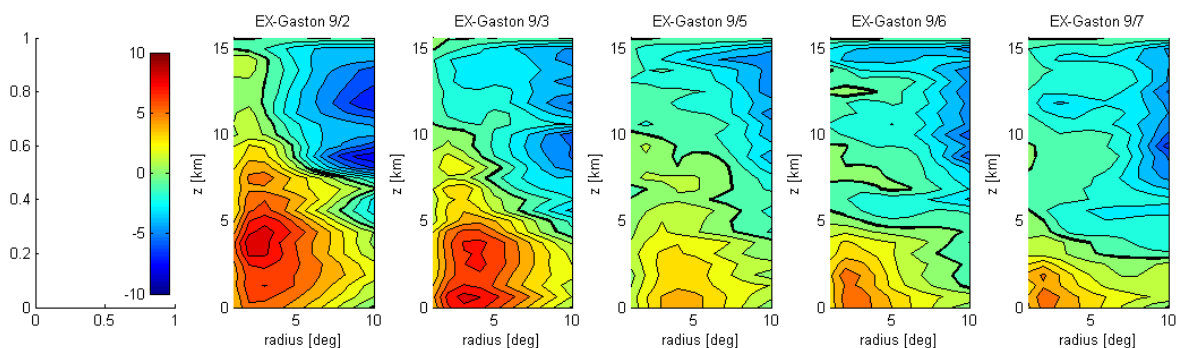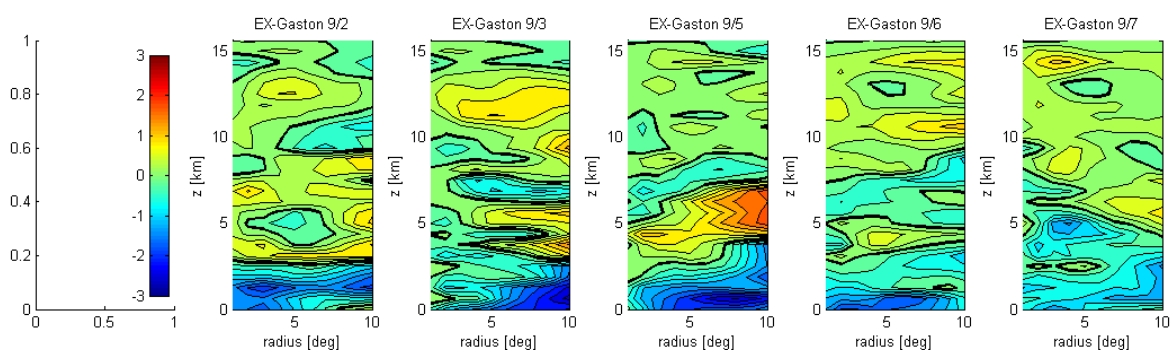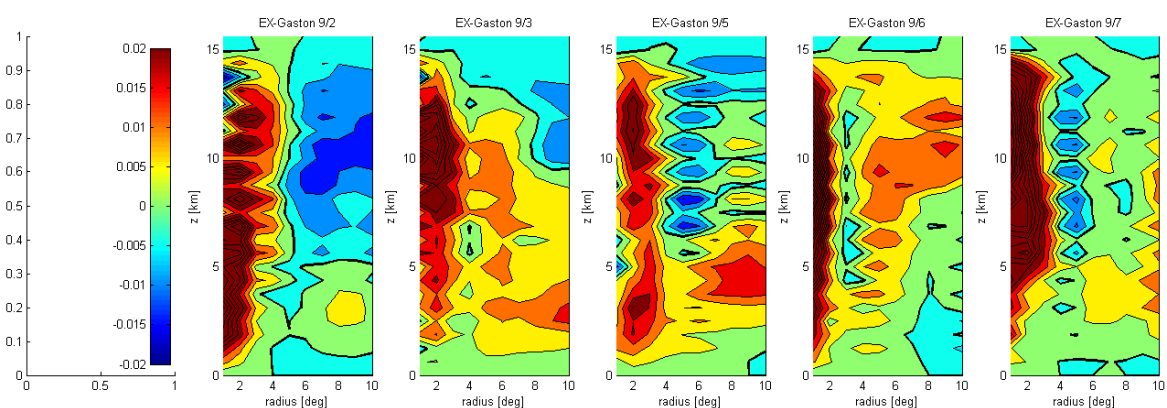
Figure 52. Vertical profile of radially averaged vertical velocity at various radii for mission (a) RF09, (b) RF10, (c) RF11, (d) RF12 and (e) RF13.
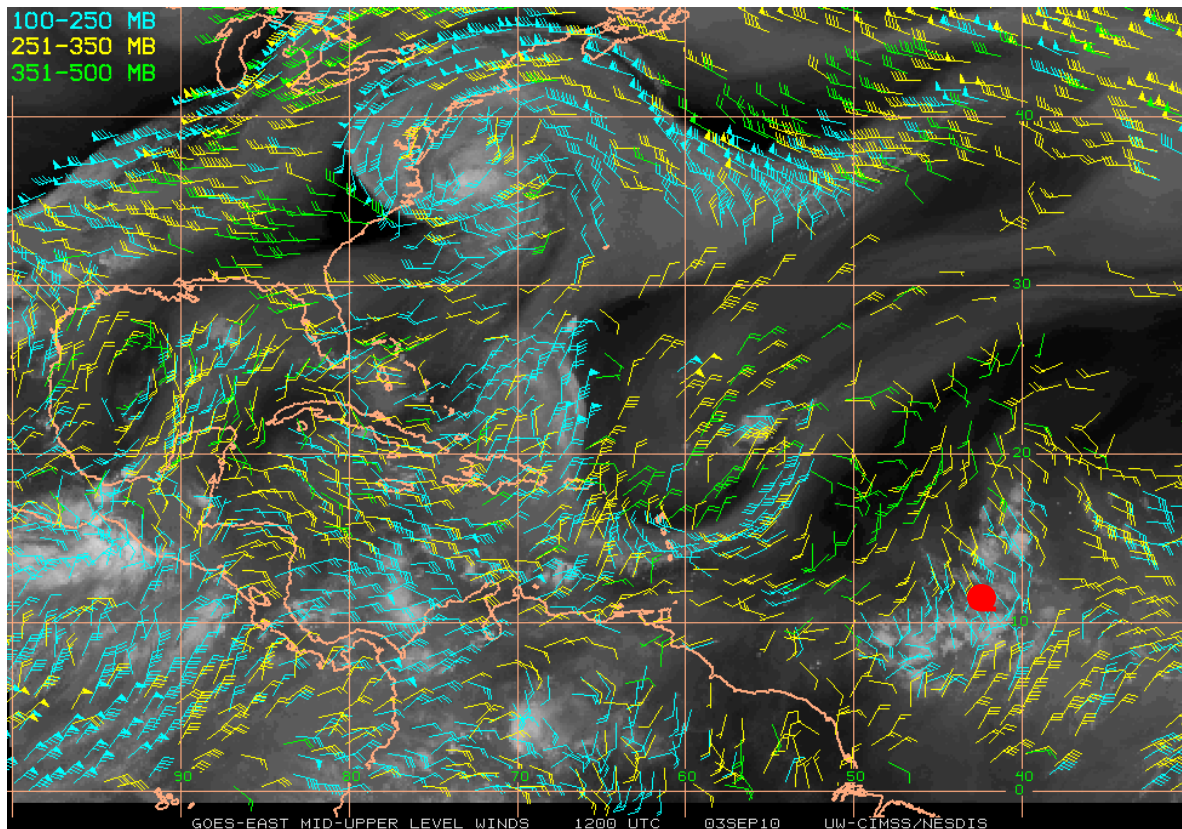
Figure 53. Raw CIMSS Satellite wind barbs for upper level winds [kts] above500hPa and IR for PGI38L (Gaston) on Sep. 3rd 12Z.

There was clearly another environmental player in this case. Dry air in the mid-levels is evident nearby PGI38 in satellite analysis (Figure 54). This dry air outbreak occurred over a several day period from August 23rd to September 6th. Without further analysis, it would be difficult to characterize this airmass as SAL or subsidence-induced dry air, but regardless, it played a role inhibiting persistent convection to establish in case. Animations of this satellite product show the dry air begins to wrap in front of the system, progressively getting closer to the central convection, and eventually entrained into (or above) the strong low level circulation that still existed.
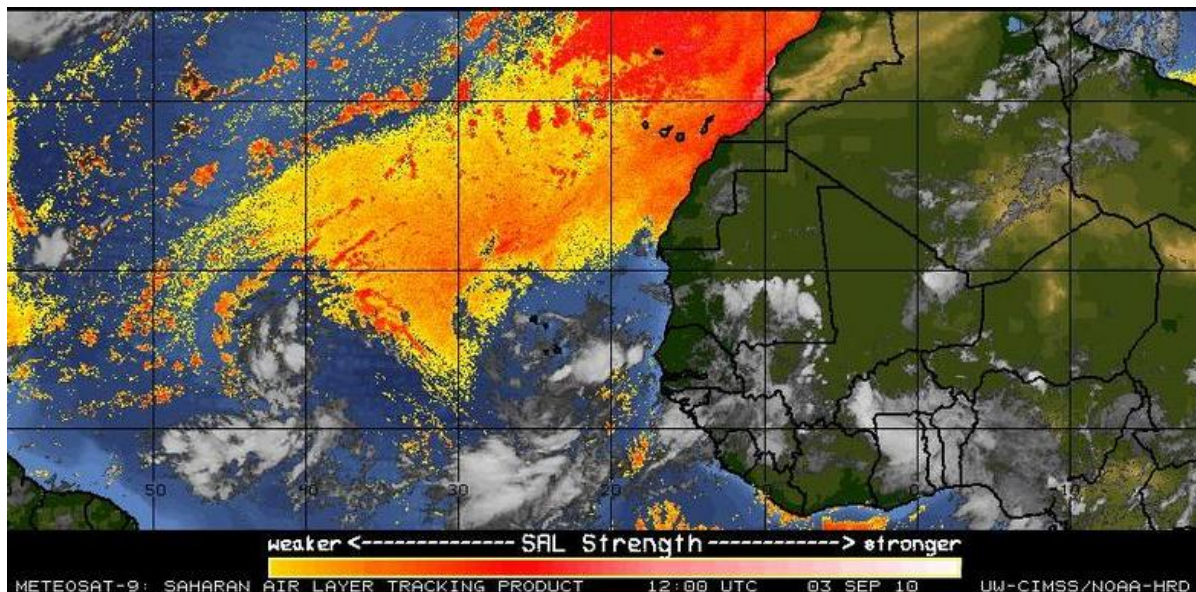
Figure 54. CIMSS satellite derived Saharan Air Layer product indicating dry, dust filled airmasses.

The IAKE analyses in this case also reveal the weak support that develops in the upper levels. On September 1 (Fig. 55), when the system was briefly TS Gaston, a region of reasonably high IAKE covers the interior radii of the storm system, extending to the west and northeast corridors. Efficient momentum transfer from the core vertical motion to horizontal outflow is less impeded in these regions, enhancing the outflow potential, and allowing the system to organize via a persistent secondary circulation.

In contrast, the IAKE field on the 4th of September when the system featured a strong low-level pouch and was attempting to organize back into a TC, features a much less favorable pattern (Figure 56). Negative or neutral IAKE values exist near the storm core, and there are no strong connections to positive IAKE channels in the near environment. This lack of positive IAKE does not promote the transition of vertical momentum into horizontal

outflow, and correspondingly, downdrafts begin to persist near the storm core, inhibiting

subsequent development.
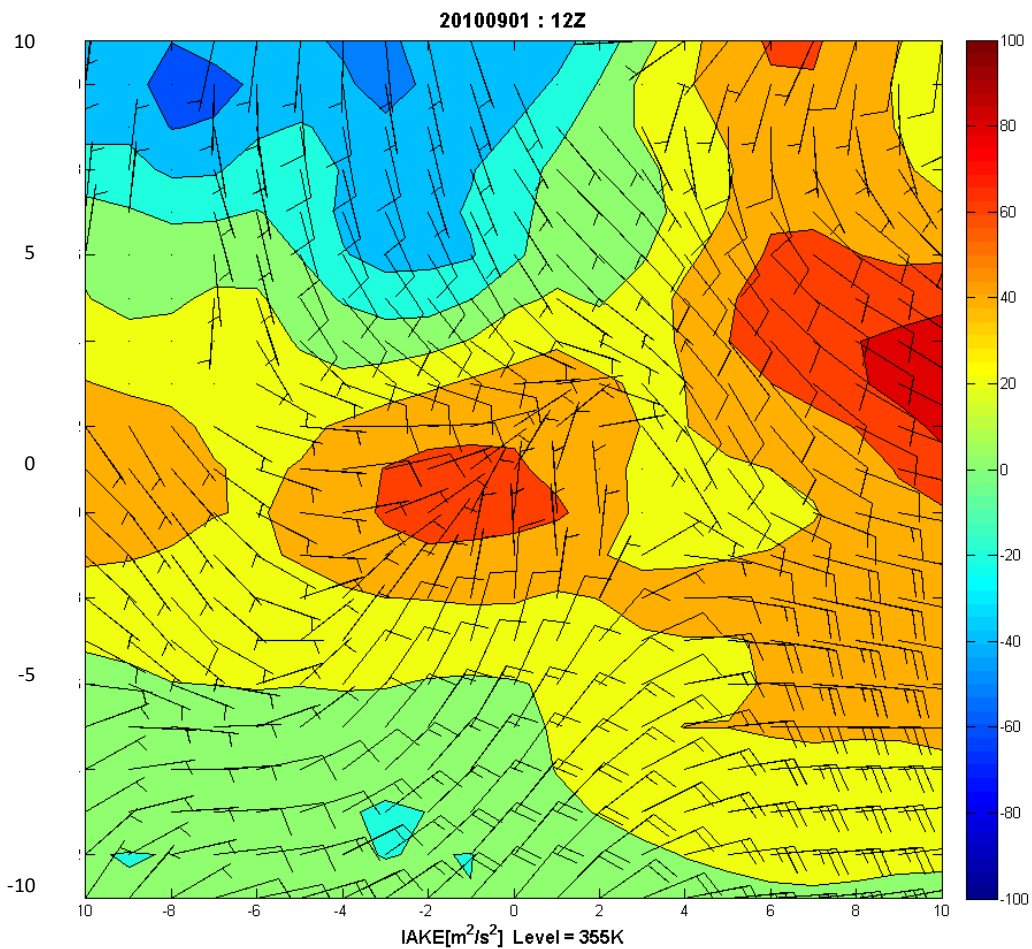
Figure 55. UW-NMS IAKE [m^2/s^2] (fill) with gridded satellite CIMSS gridded wind [m/s] at 355K on Sep.1st, 12Z.
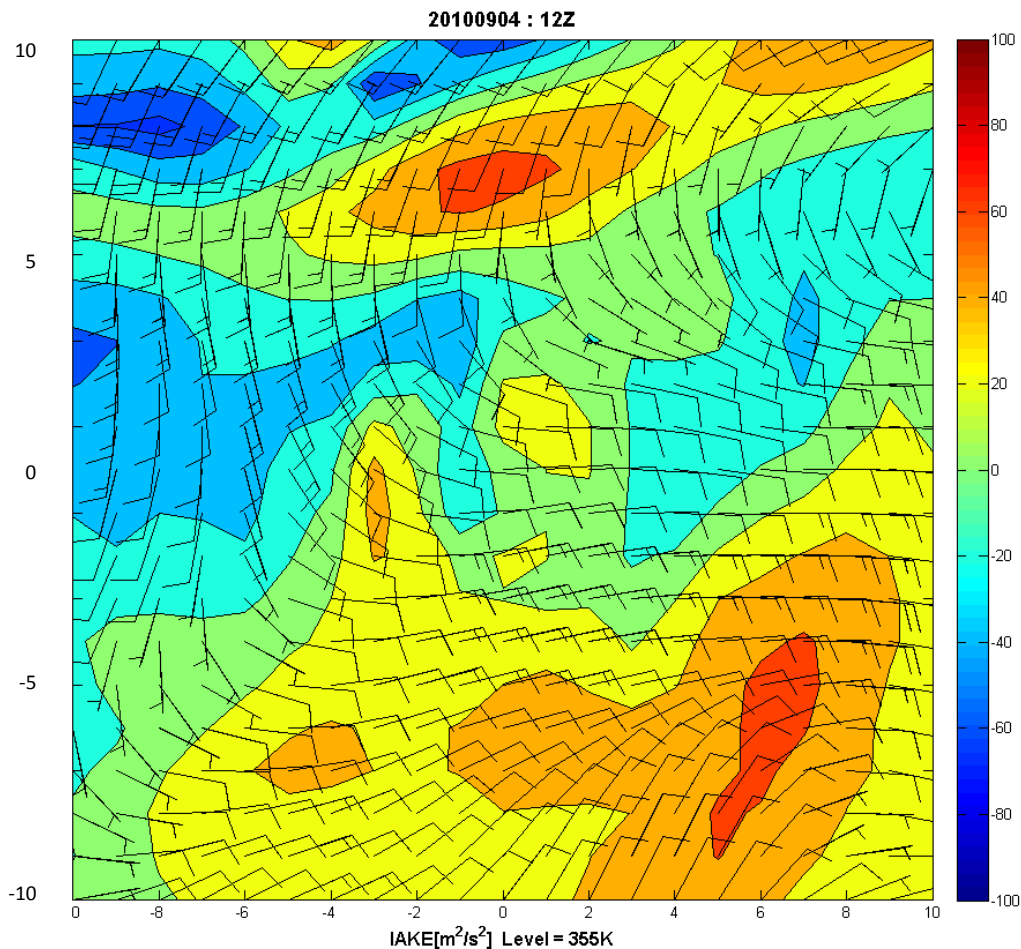
Figure 56. UW-NMS IAKE [m^2/s^2] (fill) with gridded satellite CIMSS gridded wind [m/s] at 355K on Sep.4th, 12Z.

In summary, PGI38/Gaston had the potential to develop into a sustained TC based on low level pouch characteristics. Even the numerical guidance forecast significant development during the analysis period. However, after a very brief time as a TD/TS, the strong low level circulation and the protection granted it by the "pouch" proved no match for the lack of development support in the mid and upper-levels. The non-existence of upper-level outflow channels to vent the mass and establish a strong "in, up and out" secondary circulation meant that the system could not support sustained deep convection.

This in turn allowed for environmental dry air (possibly associated with a SAL surge) to overtake the lower-level circulation and further disrupt the inner convection. This unfolding scenario led Gaston from a tropical storm/depression back to an open tropical wave, and although a detectable low level circulation was traceable until the storm had crossed well into the Caribbean, dry air and broad upper-level subsidence suppressed convection for the remainder of its lifetime.

4. Discussion

A critical distinction between developing and non-developing systems is persistent deep convection in the inner core. It has been shown that the transition from an open easterly wave with sporadic convection to an organizing system with persistent deep convection features the establishment of a strong secondary circulation. Furthermore, this circulation should feature an upper branch capable of the transport of mass out away from the developing core; or, a circulation characterized by "in, up and out" (Figure 55). This ventilation, in the form of outflow ducts or channels, is a critical piece to the "bottom-up" genesis theories such as the pouch hypothesis recently pushed by Montgomery et al. in the PREDICT campaign. Without it, the subsiding branch of the secondary circulation forced by the core upward vertical motions, and latent heat release, can occur adjacent to the organizing convection; or, "in, up and down" (Fig. 57). The subsiding dry air can then be entrained into convection at mid-levels, promoting enhanced downdrafts, or into the convergent boundary layer air feeding subsequent convection. Both processes are a

hindrance to sustaining deep convection. While we accept that precept that lower-level

conditions/forcing is necessary for TCG, we argue in some cases it may not be sufficient.
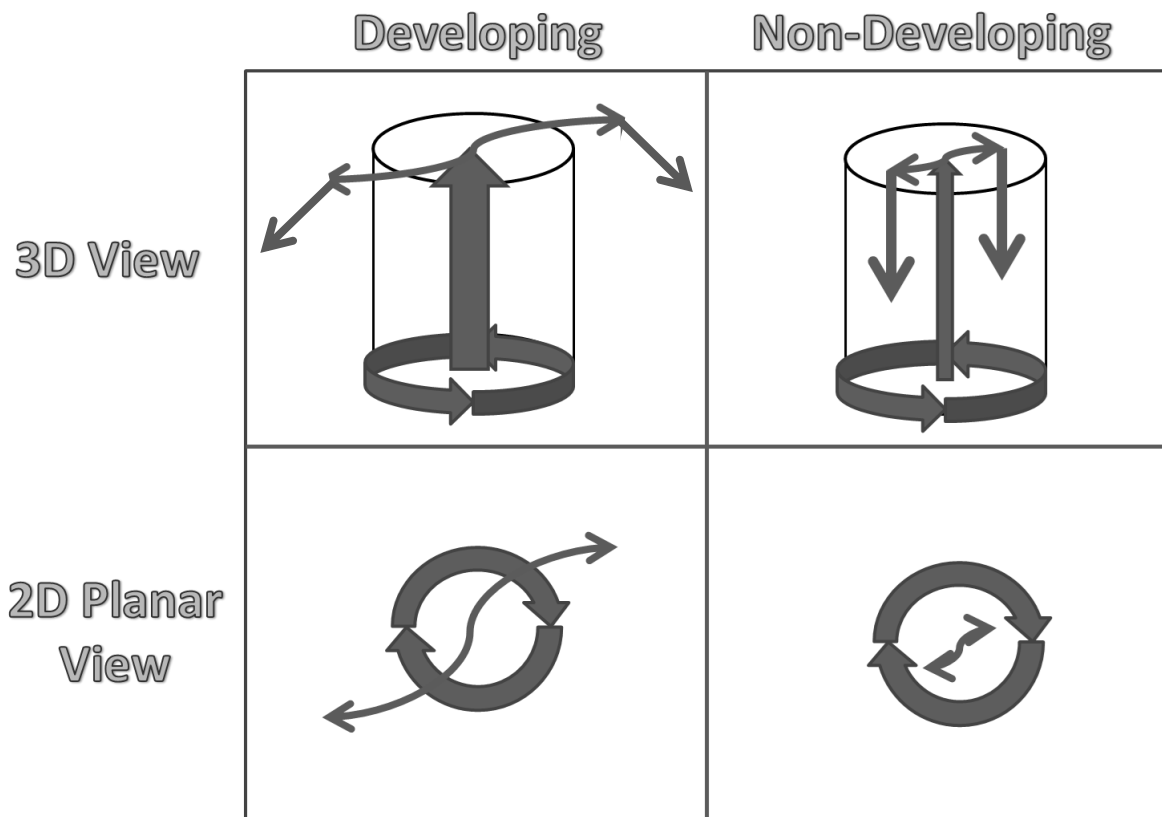
Figure 57. Simple schematic of the basic circulations between systems with outflow channels (left) and those with a non-divergent upper-level environment (right**).**

This study emphasizes the flow patterns and thermodynamic conditions in the upper

levels between developing and non-developing systems, identifying upper–tropospheric

divergent regimes specific to developing systems enabling the establishment of outflow and

mass evacuation. We find upper-level conditions that promote the establishment of outflow

channels that are connected to the environment appear to be important in some cases to

allow the genesis processes to flourish. Upper-level IAKE and PV analyses point to regions of low inertial stability, providing "soft spots" for mass being evacuated from intense core convection. The low inertial stability means less work needs to be done by the evacuating mass as it spreads horizontally upon reaching the tropopause. This allows a greater acceleration away from the inner circulation, and once linked to environmental flow, provides an effective "mass transit" from the developing disturbance. Higher mass evacuation allows a deepening of the surface pressure as well as helping to maintain the secondary circulation driving the sustained convection.

The establishment and pattern of these outflow channels is strongly dependent on ambient and evolving upper-tropospheric environmental conditions. There are several variations on efficient outflow patterns, the most common type being multiple channels to the north turning northeast and south turning southwest. The northern channel setup is often aided by transient upper level troughs that feature southwesterlies on the leading edge that can help link the outflow to the environment. Divergent patterns in the upper levels of the ITCZ can similarly provide channels for outflow to the south. Unfavorable environments are the kind that beset PGI38/Gaston described earlier, or TS Fiona where the dominant outflow channel was disrupted by converging outflow from Hurricane Earl. Dynamic structures such as these can modify the disturbance's ambient environment and aid or inhibit the upper level branch of the secondary circulation trying to develop. The ventilation of heat/mass away from the core may also prevent core stabilization, a theory promoted by Merrill (1988) in intensifying TCs.

We recognize the symbiotic nature of upper-level divergence driven by vigorous convection and that associated with larger-scale patterns is difficult to separate. Our lagged-correlation analysis identified a ~30-hour lag consistent with outflow establishing a linkage from the storm core to outer radii. This may be circumstantial evidence. However, examination of the time evolution of the upper-level divergence patterns in many cases strongly suggests that the ambient conditions preceding the disturbance (and associated convective component) plays a major factor in the overall ability of the pouch processes to flourish. Although the case-by-case magnitudes and configuration of outflow may vary, enhanced mass flux though organized outflow is shown to be important in order to sustain the inner core deep convection in developing tropical cyclones.

Another critical aspect of the establishment of an in, up and out circulation is the erosion of subsidence near the storm core. Observations have shown that dry air created from adiabatic subsidence can be entrained into convective bursts (Pratt and Evans 2009). Also, Braun (2010) showed the value of the upper levels in protecting systems from subsidence-induced dry air entrainment. Therefore, despite ample moisture and a closed circulation in the lower levels, dry air entrainment driven by subsidence can enhance downdrafts that suppress subsequent convection, in addition to stabilization by subsidence induced warming.

We also found that convective bursts on a diurnal cycle are the dominant modes of pre-depression systems in transient Atlantic easterly waves based on spectral analysis. The

transition from oscillatory to sustained intense convection is hypothesized as a necessary ingredient for TCG (Montgomery and Smith, 2011). Although a causal relationship between the existence of divergent flow aloft, core convection, and TCG cannot be stated unequivocally, our analyses strongly suggest the upper-levels at least play a modulating role. It stands to reason that strong outflow would affect the secondary circulation by curtailing subsidence adjacent to the updrafts in the storm core. A lack of this ventilation away from the core would promote compensating subsidence closer to the disturbance that could entrain dry air into the storm core and hinder further TCG (Pratt and Evans, 2009).

This work does not represent, infer or suggest a new perspective on "top-down" genesis, but serves to emphasize the role of the upper levels as a facilitator for TCG forcing processes that occur below 500hPa. Of particular importance are the processes below the boundary layer that serve a key role in genesis, as stated in the pouch hypothesis. However, upper-tropospheric conditions can regulate those processes, and in some cases unfavorable configurations can act to suppress the development of tropical cyclones along with other environmental factors such as strong vertical wind shear or cold sea surface temperatures.

5. Summary and Conclusions

This study represents a comprehensive analysis of pre-depression Atlantic tropical disturbances, with a focus on the possible roles of the upper troposphere on tropical cyclone genesis. The large-scale environment has been shown to play an important role in the genesis of African Easterly Waves as indicated in previous studies (e.g., Agudelo et al.,

2006). Upper-level conditions have also been shown to have a modulating effect on the intensification of mature TCs via ventilation processes; specifically, the presence or development of outflow channels that evacuate mass from the storm center as a branch of the TC secondary circulation and protection from dry air. Based on these two concepts, and a unique observational opportunity presented by the PREDICT field experiment, this study diagnoses the contributions of ambient upper-troposphere conditions during potential Atlantic TC genesis events.

The datasets and analyses employed in this research effort derived from several sources, some of which were a result of the PREDICT field campaign. Satellite-derived atmospheric motion vectors, produced by UW-CIMSS, were used extensively both as observations and integrated into three-dimensional analyses. Dropsonde data taken during PREDICT were used to verify the quality of the CIMSS satellite-derived wind vectors and analyses. Both were shown to be accurate, and acceptable to employ in identifying upper level flow features acting to modulate the TC genesis process.

Using the gridded satellite wind-enhanced analyses, composite and EOF fields were created covering Atlantic disturbances from 2010. The composite analyses show marked differences in the upper-level environments between pre-TCG and non-TCG systems. In particular, upper-level divergence over the center region is significantly enhanced in the developing systems, and these divergent conditions extend into the adjacent SW and NE quadrants, indicating more favorable outflow (and mass venting) conditions. These

extensions also indicate the enhanced divergence was not just a result of the internal core convection. Conversely, the non-developing sample is characterized by much weaker divergence aloft over the center, and much less divergent flow into the near-environment.

Other independent analyses were produced during PREDICT. Using the UW-NMS model analysis with GFS boundary conditions, isentropic analyses were produced and show significantly weaker inertial stability is generally found in developing systems as evidenced by lower PV through anticyclonic flow aloft, and higher Inertial Available Kinetic Energy (IAKE) near the core of the system, allowing for efficient conversion of buoyant energy to inertial energy in developing systems. This condition promotes the establishment of a sustained secondary circulation and allows deep core convection to flourish and persist. Several developing cases point to situations where concentrated outflow is directed toward regions of positive IAKE. This may signal the establishment of outflow channels (or ventilation ducts) that connect to the larger-scale environmental flow fields, and can more efficiently vent mass away from the storm center. In turn, this setup promotes sustained vortical hot tower growth, and the mechanisms for pouch theory genesis to proceed. In addition, composite mass flux diagnostics from the gridded satellite wind analyses revealed a number of characteristics specific to developing storms.

To better illuminate the concepts purported above, 2 case studies taken from the PREDICT field experiment sample of Atlantic storms in 2010 were examined; one embodying a non-developing situation and the other a developing case. The pouch

associated with post-TC Gaston featured a strong low level circulation and good "pouch

dynamics", and was forecast by analysts and numerical models to develop, but did not

regenerate as it moved eastward. This event featured a lack of coherent upper-level

outflow vents that allowed a diurnal convective cycle to dominate, as environmental dry air

was entrained into the circulation from the mid-levels.

By comparison, the disturbance (pouch) that would become TC Karl had good low-

level moisture and vorticity and looked like it should have developed on the 11th of

September (rather than the 14th) based on pouch theory parameters. However, dropsonde-

enhanced analyses showed substantial subsidence near the storm core during the diurnal

pulsation of convective activity through the 13th. Upper-level analyses indicated only a

marginal outflow environment during this time, especially impeded to the north of the

system. As the outflow became better established, the system underwent genesis and

rapidly deepened to tropical storm strength before making landfall on the Yucatan

Peninsula early on 15 Sept.

The findings in this study are significant for a number of reasons. Primarily, while the

process of TCG should continue to focus on convective forcing mechanisms and generation

of vorticity, it is shown the upper levels can provide a modulating effect and should not be

ignored. Future research should include the use of idealized high-resolution TC modeling

studies where trajectory analyses can be used to track the behavior core parcels as they

emerge at upper levels and emanate into the outflow.

Bibliography

Agudelo, P. A., J. A. Curry, C. D. Hoyos, P. J. Webster, 2006: Probabilistic discrimination between large-scale environments of intensifying and decaying African Easterly Waves. *Clim Dyn*, **36**, 1379–1401.

Bedka, Kristopher M., Christopher S. Velden, Ralph A. Petersen, Wayne F. Feltz, John R. Mecikalski, 2009: Comparisons of Satellite-Derived Atmospheric Motion Vectors, Rawinsondes, and NOAA Wind Profiler Observations. *J. Appl. Meteor. Climatol.*, **48**, 1542–1561.

Bell, M. M., and M. T. Montgomery, 2010: Sheared deep convection in pre-depression Hagupit during TCS-08. *Geophys. Res. Lett*., **37**, L06802, doi:10.1029/2009GL042313.

Bister, Marja, Kerry A. Emanuel, 1997: The Genesis of Hurricane Guillermo: TEXMEX Analyses and a Modeling Study. *Mon. Wea. Rev.*, **125**, 2662–2682.

Black, Peter G., Richard A. Anthes, 1971: On the Asymmetric Structure of the Tropical Cyclone Outflow Layer. *J. Atmos. Sci.*, **28**, 1348–1366.

Blanchard, David O., William R. Cotton, John M. Brown, 1998: Mesoscale Circulation Growth under Conditions of Weak Inertial Instability. *Mon. Wea. Rev.*, **126**, 118–140.

Braun, Scott A., 2010: Reevaluating the Role of the Saharan Air Layer in Atlantic Tropical Cyclogenesis and Evolution. *Mon. Wea. Rev.*, **138**, 2007–2037.

Challa, Malakondayya, Richard L. Pfeffer, 1990: Formation of Atlantic Hurricanes from Cloud Clusters and Depressions. *J. Atmos. Sci.*, **47**, 909–927.

Challa, Malakondayya, Richard L. Pfeffer, 1980: Effects of Eddy Fluxes of Angular Momentum on Model Hurricane Development. *J. Atmos. Sci.*, **37**, 1603–1618.

Chen, L., and W. M. Gray, 1985: Global view of the upper level outflow patterns associated with tropical cyclone intensity change during FGGE. Pap. 392, Dept. of Atmospheric Science, Colorado State University, 126 pp.

Davidson, N. E., G. J. Holland, J. L. McBride, T. D. Keenan, 1990: On the Formation of AMEX Tropical Cyclones Irma and Jason. *Mon. Wea. Rev.*,**118**, 1981–2000.

Davis, Christopher, Chris Snyder, Anthony C. Didlake, 2008: A Vortex-Based Perspective of Eastern Pacific Tropical Cyclone Formation. *Mon. Wea. Rev.*, **136**, 2461–2477.

Dunion, Jason P., Christopher S. Velden, 2004: The Impact of the Saharan Air Layer on Atlantic Tropical Cyclone Activity. *Bull. Amer. Meteor. Soc.*, **85**, 353–365.

Dunkerton, T. J., M. T. Montgomery, and Z. Wang, 2008: Tropical cyclogenesis in a tropical wave critical layer: Easterly waves. *Atmos. Chem. Phys. Disc.*, **8**, 11,149-11,292.

Emanuel, Kerry A., 1982: Inertial Instability and Mesoscale Convective Systems. part II. Symmetric CISK in a Baroclinic Flow. *J. Atmos. Sci.*, **39**, 1080–1097.

Emanuel, Kerry A., 1994: Atmospheric Convection. *Oxford University Press*, 580.

Halverson, J., and Coauthors, 2007: Nasa's Tropical Cloud Systems and Processes Experiment. *Bull. Amer. Meteor. Soc.*, **88**, 867–882.

Hanley, Deborah E., 2002: The Evolution of a Hurricane–Trough Interaction from a Satellite Perspective. *Wea. Forecasting*, **17**, 916–926.

Hendricks, Eric A., Melinda S. Peng, Bing Fu, Tim Li, 2010: Quantifying Environmental Control on Tropical Cyclone Intensity Change. *Mon. Wea. Rev.*, **138**, 3243–3271.

Holland, Greg J., 1984: Tropical Cyclone Motion. A Comparison of Theory and Observation. *J. Atmos. Sci.*, **41**, 68–75.

Holton, James R., 1992: An Introduction to Dynamic Meteorology: Third Edition. Academic Press, San Diego, California. 207– 208.

Houze, R. A., Jr., S. A. Rutledge, M. I. Biggerstaff, and B. F. Smull, 1989: Interpretation of Doppler weather radar displays of midlatitude mesoscale convective systems. Bull. *Amer. Meteor. Soc.*, **70**, 608–619.

Jordan, Elizabeth S., 1952: AN OBSERVATIONAL STUDY OF THE UPPER WIND-CIRCULATION TROPICAL STORMS. *J. Meteor.*, **9**, 340–346.

Kieu, Chanh Q., Da-Lin Zhang, 2009: Genesis of Tropical Storm Eugene (2005) from Merging Vortices Associated with ITCZ Breakdowns. Part II: Roles of Vortex Merger and Ambient Potential Vorticity. *J. Atmos. Sci.*, **66**, 1980–1996.

LeMone, M. A., 1983: Momentum transport by a line of cumulonimbus. *J. Atmos. Sci*., **40**, 1815–1834.

McBride, John L., 1981: Observational Analysis of Tropical Cyclone Formation. Part I: Basic Description of Data Sets. *J. Atmos. Sci.*, **38**, 1117–1131.

McBride, John L., Raymond Zehr, 1981: Observational Analysis of Tropical Cyclone Formation. Part II: Comparison of Non-Developing versus Developing Systems. *J. Atmos. Sci.*, **38**, 1132–1151.

Mecikalski, John R., Gregory J. Tripoli, 1998: Inertial Available Kinetic Energy and the Dynamics of Tropical Plume Formation. *Mon. Wea. Rev.*,**126**, 2200–2216.

Merrill, Robert T., 1988: Environmental Influences on Hurricane Intensification. *J. Atmos. Sci.*, **45**, 1678–1687.

Merrill, Robert T., 1988: Characteristics of the Upper-Tropospheric Environmental Flow around Hurricanes. *J. Atmos. Sci.*, **45**, 1665–1677.

Merrill, Robert T., Christopher S. Velden, 1996: A Three-Dimensional Analysis of the Outflow Layer of Supertyphoon Flo (1990). *Mon. Wea. Rev.*,**124**, 47–63.

Molinari, John, David Vollaro, 1989: External Influences on Hurricane Intensity. Part I: Outflow Layer Eddy Angular Momentum Fluxes. *J. Atmos. Sci.*, **46**, 1093–1105.

Molinari, John, David Vollaro, 1990: External Influences on Hurricane Intensity. Part II: Vertical Structure and Response of the Hurricane Vortex. *J. Atmos. Sci.*, **47**, 1902–1918.

Molinari, John, Steven Skubis, David Vollaro, 1995: External Influences on Hurricane Intensity. Part III: Potential Vorticity Structure. *J. Atmos. Sci.*,**52**, 3593–3606.

Montgomery, Michael T., Janice Enagonio, 1998: Tropical Cyclogenesis via Convectively Forced Vortex Rossby Waves in a Three-Dimensional Quasigeostrophic Model. *J. Atmos. Sci.*, **55**, 3176–3207.

Montgomery, Michael T., Brian F. Farrell, 1993: Tropical Cyclone Formation. *J. Atmos. Sci.*, **50**, 285–310.

Montgomery, M. T., M. E. Nicholls, T. A. Cramm, and A. Saunders, 2006: A vortical hot tower route to tropical cyclogenesis. *J. Atmos. Sci*., **63**, 355-386.

Montgomery, M. T., R. K. Smith, 2011: Paradigms for tropical-cyclone intensification. *Q.J.R. Meteorol. Soc., 137*, 1-31.

North, G. R., T. L. Bell, R. F. Cahalan, and F. J. Moeng. Sampling errors in the estimation of empirical orthogonal functions.*Monthly Weather Review*, **110**(7):699-7606, 1982.

Ooyama, Katsuyuki, 1969: Numerical Simulation of the Life Cycle of Tropical Cyclones. *J. Atmos. Sci.*, **26**, 3–40.

Pfeffer, Richard L., Malakondayya Challa, 1992: The Role of Environmental Asymmetries in Atlantic Hurricane Formation. *J. Atmos. Sci.*, **49**, 1051–1059.

Pratt, Aaron S., Jenni L. Evans, 2009: Potential Impacts of the Saharan Air Layer on Numerical Model Forecasts of North Atlantic Tropical Cyclogenesis. *Wea. Forecasting*, **24**, 420–435.

Ritchie, Elizabeth A., Greg J. Holland, 1997: Scale Interactions during the Formation of Typhoon Irving. *Mon. Wea. Rev.*, **125**, 1377–1396.

Rappin, Eric D., Michael C. Morgan, Gregory J. Tripoli, 2010: The Impact of Outflow Environment on Tropical Cyclone Intensification and Structure. *Preliminary Accepted Version.*

Rodgers, Edward B., Simon W. Chang, John Stout, Joseph Steranka, Jainn-Jong Shi, 1991: Satellite Observations of Variations in Tropical Cyclone Convection Caused by Upper-Tropospheric Troughs. *J. Appl. Meteor.*, **30**, 1163–1184.

Schneider, E. K., and R. S. Lindzen, 1976: A discussion of the parameterization of momentum exchange by cumulus convection. *J. Geophys. Res.*, **81**, 3158–3160.

Schubert, Wayne H., James J. Hack, 1982: Inertial Stability and Tropical Cyclone Development. *J. Atmos. Sci.*, **39**, 1687–1697.

Schumacher, Andrea B., Mark DeMaria, John A. Knaff, 2009: Objective Estimation of the 24-h Probability of Tropical Cyclone Formation. *Wea. Forecasting*, **24**, 456–471.

Shi, Jainn-Jong, Simon Wei-Jen Chang, Sethu Raman, 1990: A Numerical Study of the Outflow layer of Tropical Cyclones. *Mon. Wea. Rev.*, **118**, 2042–2055.

Shi, Jainn Jong, Simon Chang, Sethu Raman, 1997: Interaction between Hurricane Florence (1988) and an Upper-Tropospheric Westerly Trough. *J. Atmos. Sci.*, **54**, 1231–1247.

Tory, K. J., N. E. Davidson, M. T. Montgomery, 2007: Prediction and Diagnosis of Tropical Cyclone Formation in an NWP System. Part III: Diagnosis of Developing and Nondeveloping Storms. *J. Atmos. Sci.*, **64**, 3195–3213.

Tory, K. J., and W. M. Frank, 2010: Tropical cyclone formation. Chap. 2 Global Perspectives on Tropical Cyclones: From science to mitigation. World Scientific, Singapore, 55-91.

Velden, Christopher S., Kristopher M. Bedka, 2009: Identifying the Uncertainty in Determining Satellite-Derived Atmospheric Motion Vector Height Attribution. *J. Appl. Meteor. Climatol.*, **48**, 450–463.

Velden, C. S., T. Olander, and S. Wanzong, 1998: The Impact of Multispectral GOES-8 Wind Information on Atlantic Tropical Cyclone Track Forecasts in 1995. Part 1: Dataset Methodology, Description and Case Analysis. *Mon. Wea. Rev.*, **126**, 1202-1218.

Wang, Zhuo, M. T. Montgomery, T. J. Dunkerton, 2010: Genesis of Pre–Hurricane Felix (2007). Part I: The Role of the Easterly Wave Critical Layer. *J. Atmos. Sci.*, **67**, 1711–1729.

Wilks, Daniel S., 2006: Statistical Methods in the Atmospheric Sciences: Second Edition. Elsevier Inc, Burlington, Massachusetts. 352 – 357.

Wu, Chun-Chieh, Hsiu-Ju Cheng, 1999: An Observational Study of Environmental Influences on the Intensity Changes of Typhoons Flo (1990) and Gene (1990). *Mon. Wea. Rev.*, **127**, 3003–3031.

Zeng, Zhihua, Lianshou Chen, Yuqing Wang, 2008: An Observational Study of Environmental Dynamical Control of Tropical Cyclone Intensity in the Atlantic. *Mon. Wea. Rev.*, **136**, 3307–3322.

Approved: _____

Steven A. Ackerman

Professor, Department of Atmospheric & Oceanic Sciences

Date: _____

Approved: _____

Christopher S. Velden

Science Advisor, UW-CIMSS

Date: _____